2017

A Microfluidic Approach For Evaluating Novel Antithrombotic Targets

Shu Zhu
University of Pennsylvania, shuzhu@seas.upenn.edu

A Microfluidic Approach For Evaluating Novel Antithrombotic Targets

Abstract
Microfluidic systems allow precise control of the anticoagulation/pharmacology protocols, defined reactive surfaces, hemodynamic flow and optical imaging routines, and thus are ideal for studies of platelet function and coagulation response. This thesis describes the use of a microfluidic approach to investigate the role of the contact pathway factors XII and XI, platelet-derived polyphosphate, and thiol isomerases in thrombus growth and to evaluate their potential as safer antithrombotic drug targets. The use of low level of corn trypsin inhibitor allowed the study of the contact pathway on collagen/kaolin surfaces with minimally disturbed whole blood sample and we demonstrated the sensitivity of this assay to antithrombotic drugs. On collagen/tissue factor surfaces, we found the relative contributions of the extrinsic pathway, the contact pathway, and the thrombin feedback pathway vary with tissue factor surface concentration. Platelet-derived polyphosphate potentiated the thrombin feedback pathway at low tissue factor level but enhanced fibrin fiber structure regardless of tissue factor level. At locations with low tissue factor level, thrombosis may be druggable by contact pathway and polyphosphate inhibition, although thrombolytic susceptibility may benefit from polyphosphate antagonism regardless of tissue factor level. We developed a peptide-based platelet-targeting thiol reduction sensor to visualize thrombus-incorporated thiol reductase activity. Although distribution of thiol reductase activity was shown to be correlated with the level of platelet activation, protein disulfide isomerase inhibition showed a limited effect on platelet aggregation in microfluidic thrombosis assay. We also used the microfluidic system to explore the injury patch size limit for triggering clotting. We observed a full clotting response of platelet deposition, thrombin generation and fibrin polymerization on one of the smallest biological units of a single collagen fiber presenting tissue factor and von Willebrand factor suggesting the lack of physiological injury patch size limit. Finally, we made the first estimation of thrombin flux from growing thrombus under flow using the microfluidic thrombosis assay in combination with enzyme-linked immunosorbent measurement of thrombin-antithrombin complex. We found thrombin is robustly generated within clots by the extrinsic pathway, followed by late-stage factor XIa contributions, with fibrin localizing thrombin via its antithrombin activity as a self-limiting hemostatic mechanism.

Degree Type
Dissertation

Degree Name
Doctor of Philosophy (PhD)

Graduate Group
Chemical and Biomolecular Engineering

First Advisor
Scott L. Diamond

Keywords
Blood, Hemostasis, Microfluidics, Platelet, Thrombosis

A MICROFLUIDIC APPROACH FOR EVALUATING NOVEL ANTITHROMBOTIC TARGETS

Shu Zhu

A DISSERTATION

in

Chemical and Biomolecular Engineering

Presented to the Faculties of the University of Pennsylvania

in

Partial Fulfillment of the Requirements for the

Degree of Doctor of Philosophy

2017

Supervisor of Dissertation

_____

Scott L. Diamond

Professor, Chemical and Biomolecular Engineering

Graduate Group Chairperson

_____

John C. Crocker, Professor, Chemical and Biomolecular Engineering

Dissertation Committee

Lawrence F. Brass, Professor, Department of Medicine

Talid R. Sinno, Professor, Department of Chemical and Biomolecular Engineering

Daeyeon Lee, Professor, Department of Chemical and Biomolecular Engineering

A MICROFLUIDIC APPROACH FOR EVALUATING NOVEL ANTITHROMBOTIC TARGETS

ACKNOWLEDGMENT

Firstly, I would like to express my deepest gratitude to my thesis advisor Dr. Scott Diamond for the guidance and continuous support for my PhD study. I feel so privileged to conduct research with a talented, enthusiastic and devoted scientist like Dr. Diamond. I would never be able to prepare this dissertation without the training provided by the Diamond lab. I would also like to extend my thanks to my other thesis committee members, Dr. Lawrence Brass, Dr. Talid Sinno and Dr. Daeyeon Lee for their challenging questions and insightful comments on my work and for the time and effort they spent serving on my committee. I owe equal appreciation to all past and current Diamond lab members, especially those who I have worked closely with, Dr. Thomas Colace, Dr. Ryan Muthard, Dr. John Welsh, Dr. Mei Yan Lee, Dr. Ruizhi Li, Dr. Jifu Tan, Bradley Herbig, Xinren Yu, and Huiyan Jing and to all the great scientists I have collaborated with, Dr. James Morrissey, Dr. Maurizio Tomaiuolo and Dr. Juan Jimenez. I want to thank all of you for offering me precious technical support and all the joyful and inspiring discussions.

My special appreciation goes to my dearest parents for trusting my decision of studying and pursuing a doctoral degree abroad in the US. Thanks for the great internet, I can always feel the love from my family through daily conversations despite the 12-hour time difference between home and Philadelphia. Thank you dad for the encouragements whenever I am hesitant to move forward and thank you mom for all the comforting words to guide me through all the tough times. I want also to extend special thanks to my friends and other family members, especially Fay Wang, for always being curious about my research and being cheerful whenever I feel down. I feel lucky to always have this

group of optimistic and caring people backing me up throughout my life away from home.

Finally, I want to thank my husband and my best friend Yichen Lu for sharing this journey with me. I feel so fortunate to be in the same department and lab, which later led to both academic and life partners. Your intelligence, kindness, patience and devotion motivates me to be a better person. I feel truly blessed to be part of your life. Wherever the future leads us, I am excited to explore, to learn and to strive with you.

ABSTRACT

A MICROFLUIDIC APPROACH FOR EVALUATING NOVEL ANTITHROMBOTIC TARGETS

Shu Zhu

Scott L. Diamond

Microfluidic systems allow precise control of the anticoagulation/pharmacology protocols, defined reactive surfaces, hemodynamic flow and optical imaging routines, and thus are ideal for studies of platelet function and coagulation response. This thesis describes the use of a microfluidic approach to investigate the role of the contact pathway factors XII and XI, platelet-derived polyphosphate, and thiol isomerases in thrombus growth and to evaluate their potential as safer antithrombotic drug targets. The use of low level of corn trypsin inhibitor allowed the study of the contact pathway on collagen/kaolin surfaces with minimally disturbed whole blood sample and we demonstrated the sensitivity of this assay to antithrombotic drugs. On collagen/tissue factor surfaces, we found the relative contributions of the extrinsic pathway, the contact pathway, and the thrombin feedback pathway vary with tissue factor surface concentration. Platelet-derived polyphosphate potentiated the thrombin feedback pathway at low tissue factor level but enhanced fibrin fiber structure regardless of tissue factor level. At locations with low tissue factor level, thrombosis may be druggable by contact pathway and polyphosphate inhibition, although thrombolytic susceptibility may benefit from polyphosphate antagonism regardless of tissue factor level. We developed a peptide-based platelet-targeting thiol reduction sensor to visualize thrombus-incorporated thiol reductase activity. Although distribution of thiol reductase activity was shown to be

correlated with the level of platelet activation, protein disulfide isomerase inhibition showed a limited effect on platelet aggregation in microfluidic thrombosis assay. We also used the microfluidic system to explore the injury patch size limit for triggering clotting. We observed a full clotting response of platelet deposition, thrombin generation and fibrin polymerization on one of the smallest biological units of a single collagen fiber presenting tissue factor and von Willebrand factor suggesting the lack of physiological injury patch size limit. Finally, we made the first estimation of thrombin flux from growing thrombus under flow using the microfluidic thrombosis assay in combination with enzyme-linked immunosorbent measurement of thrombin-antithrombin complex. We found thrombin is robustly generated within clots by the extrinsic pathway, followed by late-stage factor XIa contributions, with fibrin localizing thrombin via its antithrombin activity as a self-limiting hemostatic mechanism.

TABLE OF CONTENTS

ACKNOWLEDGMENT ..... **III**

ABSTRACT ..... **V**

LIST OF TABLES ..... **XI**

LIST OF ILLUSTRATIONS ..... **XII**

CHAPTER 1 : INTRODUCTIONS **1**

1.1 Hemostasis and thrombosis **1**

1.2 Plasma coagulation cascade **1**

1.3 Current antithrombotic strategies **4**

1.4 Recreating *in vivo* hemodynamics using microfluidic devices **5**
1.4.1 Inhibitors and activators 8
1.4.2 Microfluidic device fabrication 9
1.4.3 Defined surfaces for coagulation studies 9
1.4.4 8-channel device 10

CHAPTER 2 : CONTACT ACTIVATION OF BLOOD COAGULATION ON A DEFINED KAOLIN/COLLAGEN SURFACE IN A MICROFLUIDIC ASSAY **13**

2.1 Introduction **13**

2.2 Materials and Methods **15**
2.2.1 Fluorescent labeling of kaolin particles 15
2.2.2 PS/PC liposomes 15
2.2.3 Thrombin biosensor on platelet surface 16
2.2.4 PDMS patterning and flow devices 16
2.2.5 Kaolin/collagen and TF/collagen surfaces 17
2.2.6 Characterization of kaolin/collagen surface 17
2.2.7 Blood collection and preparation for microfluidic assay 20
2.2.8 Microfluidic model for contact activation 20
2.2.9 Constant flow mode and pressure relief mode 21
2.2.10 Detection of thrombin activity with time in a tube clotting assay 22
2.2.11 Statistical analysis 22

2.3 Results **24**
2.3.1 Kaolin surface concentration 24
2.3.2 Effect of kaolins surface concentrations on activity of contact pathway 29
2.3.3 Effect of flow conditions on activity of contact pathway 31

2.4 Discussion **41**

2.5 Conclusions **45**

CHAPTER 3 : FXIA AND PLATELET POLYPHOSPHATE AS THERAPEUTIC TARGETS DURING HUMAN BLOOD CLOTTING ON COLLAGEN/TISSUE FACTOR SURFACES UNDER FLOW **46**

3.1 Introduction **46**

3.2 Methods **48**
3.2.1 Materials 48
3.2.2Preparation and characterization of collagen/TF surface 49
3.2.3 Blood collection and preparation 49
3.2.4 Microfluidic clotting assay on collagen/±TF surface 50
3.2.5 Preparation of PPXbd 51
3.2.6 Determination of TF surface concentrations 51
3.2.7 Scanning electronic microscopy 52
3.2.8 Statistical analysis 53

3.3 Results **56**
3.3.1 Contact pathway was indispensable for thrombin generation on collagen surface 56
3.3.3 PPXbd inhibited fibrin generation on collagen/low $[TF]_{wall}$ surface at venous shear rate 61
3.3.4 PPXbd inhibited thrombin and fibrin generation on collagen/low $[TF]_{wall}$ surface at arterial shear rate 64
3.3.5 PPXbd blocked mechanisms downstream of FXIIa on collagen/low-medium $[TF]_{wall}$ 67
3.3.6 PPXbd altered fibrin structure and promoted clot retraction upon fibrinolysis 69

3.4 Discussion and Conclusions **72**

CHAPTER 4 : PLATELET-TARGETING THIOL REDUCTION SENSOR DETECTS PROTEIN DISULFIDE ISOMERASE ACTIVITY ON ACTIVATED PLATELETS IN MOUSE AND HUMAN BLOOD UNDER FLOW **78**

4.1 Introduction **78**

4.2 Materials and Methods **81**
4.2.1 Materials 81
4.2.2 Production of disulfide-linked thiol isomerase sensitive hetero-peptide dimers (PDI-sP) 82
4.2.3 Synthesis of thiol isomerase sensitive antibody (PDI-sAb) 85
4.2.4 Microfluidic clotting assay on collagen surface 85
4.2.5 Blood collection and preparation 86
4.2.6 Mouse intravital microscopy 86

4.3 Results **87**
4.3.1 Sensitivity of PDI-sAb to reducing reagents 87
4.3.2 Sensitivity of PDI-sAb to rhPDI and psPDI 90
4.3.3 Sensitivity of PDI-sAb to PDI inhibition 95
4.3.4 Detection of PDI reductase activity in a microfluidic thrombosis model 99

4.3.5 Detection of PDI reductase activity in vivo 102

4.4 Discussion and Conclusions 104

CHAPTER 5 : MINIMUM WOUND SIZE FOR CLOTTING: FLOWING BLOOD COAGULATES ON A SINGLE COLLAGEN FIBER PRESENTING TISSUE FACTOR AND VON WILLEBRAND FACTOR 109

5.1 Introduction 109

5.2 Materials and Methods 111
5.2.1 PDMS patterning and flow devices 111
5.2.2 Preparation of small collagen patches 111
5.2.3 Blood collection and preparation 114
5.2.4 Microfluidic thrombosis model 115
5.2.5 Scanning electronic microscopy 115
5.2.6 Statistical analysis 115

5.3 Results 116
5.3.1 Micropatterned zones of collagen fibers 116
5.3.2 A single collagen fiber with tissue factor triggers coagulation at venous wall shear rate 116
5.3.3 Patch threshold on collagen/TF at arterial flows when von Willebrand Factor is absent 122
5.3.4 Single collagen fiber with TF and VWF supports coagulation at arterial shear rate 125

5.4 Discussion 129

5.5 Conclusions 132

CHAPTER 6 : DYNAMICS OF THROMBIN GENERATION AND FLUX FROM CLOTS DURING WHOLE HUMAN BLOOD FLOW OVER COLLAGEN/TISSUE FACTOR SURFACES 133

6.1 Introduction 133

6.2 Materials and Methods 135
6.2.1 Materials 135
6.2.2 PDMS patterning and flow device 136
6.2.3 Analysis of system response time 136
6.2.4 Preparation of thrombotic patches 137
6.2.5 Blood collection and sample preparation 138
6.2.6 Microfluidic thrombosis assay 138
6.2.7 TAT-ELISA assay 139

6.3 Results 139
6.3.1 Device response time 139
6.3.2 Clotting under flow: Fibrin rapidly captures thrombin 142
6.3.3 Increased surface TF concentration promotes thrombin flux 145
6.3.4 Thrombin flux amplification via thrombin feedback activation of FXI 146
6.3.5 The first layer of collagen-activated platelets generates the majority of thrombin 148

6.3.6 Longer collagen/TF zones are less efficient in thrombin production 150

6.4 Discussion and Conclusions 152

CHAPTER 7 : FUTURE WORK 157

7.1 Effect of flow pulsatility on thrombus growth 157

7.2 Microfluidic characterization of reaction dynamics of fibrin formation 163

BIBLIOGRAPHY 167

LIST OF TABLES

Table 3-1 Estimated TF surface concentration. 55

Table 4-1 PDI-P fluorescence change after addition of reducing reagent DTT. 84

LIST OF ILLUSTRATIONS

Figure 1-1 Schematic of simplified model of the coagulation cascade. 3

Figure 1-2 The initiation and pharmacological regulation of thrombin 7

Figure 1-3 8-channel device. 12

Figure 2-1 Fluorescent intensity vs. surface concentration for pure fluorescent..... 19

Figure 2-2 Experimental design..... 23

Figure 2-3 Determination of kaolin surface concentration. 26

Figure 2-4 Lipids promote platelet poor plasma clotting in the presence of kaolin. 27

Figure 2-5 Kaolin sped up thrombin generation in whole blood in a dose dependent manner..... 28

Figure 2-6 Dynamic change of platelet and fibrin fluorescent intensities on..... 30

Figure 2-7 Average platelet and fibrin signal on collagen/kaolin surface at three..... 32

Figure 2-8 Platelet aggregation on collagen/kaolin surface. 33

Figure 2-9 TF is more efficient in triggering WB clotting in well plate. 35

Figure 2-10 Dynamics of platelet deposition and fibrin formation on collagen/TF..... 36

Figure 2-11 Averaged platelet and fibrin intensities on collagen/TF and 37

Figure 2-12 Effect of antiplatelet therapies on thrombus formation on collagen..... 39

Figure 2-13 Effect of antiplatelet therapies on thrombus formation on collagen..... 40

Figure 2-14 Inhibition of fibrin formation on collagen/kaolin surface by high CTI or PPACK..... 44

Figure 3-1 Annexin V staining of TF liposomes on collagen surface. 54

Figure 3-2 14E11 and O1A6 individually block thrombin/fibrin generation on..... 57

Figure 3-3 Low level of CTI is required for blocking XIIa generation in reservoirs... 58

Figure 3-4 Potency of 14E11 and O1A6 varies depending on $[TF]_{wall}$. 60

Figure 3-5 PPXbd inhibits fibrin generation at low $[TF]_{wall}$ under venous condition. . 62

Figure 3-6 Massive XIIa dependent thrombin generation masked the effect of 63

Figure 3-7 PPXbd inhibits fibrin and thrombin generation on collagen/low $[TF]_{wall}$ at arterial shear rate. 65

Figure 3-8 PPXbd delayed occlusion on collagen surface. 66

Figure 3-9 PPXbd inhibits pathways downstream of FXIIa. 68

Figure 3-10 PPXbd reduces thrombus resistance to fibrinolysis induced by 70

Figure 3-11 PPXbd enhances clot retraction after flow cessation and alters fibrin..... 71

Figure 3-12 Role of XIIa, XIa, and polyP in thrombus formation on collagen/TF 73

Figure 3-13 Platelet and fibrin deposition on collagen/polyP surface. 77

Figure 4-1 Platelet-targeting thiol isomerase sensitive fluorogenic sensor (PDI-sAb). 80

Figure 4-2 Two step reaction for producing disulfide-linked thiol isomerase 83

Figure 4-3 PDI-sAb sensitivity to reducing reagents. 89

Figure 4-4 PDI-sAb sensitivity to exogenously added rhPDI. 92

Figure 4-5 Sensitivity of PDI-sAb to platelet-derived thiol reductase activity. 93

Figure 4-6 Platelet expression of thiol reductase activity is associated with granule release and PS expression. 94

Figure 4-7 PDI-sAb sensitivity to PDI inhibitors. 96

Figure 4-8 PDI inhibitors cause reduction in thiol reductase activity expression on platelet surface. 97

Figure 4-9 Rutin does not cause reduction in platelet PS exposure. 98

Figure 4-10 Detection of thiol reductase activity *in vitro*..... 100
Figure 4-11 Rutin causes severe reduction in platelet deposition on collagen in the... 101
Figure 4-12 Detection of thiol reductase activity *in vivo.* 103
Figure 4-13 PDI-sAb specifically detects thiol isomerase activities in blood. 108
Figure 5-1 Microfluidic perfusion and micropatterned collagen fiber surfaces. 113
Figure 5-2 Thrombus formation on collagen/TF at venous and arterial flows 118
Figure 5-3 Thrombus formation on 20-μm collagen at venous flow condition..... 120
Figure 5-4 Thrombus formation on small patches of collagen (no TF) at venous and arterial flow conditions. 121
Figure 5-5 For arterial flow, coagulation on collagen/TF fibers requires pre- 123
Figure 5-6 Incorporation of plasma vWF into formed thrombus on single..... 124
Figure 5-7 VWF and TF synergistically promote coagulation on single collagen fiber at arterial flow. 127
Figure 5-8 Surface plot of platelet deposits on a single collagen/TF/VWF fiber..... 128
Figure 6-1 Microfluidic setup for measuring thrombin flux during whole blood 141
Figure 6-2 Thrombin flux from clots growing on collagen/TF. 143
Figure 6-3 Platelet aggregation and fibrin formation on collagen/TF. 144
Figure 6-4 Thrombin flux is amplified after 500 sec of clotting via thrombin..... 147
Figure 6-5 The first layer of collagen-activated platelets support initial thrombin 149
Figure 6-6 Longer collagen/TF zones were less efficient in thrombin production. ... 151
Figure 6-7 Substantial inhibition of fibrin polymerization by GPRP under flow. 156
Figure 7-1 A LabVIEW program to control programmable syringe pump. 160
Figure 7-2 Representative shear rate profiles. 161

Figure 7-3 Dynamics of platelet adhesion and aggregation on small collagen patches. 162
Figure 7-4 Fibrin localizes free thrombin via its antithrombin activity..... 165
Figure 7-5 Cumulative FPA generation detected downstream of growing clots on... 166

Chapter 1 : Introductions

1.1 Hemostasis and thrombosis

Hemostasis refers to the rapid response from the hemostatic system to prevent excessive bleeding upon tissue injury [1]. Hemostasis requires the concerted actions from vascular, platelets and coagulation enzymes. Neurogenic constriction of damaged blood vessel immediately diminishes blood loss. Exposed collagen and von Willebrand Factor (vWF), the two major physiological platelet activators, trigger and support primary platelet aggregation over injury sites [2]. Activated platelets experience shape change and release autocrine activators such ADP and thromboxane (TXA_2), which promote platelet secondary aggregation [2]. Meanwhile, exposed tissue factor (TF) initiates plasma coagulation cascade and leads to thrombin production. Thrombin, as the principle enzyme of coagulation, promotes platelet aggregation and cleaves soluble fibrinogen to fibrin [3]. Fibrin polymerizes into fibrin network to increase clot integrity and stability [4].

Thrombosis refers to excessive clotting response usually observed in diseased vessels. Unlike a hemostatic plug whose growth is usually confined in the vessel wall and extravascular space, thrombi form exclusively in the vessel lumen [1]. Thrombosis can cause obstruction of blood flow in diseased vessel and increase the risk of numerous life threatening diseases like stroke, myocardial infarction and venous thromboembolism [1].

1.2 Plasma coagulation cascade

Plasma coagulation can be initiated via two distinctive pathways: the contact pathway and the extrinsic pathway **(Figure 1-1).** The extrinsic pathway prompts major

clotting response upon vascular injury. Disrupted endothelium exposes TF to blood stream. Circulating factor VII (FVII) subsequently forms complex TF/FVIIa with TF in its activated form. TF/FVIIa complex then activates common pathway factor X (FX) and creates crosstalk between the two initiation pathways by activating factor IX (FIX). The contact pathway is initiated by the activation of factor XII (FXII) on anionic surfaces. Clotting is dominated by this pathway when blood is exposed to foreign surfaces that are bearing negative charges. Although extracellular RNA and DNA, collagen and misfolded protein have been identified as naturally occurring FXII activators, the contact pathway is less relevant to primary hemostasis since FXII deficiency is not associated with a bleeding phenotype [5]. Upon activation, FXIIa converts downstream factor XI (FXI) to its activated form FXIa, which will then lead to the formation of intrinsic tenase FIXa/FVIIIa. Following the "waterfall" coagulation cascade, both pathways merge to the common pathway where FX is activated by either the extrinsic tenase (TF/FVIIa) or the intrinsic tenase (FIXa/FVIIIa) forming prothrombinase (FXa/FVa) complex on phospholipid membranes [6]. The prothrombinase complex catalyzes the activation of zymogen prothrombin. Thrombin, as the central protease of the coagulation cascade, can self-amplify via a FXI dependent feedback pathway and cleaves soluble fibrinogen into fibrin polymer. Calcium ions play essential roles in assisting coagulation. Both intrinsic tenase and prothrombinase complex only function in the presence of calcium ions [7]. Thus, calcium chelators (i.e. citrate) have been used as anticoagulants for blood collection.

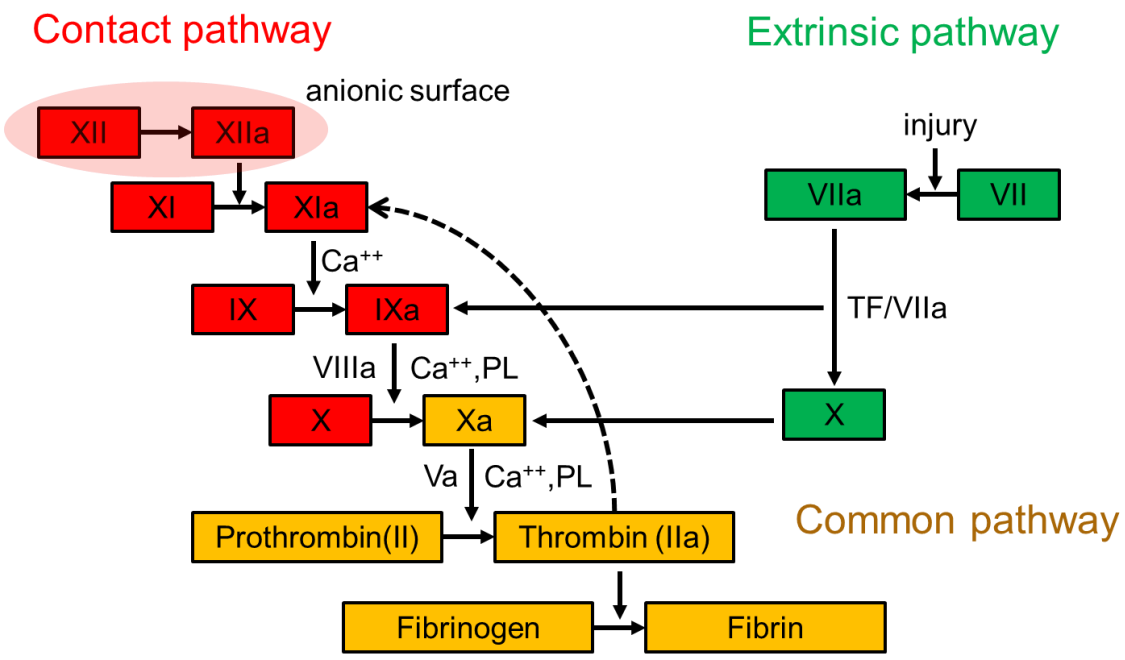

Figure 1-1 Schematic of simplified model of the coagulation cascade.

Blood coagulation can be initiated via two distinctive pathways. Contact pathway is triggered when blood is exposed to negatively charged surfaces on which FXII is converted to FXIIa. FXIIa can activate FXI and lead to the activation of FIX and subsequent FXa generation. Extrinsic pathway is initiated by exposed TF at injury site. TF complexes with FVIIa and robustly activate FX and FIX. Both pathways merge into common pathway where thrombin is generated. Thrombin, as the central protease in the coagulation cascade, can amplify coagulation via contact pathway by activating FXI and can also convert soluble fibrinogen to insoluble fibrin fibers.

1.3 Current antithrombotic strategies

Antithrombotic therapies have been widely used in clinical practices for more than 50 years. Current antithrombotic therapies can be divided into two major categories: anticoagulant and antiplatelet drugs. Anticoagulant drugs target and inhibit coagulation, thereby limiting thrombin and fibrin formation and preventing unlimited clot growth. The most commonly used anticoagulant drug in the U.S is warfarin, a traditional drug that inhibits vitamin K-dependent synthesis of calcium-dependent coagulation factors [8]. More recently, direct acting oral anticoagulants (DOACs) have been introduced into market. DOACs are direct inhibitors for thrombin (dabigatran) and coagulation factor Xa (FXa, rivaroxaban and apixaban), which are the two key coagulation factors belong to the final common pathway of the coagulation cascade [9, 10]. Antiplatelet drugs limit clot growth by inhibiting platelet aggregation. Aspirin is one representative antiplatelet drug. It suppresses the production of the autocrine platelet activator TXA2, therefore inhibiting platelet aggregation [2].

Despite the fact that antithrombotic drugs have been widely used for treating thrombosis for decades, thromboembolic disorder is still one of the leading causes of morbidities and mortality worldwide indicating the inefficiency of the current therapies [10]. Additionally, most of the antithrombotic drugs are associated with bleeding risks. Studies have shown over 10% of annual bleeding rates by warfarin administration. Elderly patients are more prone to cardiovascular diseases requiring antithrombotic treatment but are also at higher risk of bleeding with current antithrombotic drugs [11].

Due to the unmet medical needs in thrombosis treatment, researchers are still seeking for safer and more effective antithrombotic strategies.

1.4 Recreating *in vivo* hemodynamics using microfluidic devices

The ***in vivo*** cardiovasculature achieves robust oxygen delivery by pumping blood from the heart to the smallest of capillaries. Composed of diverse cell types, blood flows through a branched and flexible geometry of living vessels. Biorheological complexity arises from single protein and protein ensemble mechanics, single cell biomechanics, dense suspensions of cells in time-dependent flows, and cellular mechanobiological response to forces transmitted by and through fluids and tissues. In contrast, the ***in vitro*** setting, once a single glass dish (now plastic), is a sterile environment lacking both flow and forces, which has at least progressed to the 96-well plate format and beyond. Bridging these two extremes is the ***in microfluidico*** setting that combines flow and high replicates at small length scales to recreate biochemical and biological complexity under the dynamic conditions of the vasculature.

For blood research, the microfluidic device can be considered an "open" reactor system that contains a small reservoir on or off the device from which blood flows directly into the microfluidic channel(s). While blood is held by the perfect *in vivo* container (the endothelium), blood should be considered perturbed when it is obtained by phlebotomy and delivered to the reservoir of the device. Using fresh human blood *ex vivo* in flow experiments requires precise consideration of anticoagulation so that the blood is minimally perturbed prior to introduction into the microfluidic channel. For coagulation research in which blood generates thrombin, several triggers should be considered and

controlled: (i) air/biomaterial activation of the contact pathway factor FXII, (ii) platelet dependent activation of the contact pathway (via polyphosphate release and other FXIIa activators), (iii) extrinsic activation by endogenous tissue factor (from phlebotomy or from a disease state in the donor) or exogenous TF added by the experimentalist to the reservoir or affixed to the surface of the microchannel **(Figure 1-2A).** Numerous inhibitors and experimental designs allow control of these pathways to obtain clotting conditions that range from contact dominated to extrinsic pathway dominated **(Figure 1-2B)** [12, 13]**.**

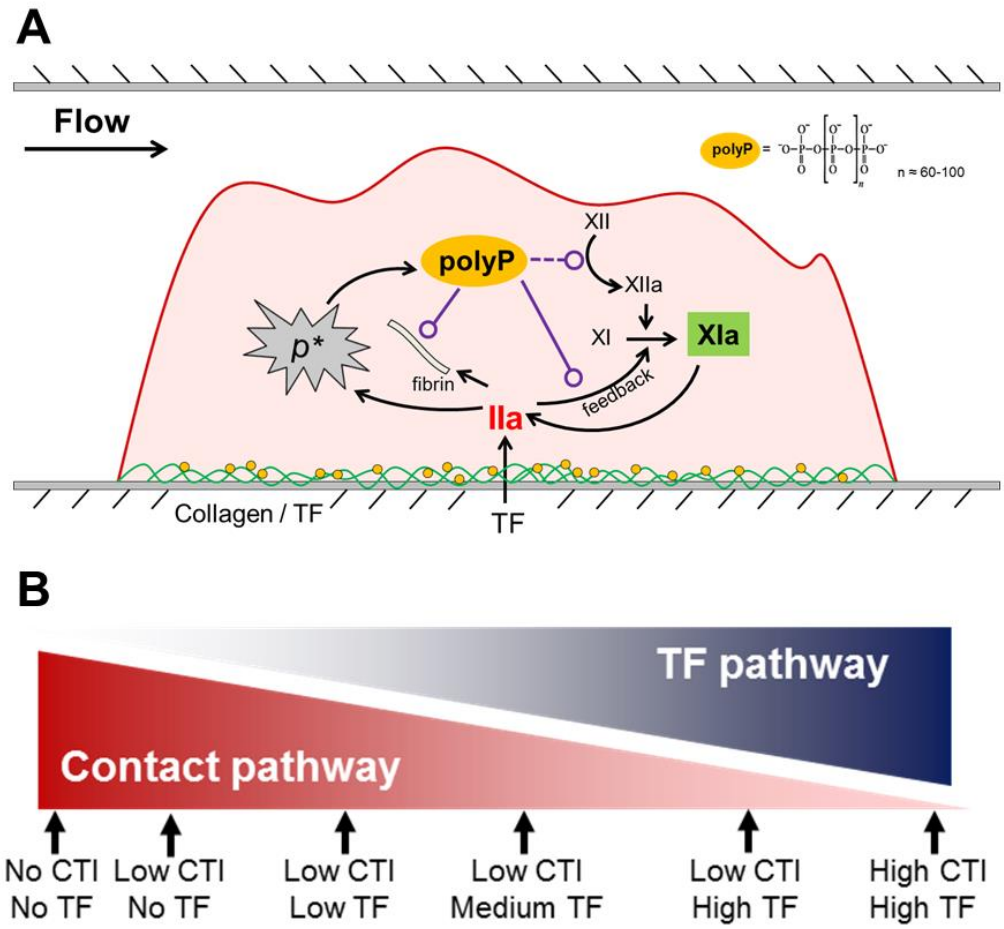

Figure 1-2 The initiation and pharmacological regulation of thrombin production and coagulation using whole blood in microfluidic devices.

A, Pre-patterned collagen/TF surface can simultaneously trigger thrombin generation and support platelet aggregation. As thrombi builds up, packed activated platelets secret high concentration of polyphosphate (polyP), which promotes contact activation and thrombin feedback activation of FXI and enhances fibrin physical structure. **B,** By varing TF surface concentration and CTI concentration used for anticoagulation, Zhu et al. in 2015 generated various coagulation conditions under which thrombin generation can be primarily dominated by the contact pathway (low/no CTI, no TF) or the extrinsic pathway (high/low CTI, high TF) or regulated by both pathways with comparable contributions (low CTI, low-medium TF).

1.4.1 Inhibitors and activators

Sodium citrate, a calcium chelating reagent, is typically used as anticoagulant to inhibit calcium dependent mechanisms in the coagulation cascade [14]. Clotting resumes upon recalcification prior to flow into the microfluidic device. However, FXII activation can proceed in the absence of calcium and prime the contact pathway. Because resting time of citrated blood is often an uncontrolled variable, corn trypsin inhibitor (CTI), a β-FXIIa inhibitor at a low level of 4 μg/mL can be used to study the contact pathway by providing partial blockade of contact activation during blood collection but still allowing FXIIa generation on a prothrombotic surface. High level of CTI (40-100 μg/mL) provides strong blockade of β-FXIIa thus allowing the study of the extrinsic pathway. CTI at high concentrations may have some activity on Factor XIa (FXIa) [15, 16]. Antibodies such as 14E11 prevent activation of FXI by FXIIa and are analogous to CTI in their use [17-19]. For either CTI or 14E11, thrombin can still feedback activate FXI to FXIa. Antibodies against FXI/FXIa that prevent activation of Factor IX (of the intrinsic tenase Factor IXa/Factor VIIIa) eliminate both the contact pathway and the thrombin feedback activation of FXI, replicating a FXI-deficiency (hemophilia C). A procoagulant surface can be created in the microchannel by patterning collagen which causes platelet activation via GPVI and mediates adhesion through activated platelet integrin $\alpha_2\beta_1$ [20-22]. Addition of kaolin to collagen will enhance contact activation of FXII [12], while addition of lipidated TF to collagen (0.1 to 10 molecules/μm^2) [23-25] spans the relevant dose-response regime for triggering the extrinsic pathway. Use of direct Factor Xa or thrombin inhibitors (eg. 1 μM apixaban or 100 μM PPACK, respectively) prevent clotting and allow the study of platelet, red blood cell, and neutrophil function in flowing

whole blood without the confounding influence of thrombin and fibrin. Additionally, pharmacological modulators of clotting (recombinant FVIIa, anti-TFPI) [26] or platelet activation (aspirin, $P2Y_{12}$ inhibitors, protease activated receptor-1 inhibitors) can be used as part of the experimental design [12, 27-29].

1.4.2 Microfluidic device fabrication

Microfluidic devices are fabricated by soft lithography with PDMS. High quality photomasks (10,000 dpi) are designed in computer-aided design programs (i.e. DraftSight and LayoutEditor) and are sent for manufacture at OutputCity (Bandon, OR). Designed features on photomasks can be transferred onto silicon wafers using standard photolithograph [30]. Mixed PDMS prepolymer and curing reagent are cured over the master. The molded PDMS are then cut into individual devices. Fluidic and vacuum ports are added using microfluidic biopsy punch.

1.4.3 Defined surfaces for coagulation studies

Neeves et al. [22] demonstrated the technique of patterning fibril collagen onto glass surface with a single channel PDMS device. This technique can be applied to generate focal thrombosis within defined prothrombotic regions. In fact, surface-immobilized collagen fibrils not only activate platelets and support platelet aggregation but also serve as substrates for other hemostatically active proteins and/or particles. Colace et al. [23] linked TF-incorporated lipid liposomes to collagen surface by biotin-avidin interaction to create defined prothrombotic surfaces mimicking *in vivo* injuries. Zhu et al. [12] utilized electrostatic interaction to decorate collagen surfaces with kaolin

(FXII activator) nanoparticles or lipidated TF that can trigger thrombin generation via the contact pathway or via both the contact and the extrinsic pathways **(Figure 1-2B)**.

1.4.4 8-channel device

A microfluidic device that consists of 8 flow channels was developed by Maloney et al. in 2010 [20], which was subsequently used in several works to generate focal thrombosis on micro-patterned collagen surfaces [12, 13, 23, 24, 26, 28, 31, 32] (**Figure 1-3A**). The vast majority of microfluidic models used to study the hemostatic mechanism under relevant local wall shear rate conditions are driven by constant flow rate (Const Q) syringe pumps. Instead, the *in vivo* pump, the heart, operates in a constant pressure drop mode and the branchlike networks of the vasculature ensure that Const Q in any vessel is unlikely. In 2012 Colace et al. [24] demonstrated that a platelet/fibrin aggregate depositing under Const Q in a fixed volume experiences a nonlinear increase in local wall shear rate (**Figure 1-3C**) whereas a platelet/fibrin mass forming under constant pressure drop conditions (Const ΔP) experiences an initial increase in local wall shear rate followed by a decline (**Figure 1-3D**), caused by a decrease in flow rate during the formation of the thrombus (**Figure 1-3D**, bottom panel). The authors were able to achieve Const Q vs. Const ΔP conditions by employing the 8-channel flow device. Under Const Q conditions whole blood was run through all 8 channels, while under Const ΔP conditions, channels with whole blood were staggered with channels of whole blood treated with EDTA to chelate Ca^{2+}, an essential component of platelet adhesion. Platelet/fibrin masses formed under Const Q conditions grew more rapidly than those under Const ΔP, perhaps due to increased VWF function under increased shear rate [33]

and always ruptured (formed in vitro emboli, **Figure 1-3C**) from the pro-aggregatory surface. Those *in vitro* thrombi developed under Const P conditions, however, grew to fully occlude their containing vessels and divert flow through the EDTA containing channels (**Figure 1-3D**). The Const ΔP mode is the more physiological relevant mode of operation; in which thrombotic occlusion can be achieved by diverting flow to a paired open channel. However, under this operation mode, the requirement of pressure relieving channels reduced the availability of the assay channels on a single device, which can be potentially changed by employing a pressure sensing and controlling system in each channel.

Local hemodynamic conditions around a developing microfluidic thrombus can be calculated using both 2-D and 3-D COMSOL models in conjunction with epifluorescence microscopy to quantify platelet and fibrin deposition. When whole blood was treated with GPRP, a peptide inhibitor of fibrin polymerization, the resulting thrombi were unable to resist local wall shear rates of 2,900 s^{-1} (**Figure 1-3C-D, open circles**). Although fibrin, the polymeric protein that weaves a tight mesh around platelet aggregates, was already believed to provide clots with structure [34], this study was the first to quantify a dramatic increase in the shear resistance of clots formed with fibrin as opposed to those formed in the presence of GPRP.

This 8-channel device allowed for simultaneous evaluation of platelet responsiveness to multiple inhibitors under precisely controlled surface and hemodynamic conditions without requiring large volume of whole blood. This high-throughput microfluidic thrombosis model has been used to evaluate platelet function and coagulation from patients with congenital bleeding disorders [26, 31].

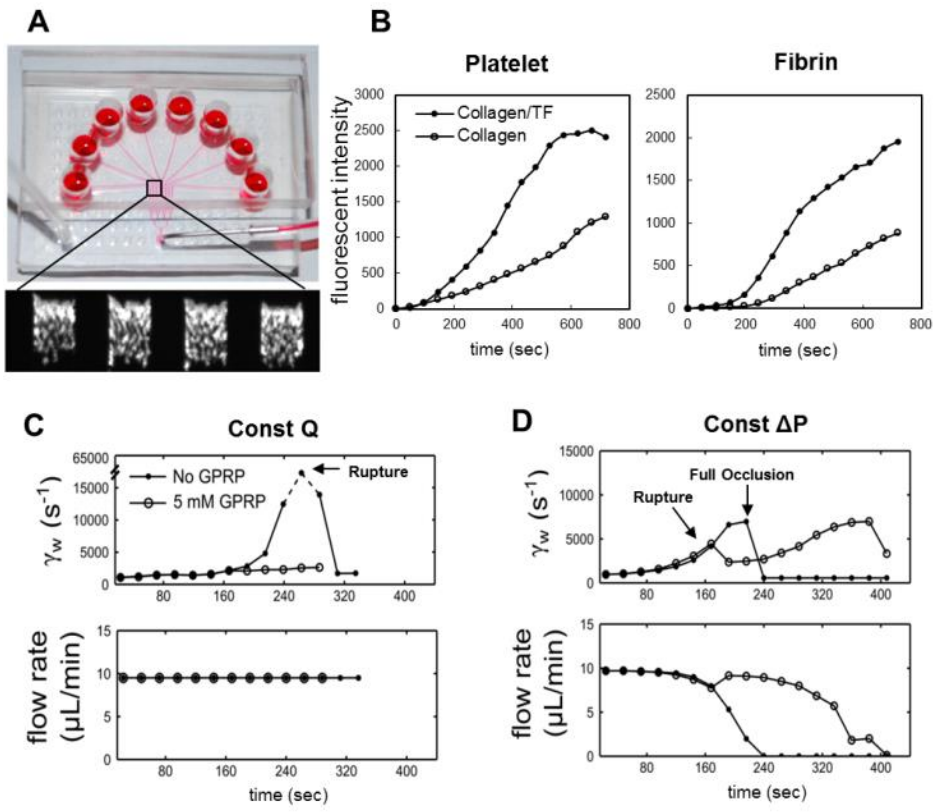

Figure 1-3 8-channel device.

A, A microfluidic device consisting of 8 separate inlets perfused by a single outlet (top). This device can be run under Const Q by perfusing all 8 channels with whole blood or under Const ΔP by staggering channels of whole blood with channels of whole blood treated with EDTA to prevent platelet deposition. The bottom panel illustrates 4 platelet masses (of 8) depositing in parallel under whole blood perfusion at 1000 s^{-1} at Const Q (platelets were labeled with a fluorescently tagged antibody). The channel width is 250 μm. **B,** At Const Q, when whole blood was perfused over collagen surface at 100 s^{-1}, both platelet aggregation and fibrin formation were promoted in the presence of high level of surface immobolized TF (~ 5-10 molec/μm^2). In Colace et al. 2012, local wall shear rate was calculated using a two-dimensional COMSOL model at a representative platelet surface by assuming that the aggregate height was proportional to its epifluorescence. **C,** Platelet/fibrin masses (closed circles) experienced an increase in shear rate until rupture. Samples treated with GPRP to inhibit fibrin formation (open circles) did not withstand shear rates greater than 2900 s^{-1}. **D,** Platelet/fibrin masses formed under Const ΔP experienced a biphasic local wall shear rate profile. When aggregates approached 75% of full channel occlusion, a steep drop in channel flow rate was calculated. A representative samples treated with GPRP (open circles) began to occlude the channel but ruptured at ~150 sec and organized into a more hemodynamically favorable conformation such that the local wall shear rates could not be accurately predicted.

Chapter 2 : Contact activation of blood coagulation on a defined kaolin/collagen surface in a microfluidic assay

2.1 Introduction

Contact pathway can be strongly triggered by negatively charged surfaces such as glass, kaolin and celite [35]. Zymogen factor XII (FXII) is activated to FXIIa upon contacting with anionic surfaces and leads to a multistep cascade, whereby thrombin (FIIa) forms as a potent platelet activator and trigger of fibrin polymerization [36, 37]. The pathophysiology of contact pathway is not fully elucidated. While tissue factor triggered extrinsic pathway prompts major response to vascular injury, contact pathway likely has a minor role in hemostasis since factor XII deficiency is not associated with a bleeding defect. However, recent experiments revealed that FXII-mediated fibrin formation is essential for thrombus stability in a mice model [38-40]. In contrast, FXI-deficient (hemophilia C) patients display little spontaneous bleeding but at elevated risk of bleeding post-injury or post-operative, especially at sites with high fibrinolysis [41]. It has been suggested that pharmacological inhibitors of FXIIa or FXIa may be drugs useful for limiting thrombosis with reduced risk of bleeding side effects [42-44].

Many studies of contact pathway have been conducted for the purpose of investigating unfavorable thrombosis on blood-contacting medical devices. Most of these studies mainly focus on the activation mechanism of FXII. The approach often eliminates blood flow and cellular components, which then allows contact activation in static tubes with plasma [45-47]. However, flow and cellular constituents are both present in human blood vessels, fundamentally altering reaction dynamics as compared to a cell-free system under static conditions. Flow based studies designed to intentionally trigger and

measure contact pathway are less common. Glass capillary flow reactor has been used to study plasma coagulation via artificial surface activation [48]. Kaolin-activated thromboelastography (TEG) has been applied as a predictive test for post-operative bleeding to assess clotting factors (i.e. rate, strength, and stability) under non-flow condition [49, 50]. Typically, citrate is used as an anticoagulant which allows recalcification immediately prior to an experiment. However, FXIIa can be formed under calcium-free conditions and the resting time in citrate is often an uncontrolled variable. In contrast, corn trypsin inhibitor (CTI) is a potent and selective inhibitor of βFXIIa (but not αFXIIa). Blood will eventually clot by the contact pathway even in the presence of high dose CTI (40 to 100 μg/mL) [51]. The use of low dose CTI (4 μg/mL) provides a ~30-minute window from blood draw to last data point whereby blood does not clot in the tube but will generate thrombin at the site of a thrombotic trigger such as collagen.

Microfluidic devices allow the study of thrombotic events by perfusion of whole blood over well-defined prothrombotic surfaces [20, 22, 23, 52]. Microfluidics enables precise control of flow condition and real-time observation of thrombus structure. In this chapter, Zhu and Diamond describe a prothrombotic surface composed of collagen and kaolin that is capable of activating blood coagulation via the contact pathway, independent of tissue factor (TF). This surface also serves as a biologically important substrate for anchoring activated platelets and polymerized fibrin. Engagement of contact pathway was evaluated by dynamic accumulation of localized platelets and fibrin on the collagen/kaolin surface. This microfluidic assay allowed a controlled study of the sensitivity of contact pathway function to wall shear rate.

2.2 Materials and Methods

2.2.1 Fluorescent labeling of kaolin particles

For imaging of kaolin on collagen, fluorescent labeling of kaolin particles was carried out in a two-step reaction [53]. Kaolin was mixed with 3-mercaptopropyl-trimethoxysilane in 80% methanol (50 mL methanol/g kaolin) in a 3:1 mass ratio. The mixture was stirred at room temperature for 6 hr to activate kaolin surface by converting surface hydroxyl groups to thiol groups, filtered, and washed 3 times with 80% methanol. The residue was collected and vacuum-dried for 12 hr. Powdered kaolin was then dried at 80 ºC for 5 hr. Labeling solution was prepared by adding 5 mg fluorescein-5-maleimide into 120 mL phosphate buffered saline (PBS). Activated kaolin (125 mg) along with 50 mL ethanol was mixed with labeling solution for 1 hr. Kaolin was centrifuged (5000 g, 1 min) and supernatant was discarded. The pellet was resuspended in 1 mL PBS buffer. Centrifugation and re-suspension were repeated several times until supernatant was clear. Fluorescent kaolin pellet was vacuum-dried (12 hr) and stored to avoid light and moisture.

2.2.2 PS/PC liposomes

Liposomes were prepared according to a previous reported technique [54]. L-α-phosphatidylcholine (PC) and L-α-phosphatidylserine (PS) (Avanti Polar Lipids, Alabaster, AL) were vacuum-dried in an 80:20 molar ratio. The dried film was resuspended in 1 mL HEPES buffered saline (HBS) at 2.3 mg-lipid/mL. A size extruder generated <100 nm diameter liposomes.

2.2.3 Thrombin biosensor on platelet surface

Soluble thrombin was detected under flow conditions using a platelet-linked thrombin biosensor [55]. A total of 4 µL of anti-human CD61 antibody (5 mg/mL, Biolegend, San Diego, CA) was mixed with 8 µL of 900 µM DBCO-sulfo-NHS ester (Click Chemistry Tools, Scottsdale, AZ) in 28 µL of HBS buffer. The mixture was incubated at room temperature for 30 min. A volume of 2.5 µL of Tris-HCl (1M, pH 8) was then added to quench the DBCO linking of anti-human CD61. Diluted peptide thrombin sensitive peptide (4 µL of 4 mM) was added into the reaction to initiate labeling reaction and incubated in the dark at room temperature for 4 hr. The thrombin sensor was then gel filtrated with P6-Gel beads (hydrated in HBS buffer) yielding approximately 100 µL of platelet binding thrombin sensor (5 µg/mL).

2.2.4 PDMS patterning and flow devices

The microfluidic patterning device and the 8-channel microfluidic flow device were fabricated with poly(dimethylsiloxane) (PDMS, Ellsworth Adhesives, Germantown, WI) as previous described [22]. The protein patterning device has a single channel (250 µm in width, 60 µm in height) and two outlets at both ends of the channel allowing protein infusion for coating. The flow device has 8 cylindrical reservoirs connecting to 8 evenly spaced channels that merge to a single outlet. Both devices have a vacuum groove that allows them to be reversibly vacuum bonded onto glass slides.

2.2.5 Kaolin/collagen and TF/collagen surfaces

Glass slides were rinsed with ethanol for 15 sec followed by DI water for 30 sec and were dried with compressed filtered air. The patterning device was vacuum bonded onto a cleaned glass slide. A volume of 5 µL of acid insoluble collagen type I (Chronolog Corp, Havertown, PA) followed by 20 µL bovine serum albumin (0.5% BSA in HBS) perfusion through the channel forming an immobilized thin matrix of well aligned collagen fibrils. Kaolin suspension (50 mg/mL HBS) was centrifuged briefly (500 g, 15sec) to remove aggregates and supernatant was mixed with prepared PS/PC liposomes in a 3:1 volume ratio. Kaolin surface concentration can be varied via changing the centrifugation time: 5 sec centrifugation gives highly packed kaolin surface; 30 sec centrifugation gives sparse kaolin deposition while 15 sec centrifugation gives a medium density of localized kaolin on collage fibrils. A volume of 10 µL of kaolin/lipids suspension or Dade Innovin recombinant human tissue factor (50% in HBS, VWR Corp, Radnor, PA) was pulled through the channel and allowed to settle over collagen for at least 30 min before rinsing with 10 µL BSA to remove excessed kaolin, TF or lipids.

2.2.6 Characterization of kaolin/collagen surface

For calibration, fluorescent kaolin was suspended in HBS buffer to five concentrations (0, 10, 20, 30, 40 mg/mL) and allowed to completely fill the main channel of the patterning devices and to settle overnight at 65ºC forming five dried fluorescent kaolin (without collagen) films with surface concentrations from 0-2.4 pg/µm^2. Fluorescent intensity was measured by imaging. A fluorescent intensity vs. mass curve was then constructed (**Figure 2-1**). Four fluorescent kaolin/collagen surfaces with zero,

low, medium and high amount of kaolin were made. Their surface mass concentrations were extrapolated from the mass vs. fluorescent intensity curve. Surface coverage of kaolin/collagen surface was calculated with thresholding tool in ImageJ (NIH). A calibration curve was made by relating surface concentration to surface coverage.

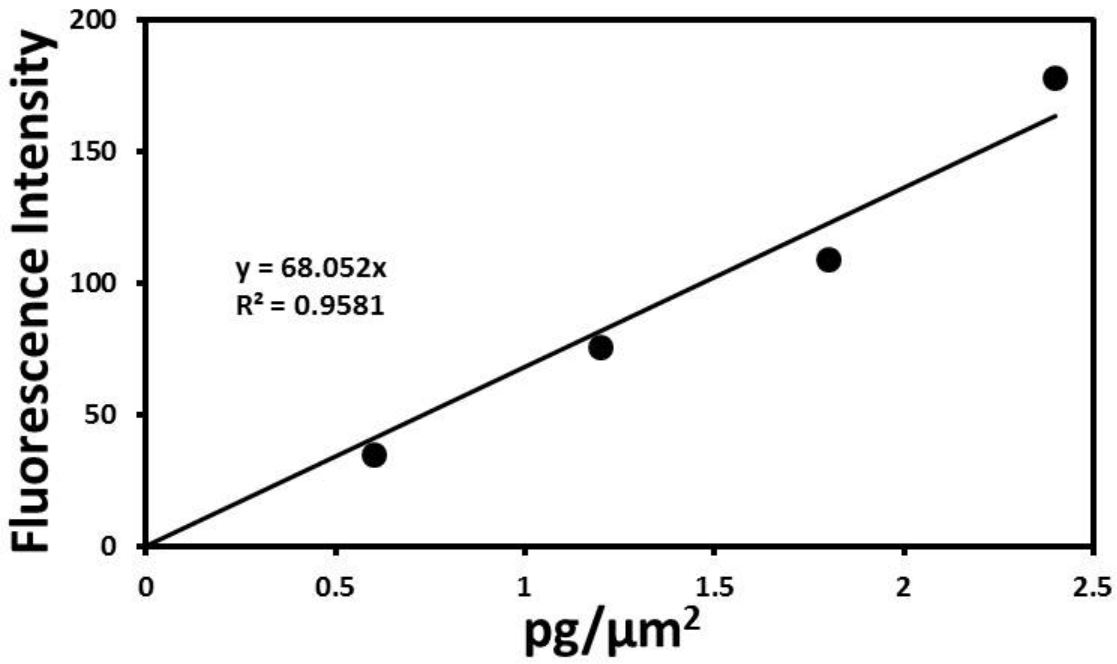

Figure 2-1 Fluorescent intensity vs. surface concentration for pure fluorescent kaolin surface.

A linear dependency of fluorescent intensity of kaolin particles on its surface concentration was observed.

2.2.7 Blood collection and preparation for microfluidic assay

Blood was collected via venipuncture from health donors (who were free of alcohol and medication for 72 hr prior to experiments) into corn trypsin inhibitor (CTI, 4 μg/mL WB, Haematologic Technologies, Essex Junction, VT). All donors were consent under approval of University of Pennsylvania Institutional Review Board. First 5 mL of blood was discarded to avoid tissue factor contamination. Blood was treated with anti-human CD61 antibody (BD Biosciences, San Jose, California) for platelet detection and Alexa Fluor 488 fluorescent fibrinogen (Life Technologies, Grand Island, NY) for observation of fibrin generation. All experiments were initiated within 5 min after venous phlebotomy. For antithrombotic therapy tests, platelet thrombin biosensor was added into blood in 1:9 ratio for the measurement of thrombin level. Anti-human CD41a antibody and Fluor 647 fluorescent fibrinogen were added for platelet and fibrin detection, respectively.

2.2.8 Microfluidic model for contact activation

The 8-channel flow device was vacuum bonded to a glass slide with its flow channels mounted perpendicularly to the pattered kaolin/collagen surface, forming eight evenly spaced 250μm×250μm prothrombotic patches (**Figure 2-2**). Blood was perfused over prothrombotic surfaces under either venous (100 s^{-1}) or arterial wall shear rates (1000 s^{-1}) controlled by a syringe pump (Harvard Apparatus PHD 2000, Holliston, MA) (**Figure 2-2**). A custom stage held 3 flow devices allowing up to 24 conditions to be imaged simultaneously in single experiment. Platelet accumulation, fibrin generation,

and thrombin formation were monitored by 3-color imaging with a fluorescence microscope (IX81, Olympus America Inc., Center Valley, PA) with specified time intervals. Images were captured with a CCD camera (Hamamatsu, Bridgewater, NJ) and were analyzed with ImageJ (NIH). All images were background subtracted. The center 65% of the prothrombotic region was selected to avoid edge effects and fluorescent intensities of the selected region were recorded for analysis.

2.2.9 Constant flow mode and pressure relief mode

By changing the inlet condition of each well of the 8-channel device, thrombus could form under either constant flow mode or pressure relief mode [24]. As a clot approaches channel occlusion, shear rates on the thrombus surface become very large under constant flow mode. Given the power of the syringe pump, a 60-micron thick clot can never block the channel in the constant flow rate mode. The pressure relief mode approaches a constant pressure drop driven flow allowing an occlusive clot to stop flow and divert flow to a relief channel. Constant flow mode: CTI treated blood was perfused in all eight channels and inlet wall shear rate was maintained in all channels before full channel occlusion. Pressure relief mode: EDTA (8 mmol/L, ethylenediaminetetraacetic acid) treated blood was fed into every other channel to ablate platelet deposition and clotting. The matched EDTA channel allows clot formation to proceed at essentially constant pressure drop in the matched, active assay channel (no EDTA present).

2.2.10 Detection of thrombin activity with time in a tube clotting assay

Citrated (1:9 WB) and CTI-treated (4 μg/mL) whole blood was diluted 1:4 HBS buffer and recalcified to 10 mM final calcium concentration in 384-well plate (65 μL/well) right before experiment. A thrombin specific fluorogenic substrate Boc-Asp(OBzl)-Pro-Arg-AMC (10 μmol/L, peptide international) was added to detect thrombin generation in terms of fluorescence of released aminomethylcoumarin (AMC) [51, 56]. Kaolin or recombinant TF was added into wells to trigger clotting. Fluorescence was measured with Thermo Fluoroskan in 15 sec time intervals for 1 hr. Fraction conversion of thrombin substrate f was calculated with following equation: $f(t) = [\mathbf{F}(t) - F(0)]/[F_{max} - F(0)]$ where F(t) is the instantaneous fluorescent reading in the well, F_{max} is the maximum readings in the well. f(t) was calculated for each well and was averaged over all replicated wells. The initiation time T_i of thrombin generation was defined at the time point when 5% of the thrombin substrate was converted (f=0.05). A large burst in thrombin always occurs promptly after T_i.

2.2.11 Statistical analysis

Data were compared to controls using two-tail Student's t-test. P-value < 0.05 was considered statistical significant. For antithrombotic therapy tests, Bonferroni correction was performed since multiple statistical tests were being performed simultaneously.

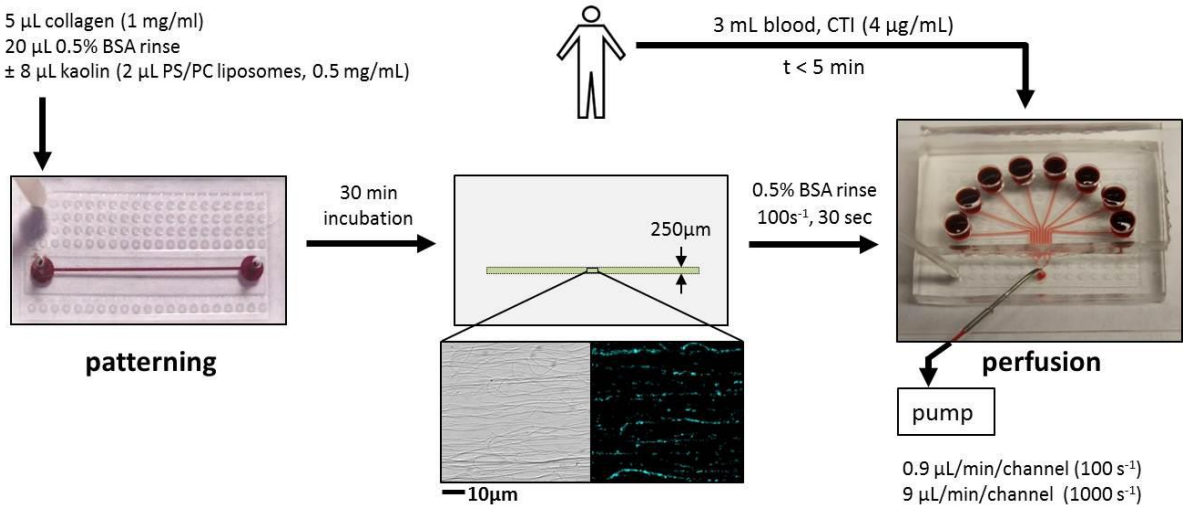

Figure 2-2 Experimental design.

Collagen was patterned with a single channel device that was vacuum bonded on a glass slide (left, red dye to show flow path). After BSA-blocking, a mixture of kaolin and PS/PC liposome was pulled through the main channel and allowed to settle for 30 min, forming a 250-µm wide immobilized kaolin/collagen film (middle). The patterning device was then replaced by an 8-channel device that was mounted perpendicular to kaolin/collagen strip forming 8 evenly spaced 250 µm × 250 µm procoagulant zones. CTI (4µg/mL) treated blood was perfused over kaolin/collagen surfaces in the presence of fluorescent conjugated platelet and fibrinogen labels (right). Flow was initiated within 5 min after venous phlebotomy and shear rate was controlled by a syringe pump. In some experiments, EDTA was added to blood in lanes 2, 4, 6, 8 to operate in a constant pressure drop mode.

2.3 Results

2.3.1 Kaolin surface concentration

Kaolin particles displayed flow-resistant adsorption to collagen (up to 1000 s^{-1}), an adsorption likely depending on electrostatic attraction between anionic kaolin surface and cationic regions on collagen fibrils. This kaolin adsorption occurred even with precoating of collagen with BSA. A calibration experiment demonstrated a linear dependency between kaolin surface concentration and % area surface coverage (**Figure 2-3B**) as expected for the thin collagen matrix. **Figure 2-3C-F** correspond to collagen surfaces with no, low, medium, and high level of florescent kaolin. Surface concentrations were determined from the calibration line and converted to surface ratio (μm^2 kaolin/ μm^2 glass) using the specific surface area of kaolin particles of 16 $\mu m^2/\mu g$-kaolin [57, 58]. Addition of PC/PS liposomes to the kaolin/collagen was designed to promote contact-triggered coagulation by providing an anionic lipid surface for prothrombinase formation (Factor Xa/Va) even in the absence of activated platelets. In well plate assay of thrombin generation, initiation of thrombin generation was accelerated when PC/PS (2.3 μg/mL final concentration) was added into 5-fold diluted, 40 μg/mL CTI-treated, recalcified citrated PPP (**Figure 2-4**). Using fluorescent annexin V binding assay, we also determined that PS/PC deposition was controlled by collagen and was not affected by kaolin (data not shown). To delineate the effect of PC/PS, same amount of liposomes were patterned onto all surfaces including kaolin free collagen surface. To demonstrate that kaolin could trigger contact activation in a well plate assay (no flow), citrated WB (4 μg/mL CTI, 5-fold diluted) initiated thrombin generation at ~25 min after

recalcification and addition of kaolin (0.3-300 μg/mL) shortened the time lag in a dose dependent manner (**Figure 2-5**). The fastest thrombin generation was observed at about 10min after recalcification.

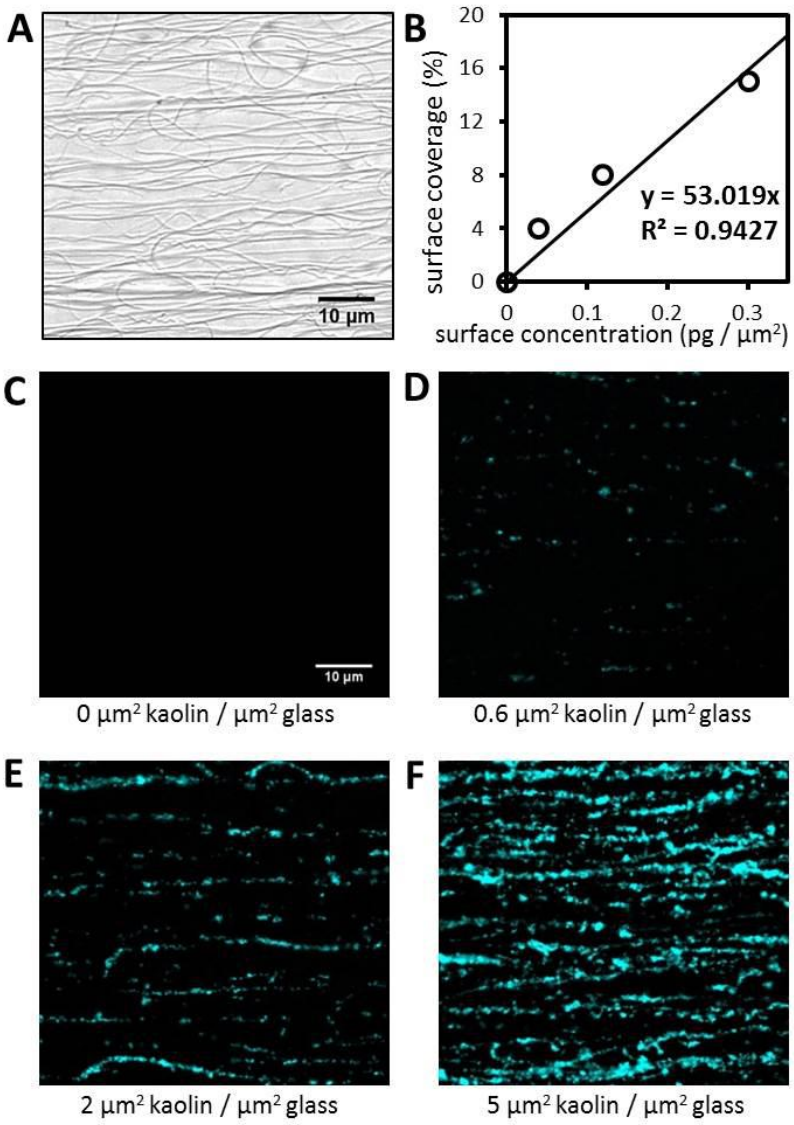

Figure 2-3 Determination of kaolin surface concentration.

A, Kaolin/collagen surface (with not PS/PC) was visualized using scanning electron microscopy (black bar represents 5 µm). White particles are kaolin and grey lines in the background are collagen fibrils. **B,** A calibration curve of fluorescent kaolin surface concentration was constructed. **C-F,** Surface with no, low, medium and high level of fluorescently labeled kaolin particles were visualized with fluorescent microscope. Surface concentrations were determined from B.

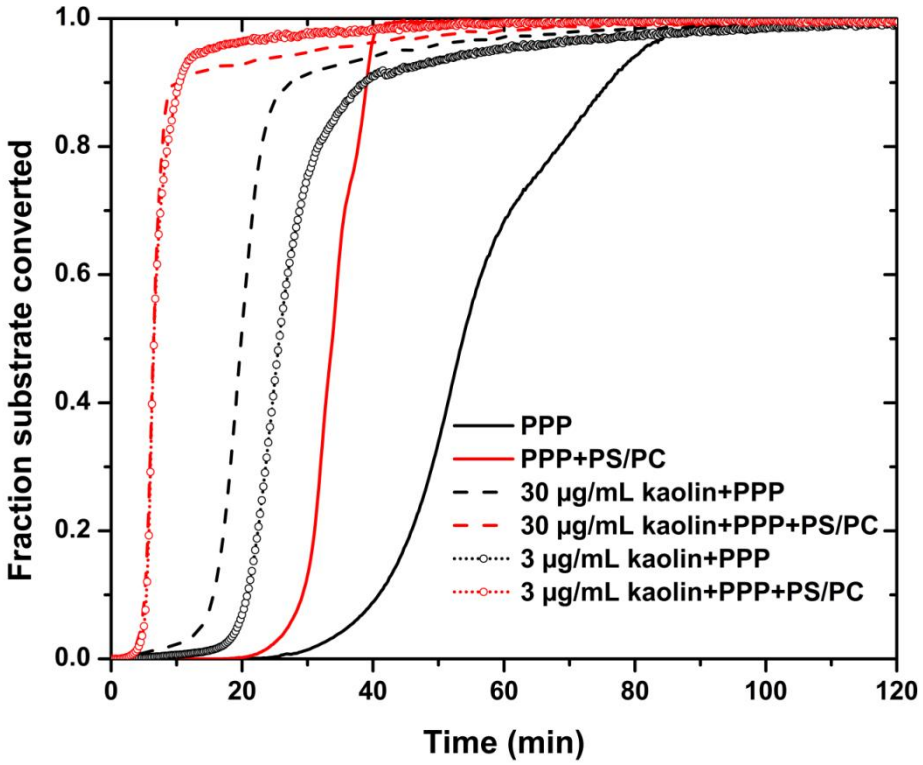

Figure 2-4 Lipids promote platelet poor plasma clotting in the presence of kaolin.

PPP was prepared from whole blood treated with both citrate (1:9 WB) and high CTI (40 µg/mL). A thrombin specific fluogenic substrate Boc-Asp(OBzl)-Pro-Arg-AMC was added into re-calcified (10 mM) PPP to detect thrombin generation in. A blend of lipids shortened the initiation time of thrombin generation (5% substrate converted) in PPP by about 10 min. The prothrombotic effects of kaolin was enhanced with the presence of lipids. However, lipids failed to further advance the initiation time when kaolin concentration increased from 3 to 30 µg/mL.

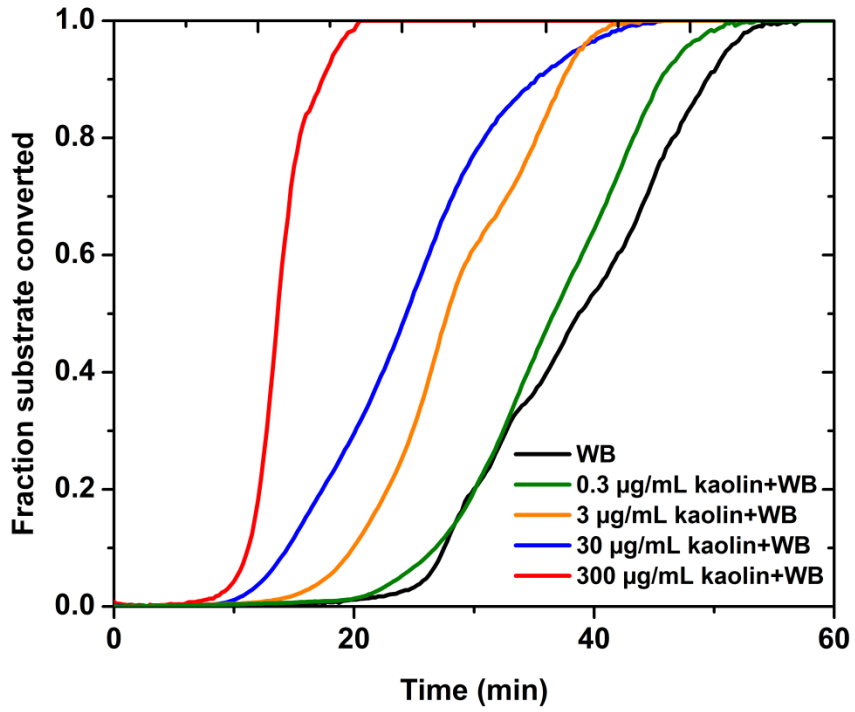

Figure 2-5 Kaolin sped up thrombin generation in whole blood in a dose dependent manner.

Citrate (1:9 WB) and CTI (4 µg/mL) treated whole blood (1:4 HBS) was recalcified (10 mM) right before measurements. Kaolin was added to trigger contact pathway. A thrombin specific fluorogenic substrate Boc-Asp(OBzl)-Pro-Arg-AMC was used to monitor the thrombin generation. Kaolin sped up thrombin formation in a dose dependent manner. Fastest thrombin generation was observed at 10 min with 300 µg/mL kaolin, which is a comparable concentration with kaolin suspension used for kaolin/collagen surface preparation.

2.3.2 Effect of kaolins surface concentrations on activity of contact pathway

In the microfluidic assay, highly concentrated kaolin (> 0.3 pg/μm^2) blocked collagen fibrils and resulted in severe reduction in platelet deposition (data not shown) and was excluded from further experiments. Platelet deposition was not affected by medium or low kaolin concentration under either pressure relief or constant flow mode (**Figure 2-6A-B**). However, presence of medium level of kaolin (0.12 pg/μm^2) accelerated onset of fibrin generation by over 100 sec and quantitatively promoted fibrin formation for both pressure relief and constant flow modes (**Figure 2-6C-D**). Depending on the donor, low level of kaolin (0.03 pg/μm^2) could either enhance or had no effect on fibrin formation suggesting a modest inter-donor variation in response to the lowest dose kaolin (data not shown). All subsequent experiments used a medium level of kaolin, which always promoted fibrin formation under flow for all donors.

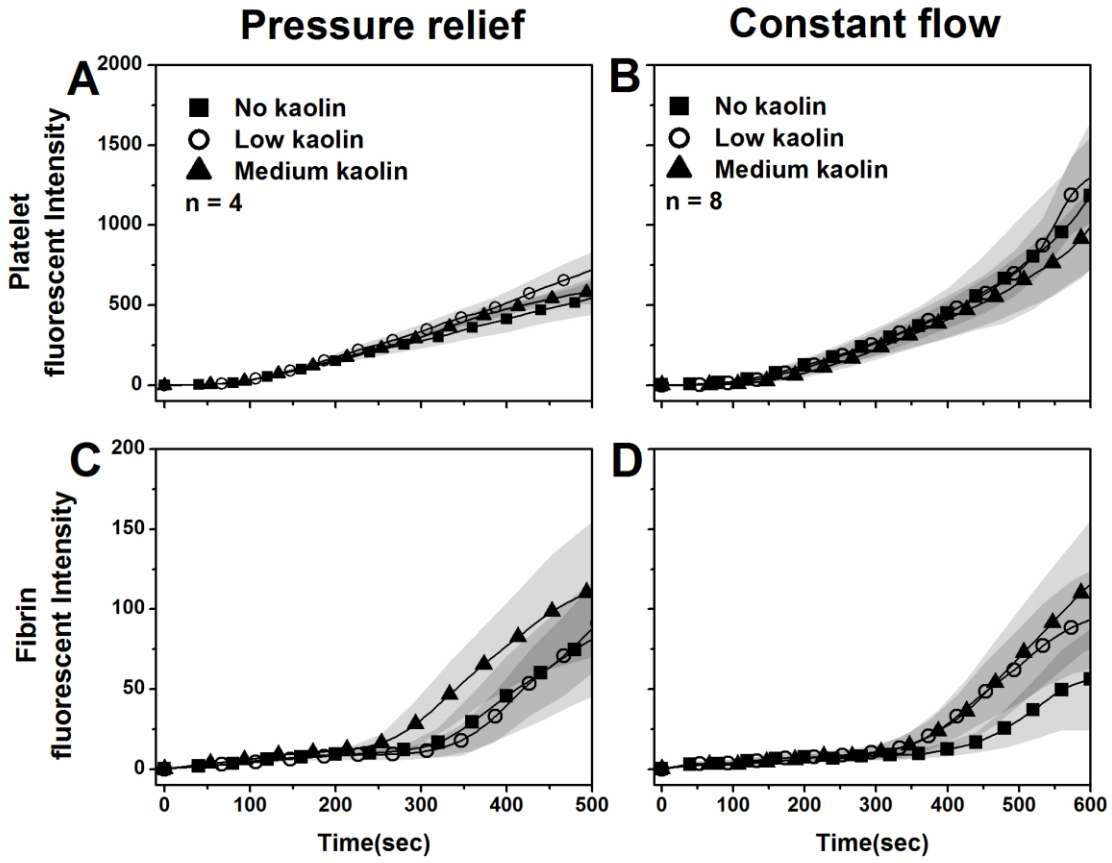

Figure 2-6 Dynamic change of platelet and fibrin fluorescent intensities on kaolin/collagen surface.

A-B, Dynamic change of platelet and fibrin fluorescent intensities on kaolin/collagen surface. CTI (4μg/mL) treated whole blood was perfused over kaolin/collagen surface at 100 s^{-1}. Platelet deposition (± SD, shaded) for different kaolin concentrations are identical indicating kaolin is not interfering with platelet deposition under either pressure relief or constant flow mode. **C-D,** Medium level of kaolin accelerated the onset of fibrin formation under both pressure relief mode and constant flow mode.

2.3.3 Effect of flow conditions on activity of contact pathway

Averaged results (**Figure 2-7**) showed that fibrin generation was favored at venous shear rate (100 s^{-1}) compare to arterial shear rate (1000 s^{-1}) for either constant flow or pressure relief mode. Under pressure relief mode, no significant difference was observed between the level of platelet depostion at arterial shear rate and at venous shear rate. Platelet deposition always preceded fibrin formation. At venous shear rate, fibrin generation was significantly more efficient under constant flow mode. However, at arterial shear rate, fibrin generation was diminished regardless of the flow modes. Under constant flow mode, reduced platelet deposition at arterial shear rate significantly delayed occlusion time. However, under pressure relief mode, there was no clear dependency of occlusion time on the degree of platelet deposition. Consistent with a previous study on TF bearing collagen surface, platelets tend to form plug at upstream of kaolin/collage patches at venous shear rate [24]. In contrast, a more homogenous platelet distribution with a heavy tail at the downstream region was observed at arterial shear rate (**Figure 2-8**). It is possible that under pressure relief mode, full channel occlusion is affected more by the spatial distribution of platelet mass on collagen matrix.

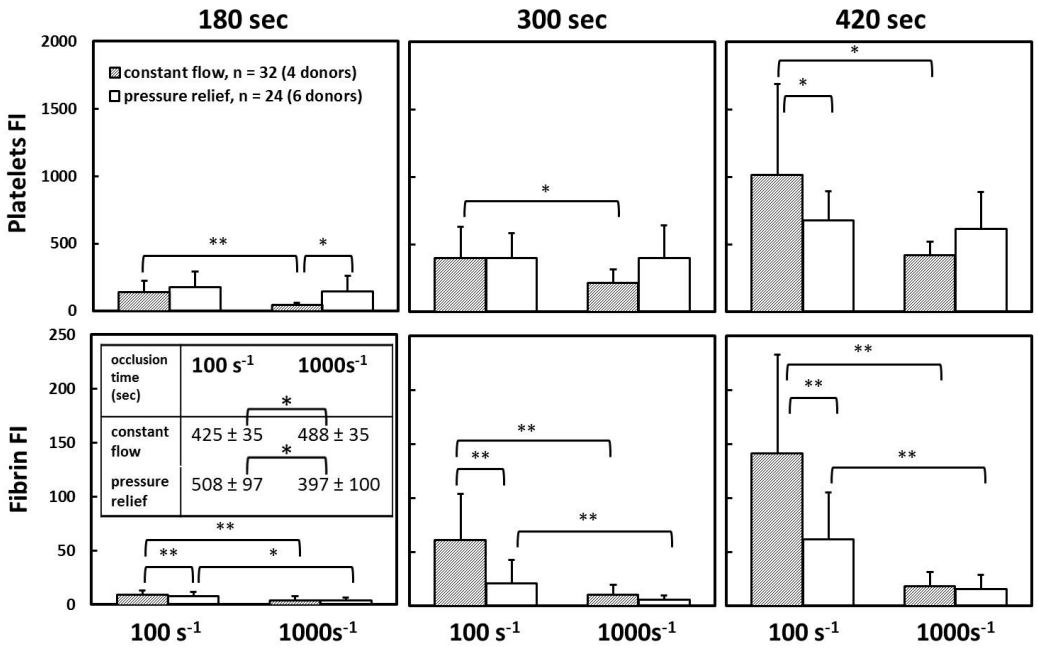

Figure 2-7 Average platelet and fibrin signal on collagen/kaolin surface at three representative time points.

Full channel occlusion times are included in an embedded table. Student's t-test was applied to compare the differences on platelet and fibrin signal and occlusion time under different flow conditions ($p<0.05$; **, $p<0.01$).

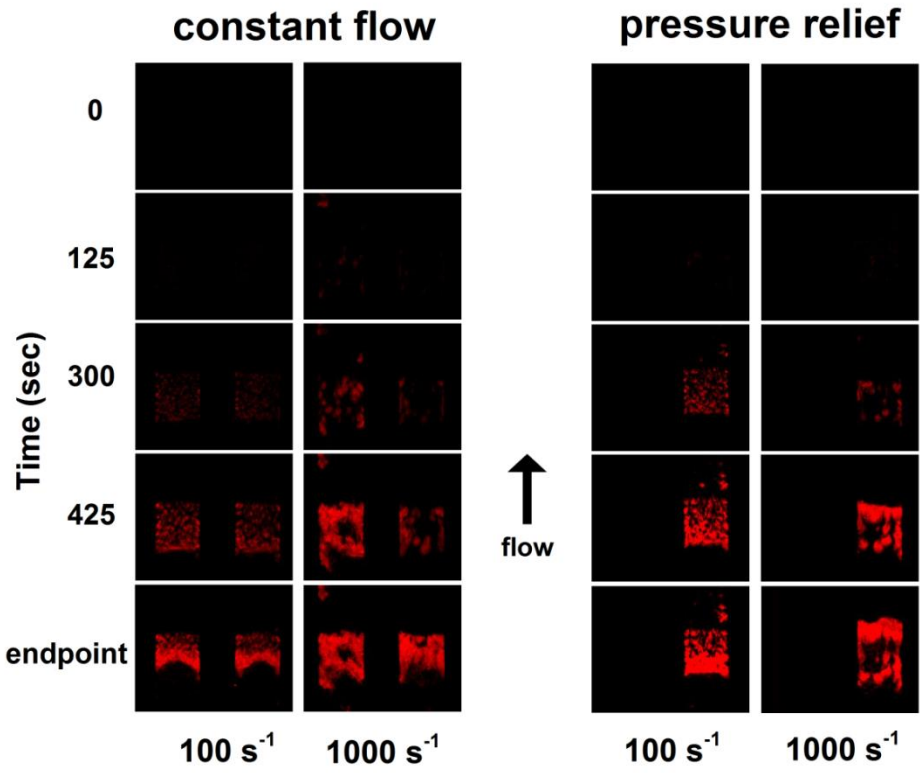

Figure 2-8 Platelet aggregation on collagen/kaolin surface.

Platelet (red) aggregation on kaolin/collagen surface at 5 representative time points under four flow conditions. Arrow indicates flow direction. Platelets tend to form plugs at front side of kaolin/collagen surface at low shear rate. High shear rate forced platelet mass downstream forming more elongated thrombi along the flow direction. Embolization or partial dislocation of thrombi was rarely seen under pressure relief mode since excessive pressure was released through the adjacent empty channels.

2.3.4 Kaolin/collagen vs. TF/collagen surfaces

We compared the flow sensitivity of contact activation with that of extrinsic activation by TF. To avoid thrombi embolization as they grew in the presence of thrombin generation, all dynamic data was obtained under pressure relief mode. TF was more efficient in terms of stimulating thrombin formation in well plate (**Figure 2-9**). A level of 2.3 pM TF induced faster thrombin generation than 0.78 mg/mL kaolin (comparable to concentration of kaolin suspension used for surface preparation). Under flow condition, platelet aggregation initiated slightly earlier on TF/collagen surface, but after the early phase (first 180 sec), platelet signal on kaolin/collagen and TF/collagen surface were statistically identical (**Figure 2-10A-B and Figure 2-11**). Fibrin formation was faster on TF/collagen surface at both venous and arterial shear rates. But at arterial shear rate, fibrin onset was substantially delayed and suppressed on both kaolin/collagen and TF/collagen surfaces (**Figure 2-10 C-D and Figure 2-11**). Interestingly, at arterial shear rate, final fibrin fluorescent intensity was statistically identical on two surfaces (**Figure 2-11**).

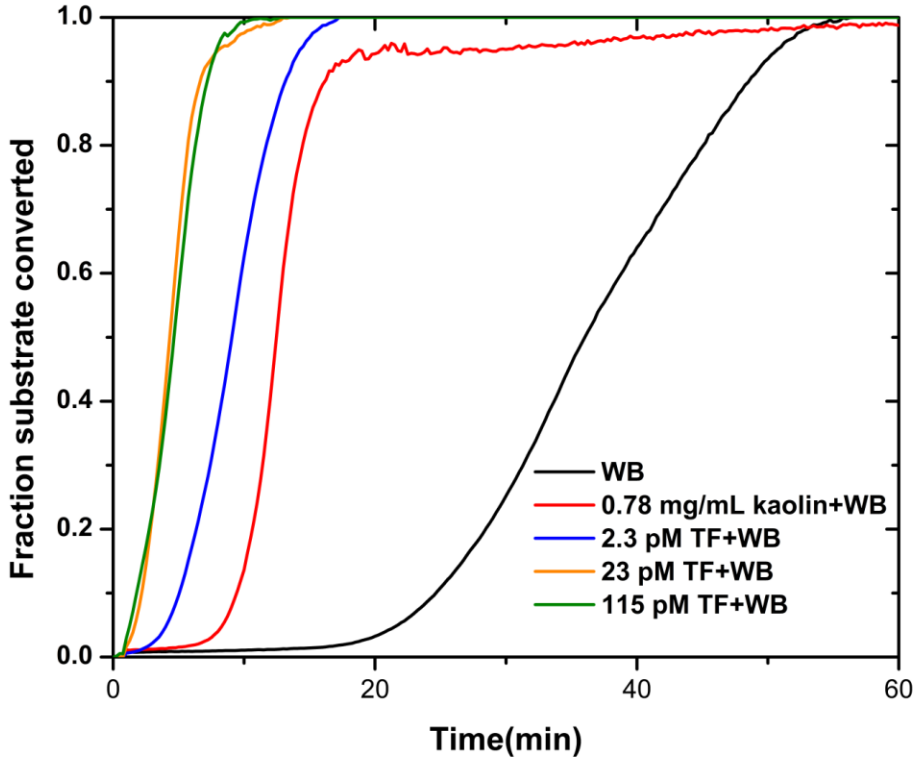

Figure 2-9 TF is more efficient in triggering WB clotting in well plate.

Citrate (1:9 WB) and CTI (4 µg/mL) treated whole blood (1:4 HBS) was recalcified (10 mM) right before measurements. Kaolin or diluted recombinant tissue factor was added to trigger either extrinsic or contact pathway. A thrombin specific fluorogenic substrate Boc-Asp(OBzl)-Pro-Arg-AMC was used to monitor the thrombin generation. Tissue factor induced faster thrombin generation.

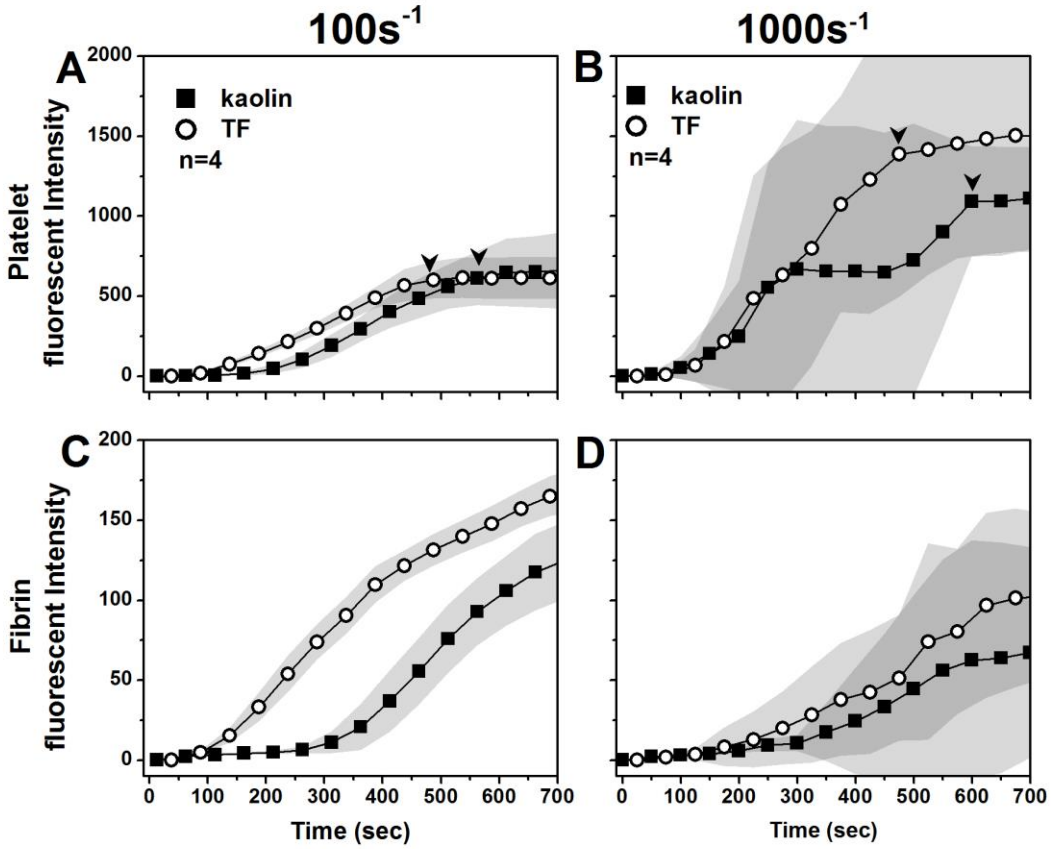

Figure 2-10 Dynamics of platelet deposition and fibrin formation on collagen/TF and collagen/kaolin at venous and arterial shear rates.

A-B, CTI-treated whole blood (4 μg/mL) was purfused over kaolin/collagen or TF/collagen surface at either venous ($100s^{-1}$) or arterial ($1000s^{-1}$) shear rate under pressure relief mode. No significant difference was observed in platelet mass growth on two surfaces. **C-D,** TF significantly accelerated fibrin generation at low shear rate (C) but not at high shear rate (black arrows indicate occlusion time).

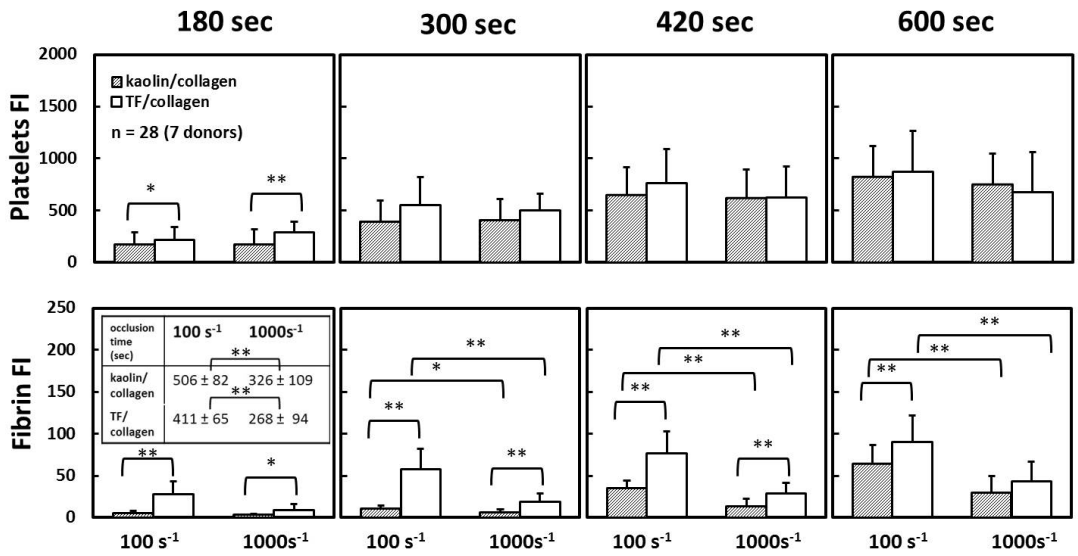

Figure 2-11 Averaged platelet and fibrin intensities on collagen/TF and collagen/kaolin surfaces at three representative time points.

No significant difference on platelet aggregation was seen on two surfaces after the first 180 sec. TF induced faster fibrin generation. However, at arterial shear rate, endpoint fibrin level was not significantly different on two surfaces. Full channel occlusion time points are included in an embedded table. T test was applied to compare the platelet and fibrin signal and occlusion time on two surfaces (*, $p<0.05$; **, $p<0.01$).

2.3.5 Pharmacological effect of antithrombotic therapies

Concentrations of antithrombotic therapies were either based on the dose level resulting in 50%-70% reduction in platelet aggregation in the flow assay (data not shown) or doses from previous studies [20]. MRS 2197 and 2-MeSAMP block P2-family $P2Y_1$ and $P2Y_{12}$ receptors, respectively [59, 60]. Both inhibitors showed robust inhibitory effect on platelet deposition (**Figure 2-12A-B**), which is consistent with previous observation in a similar microfluidic model lacking thrombin production [20]. Aspirin inhibits thromboxane A2 production by acetylating cyclo-oxygenase 1 (COX -1). 250 μM aspirin was required for significant reduction in platelet aggregation in this assay with thrombin generation. Thrombin and fibrin formation were also delayed with the presence of these three antiplatelet reagents. GSNO is a nitric oxide (NO) donor under physiological condition and had been known to inhibit platelet adhesion to collagen fibrils [61]. Iloprost, as a prostacyclin (PGI_2) analog, is an effective inhibitor of collagen-induced platelet aggregation [62, 63]. Both reagents resulted in significant delay in platelet aggregation as well as reduction in fibrin accumulation (**Figure 2-13A-D**). Thrombin level was lowered by both reagents but the effect of GSNO on thrombin was not statistical significant.

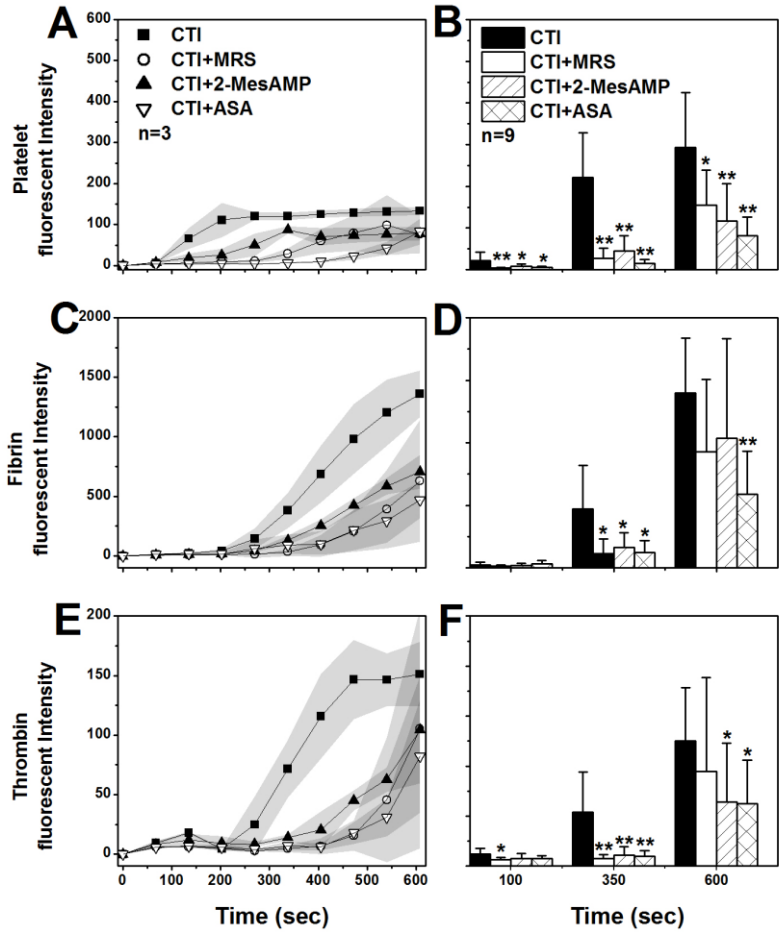

Figure 2-12 Effect of antiplatelet therapies on thrombus formation on collagen /kaolin surface.

Anticoagulated blood (CTI, 4μg/mL) was treated with MRS (10 μM), 2-MeSAMP (100 μM) or ASA (250 μM) right before experiment and perfused over kaolin/collagen surface at $1000s^{-1}$ under constant pressure mode. **A, C, E,** Dynamic changes of platelet aggregation, fibrin formation and thrombin generation on kaolin/collagen surface are based on a representative experiment (± STD, shaded). **B, D, F,** Averaged fluorescent intensities from three experiments for platelet, fibrin and thrombin are presented at three representative time points (*, $p<0.05$; **, $p<0.01$).

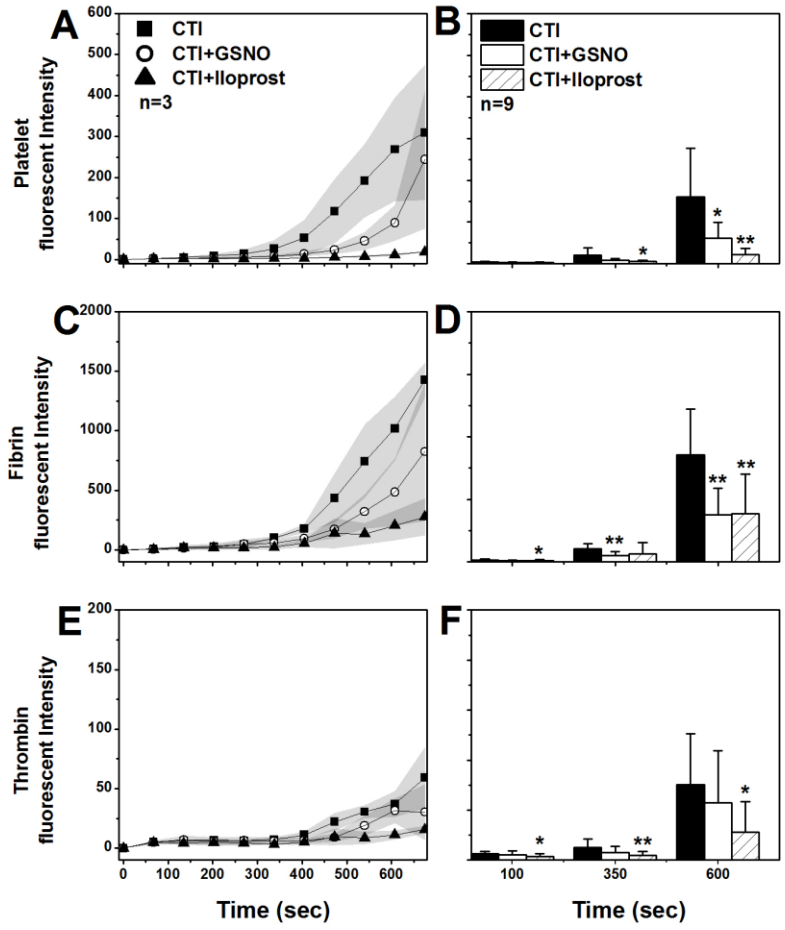

Figure 2-13 Effect of antiplatelet therapies on thrombus formation on collagen /kaolin surface.

Anticoagulated blood (CTI, 4μg/mL) was treated with Iloprost (5 nM) or GSNO (70 μM) right before experiment and perfused over kaolin/collagen surface at $1000s^{-1}$ under constant pressure mode. **A, C, E,** Representative dynamic changes of platelet, fibrin and thrombin on kaolin/collagen surface is based on a single experiment (± STD, shaded). **B, D, F,** Averaged fluorescent intensities from three experiments for platelet, fibrin and thrombin are presented at three representative time points (*, $p<0.05$; **, $p<0.01$).

2.4 Discussion

A surface was designed to activate contact pathway and allow for platelet capture. The activity of contact activation in this microfluidic assay was evaluated by initiation time and dynamics of platelet and fibrin deposition on kaolin/collagen surface. Additionally, collagen and platelets on their own can trigger the contact pathway [64]. However, Kaolin induced more efficient contact activation compare to collagen alone. Collagen stimulated platelets could enhance both coagulant activity and proteolytic cleavage of FXII and of FXI [65]. The presence of a medium level of kaolin (0.12 $pg/\mu m^2$) accelerated fibrin generation but did not interfere with platelet activation or platelet deposition on collagen. Fibrin generation was completely abolished by high dose of CTI (40 µg/mL) confirming the enhancement of fibrin generation by kaolin was FXIIa dependent (**Figure 2-14**). Inhibition of FXIIa accelerated thrombus embolization, which is consistent with our previous finding that fibrin deficient thrombus exhibits lower stability [24]. A direct comparison between FXII and FXI inhibition in a baboon model suggests FXI inhibition has more significant antithrombotic effect than FXII inhibition [66]. We've previously observed striking defects in both platelet and fibrin deposition when blood from severe hemophilia C patient was perfused over collagen [31]. A future comparison of FXII and FXI knockout in this assay would provide useful information for developing safe and effective antithrombotic therapy.

The prothrombotic effect of kaolin/collagen surface can be affected by different flow conditions. In this study, initial wall shear rate (100 s^{-1} and 1000 s^{-1}) and flow mode (pressure relief and constant flow) were the two variables in flow condition. A previous

reported COMSOL model showed that under constant flow mode, wall shear rate increases dramatically when thrombus approaches to full channel occlusion [24]. At arterial shear rate, fibrin formation was suppressed under both flow modes. High shear rate probably caused enhanced dilution of coagulation factors and inhibition of fibrin assembly. Our results suggested that at low shear condition when platelet plug forms at upstream side of kaolin/collagen patch, pressure driven convective transport of activated coagulation factors and fibrin monomers could aid coagulation reactions while at high shear condition excessive fast convection severely disturbed coagulation reactions.

We conclude that surface-linked kaolin can activate contact pathway under flow conditions but is not nearly as potent as insoluble particles added to a closed systems lacking flow. In the flow assay, TF/collagen surface triggered extrinsic pathway particularly well to allow fibrin generation, especially at venous shear rate. In well plate, TF was much more potent than kaolin in terms of stimulating thrombin generation. Compare to contact pathway, extrinsic pathway is also a much shorter reaction pathway leading to prothrombinase (FXa/FVa), which may contribute to the stronger potency of TF than kaolin under either static or flow condition.

Antithrombotic reagents targeting $P2Y_1$, $P2Y_{12}$, cyclooxygenase-1 or activating IP-receptor or guanylate cyclase were tested in the microfluidic model. To explore occlusive thrombus growth under flow in the presence of thrombin, tests were conducted at arterial wall shear rate and under pressure relief mode. All tested anti-platelet agents showed inhibitory effect on platelet deposition. Under flow condition, platelets could aid coagulation reactions by helping localizing coagulation proteins and providing required

phospholipid surface. Delay and reduction in thrombin and fibrin generation was observed as expected as platelet deposition was disturbed by antithrombotic reagents.

The role of FXII in coagulation has been investigated in several animal models. FXII-mediated fibrin formation contributes to thrombus stability in mouse models [38-40]. Antibodiy targeting heavy chain of FXII and antibody blocking FXI activation by FXIIa both reduces thrombus growth in baboon arteriovenous shunt thrombosis model [17, 66]. Knocking out FXIIa provides thromboprotection without increasing bleeding risk in an extracorporeal bypass system in rabbits under TF deficient condition wherein the thrombin generation is mainly driven by contact activation on non-physiological surface [67]. The role of FXII in thrombus formation in human is however not elucidated. Individuals with complete deficiency (<10%) of FXII is protected from myocardial infarction, whereas mild FXII deficiency (10-50%) increases the risk of myocardial infarction [68] indicating the effect of FXIIa is complicated and yet to be established when thrombus formation is initiated by extrinsic pathway. It's revealed in a recent study that extrinsic pathway prompts the initial pathological thrombosis formation whereas FXIIa promotes the stability of thrombi in later phase [69] suggesting the complementary roles extrinsic and contact pathway played in pathological thrombosis. Here we are, as the first to explore the activity of contact pathway under controlled flow and defined surface conditions in the presence of anti-platelet agents. It is a potential interest to incorporate TF into the microfluidic assay and study the activity of contact pathway with TF exposure.

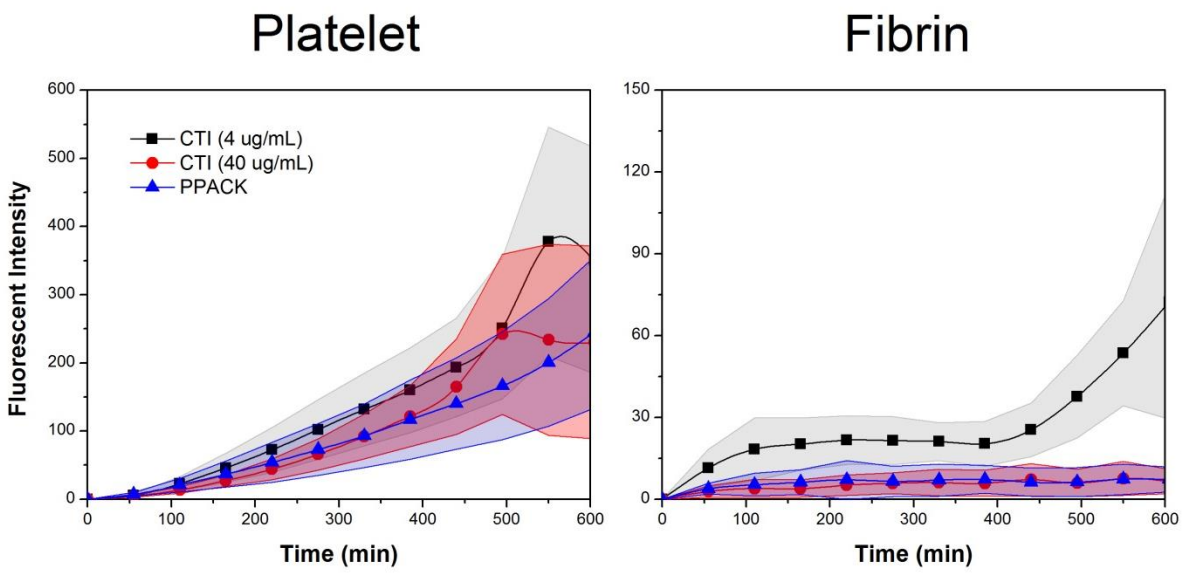

Figure 2-14 Inhibition of fibrin formation on collagen/kaolin surface by high CTI or PPACK.

Platelet deposition and fibrin generation on kaolin/collagen surface with blood treated with CTI (4 and 40 μg/mL) and PPACK (100 μM). The kinetic data was obtained at venous shear rate under constant flow mode.

2.5 Conclusions

The primary goal of this study was to develop a microfluidic model that can be used to assess the activity of contact pathway under flow conditions. Our approach was to bind kaolin to collagen, thus forming a substrate that can simultaneously induce contact activation and platelet activation/binding. Perfusion of whole blood over the kaolin/collagen surface in microfluidic flow chamber allowed observation of thrombus structure, specifically platelets and fibrin formation on the surface. Instead of directly measuring the bulk level of FXIIa, we evaluated the activity of contact pathway by dynamic change of platelet and fibrin, as they have the critical effects on thrombus structure. Fibrin formed distal of FXIIa was subject to reduced assembly at arterial flow conditions. We found that TF-triggered extrinsic pathway is more potent than kaolin initiated contact pathway in terms of stimulating thrombin formation under both static and low shear condition, but both surfaces showed a similar sensitivity to high shear rate despite different pathways they triggered. This microfluidic assay was also sensitive to inhibitory effect of antithrombotic therapies targeting $P2Y_1$, $P2Y_{12}$, cyclooxygenase-1 or activating IP-receptor or guanylate cyclase. The sensitivity of this microfluidic assay to antithrombotic drugs makes it a good candidate for potential drug screening tests and clinical diagnostic assays of antithrombotic therapy targeting contact pathway.

Chapter 3 : FXIa and platelet polyphosphate as therapeutic targets during human blood clotting on collagen/tissue factor surfaces under flow

3.1 Introduction

Many anticoagulants target prothrombinase formation or thrombin, but can be associated with bleeding risks.[11, 70] Reducing thrombotic risk without effect on normal hemostasis may require targeting factors that promote thrombus propagation and stability.[71] The contact pathway is not essential for hemostasis since factor XII (FXII) deficiency is not associated with a bleeding phenotype and factor XI (FXI)-deficient (hemophilia C) patients display a relatively mild bleeding disorder.[41] The prothrombotic function of FXII and FXI has been demonstrated in several animal vessel injury models.[38, 69, 72-80] Additionally, platelet derived polyphosphate (polyP, ~ 60-70mer) has recently been identified as a weak FXII activator[81] that also promotes the feedback activation of FXI by thrombin,[82] FV activation by FXIa, FXa, or thrombin[83, 84] and enhances fibrin physical structure.[85, 86] Also, cationic inhibitors of polyP reduce venous and arterial thrombosis in animal injury models.[87] These observations suggest that the contact pathway is a potential source of therapeutic targets for safer antithrombotic therapies.[88] Distinct from animal models, testing inhibitors of FXIa and polyP in human blood under thrombotic flow conditions helps to prioritize and inform inhibitor development against these targets. Importantly, platelet concentrations in wall-attached thrombi forming under flow are 50 to 200-fold greater than those found in whole blood, a complexity that distinguishes microfluidic flow studies from test tube studies.[20, 24, 89]

Recently, a Phase 2 trial demonstrated that FXI-antisense oligonucleotide (FXI-ASO) reduced FXI levels and decreased the incidence of deep vein thrombosis (DVT) after knee arthroplasty without increasing bleeding, thus providing evidence that FXIa can contribute to thrombosis in humans.[90] However, postoperative bleeding in knee arthroplasty is relatively uncommon and the rate of bleeding with FXI-ASO was not significantly lower than that seen with enoxaparin.[91, 92] The FXI-ASO trial demonstrates a role for FXIa in DVT, but does not resolve the role of either platelet polyP or FXIIa in post-arthroplasty DVT since FXIa can inactivate tissue factor pathway inhibitor (TFPI)[93] and FXI can be feedback-activated by thrombin.[94] During knee arthroplasty, FXIIa may (or may not) be activated by polyP, DNA/histones, RNA, sulfatides, or other factors.[95]

We used a microfluidic assay of platelet deposition and coagulation on a type I fibrillar collagen/lipidated tissue factor (TF) surface that can trigger thrombin generation via the contact pathway and/or extrinsic pathway.[12, 24] We utilized two distinct monoclonal anti-FXI antibodies, 14E11 and O1A6, to explore the role of FXI in contact activation and in promoting thrombin amplification. 14E11 selectively inhibits FXI activation by FXIIa but not FXI activation by thrombin, and O1A6 interferes with both FXI activation by FXIIa and FIX and FV activation by FXIa.[17-19] O1A6 does not directly inhibit FXI activation by thrombin but disrupts FXIa dependent thrombin amplification mechanism by inhibiting FIX activation by FXIa, which is the downstream reaction of FXI feedback activation in the thrombin feedback loop. By use of low level corn trypsin inhibitor (CTI, 4 μg/mL), the contact pathway contributions can be studied in whole blood *in vitro* without the overwhelming dominance of the "container." With 4

μg/mL CTI, drawn blood does not clot in the reservoir during the experiment but will generate thrombin via FXIIa in ~300 sec when perfused over collagen or surface-linked contact activators.[12] We investigated the role of platelet-derived polyP in promoting thrombin generation and enhancing fibrin structure and clot stability by inhibiting polyP with PPXbd, the recombinant polyP-binding domain of *E. coli* exopolyphosphatase (IC_{50}, 8.5 μg/mL).[82, 87] This microfluidic data with human blood demonstrated specific conditions when FXIa and platelet polyP play a kinetically significant role in clotting under flow conditions that can be targeted with inhibitors.

3.2 Methods

3.2.1 Materials

Reagents were obtained as follows: DBCO-*Sulfo*-NHS Ester (Click Chemistry Tools, Scottsdale, AZ, USA), azide free anti-human CD61 antibody (BioLegend, San Diego, CA, USA), annexin V-FITC, anti-human CD41a, antibody anti-human CD61 antibody (BD Biosciences, San Jose, CA, USA), Alexa Fluor 647 conjugated human fibrinogen (Life Technologies, Grand Island, NY, USA), corn trypsin inhibitor (CTI, Haematologic Technologies, Essex Junction ,VT, USA), Dade® Innovin® PT reagent (Siemens, Malvern, PA, USA), collagen (type I, Chrono-log, PA, USA), recombinant human tissue plasminogen activator (tPA, abcam, MA, USA), ethylenediaminetetraacetic acid (EDTA), grade I glutaraldehyde, sodium cacodylate, hexamethyldisilane (sigma, St. Louis, MO, USA) and H-Gly-Pro-Arg-Pro-OH (GPRP, EMD Chemicals, San Diego, CA, USA). The murine anti-human FXI monoclonal antibodies O1A6 and 14E11 were gifts from Dr. Andras Gruber (Oregon Health & Science University). Polyphosphate binding

protein (PPXbd) was prepared as described in the supplemental material.[82] A custom made thrombin sensitive peptide *azidoacetyl-AK(5FAM)-GALVPRGSAGK(CPQ2)-NH2* was obtained from CPC scientific (Sunnyvale, CA, USA) for click reactions to anti-CD61 as previously described.[55]

3.2.2Preparation and characterization of collagen/TF surface

Glass slides were rinsed with ethanol followed by deionized water and dried with filtered air. A volume of 5 μL collagen was perfused through the patterning channel (250 μm wide x 60 μm high) of a microfluidic device to create a single stripe of fibrillar collagen as previously described.[22] Lipidated TF was then sorbed to the collagen surface by introduction of 5 μL of Dade® Innovin® PT reagent (20 nM stock concentration)[96] diluted 300, 100, and 5-fold with HEPES buffered saline to obtain low, medium, and high $[TF]_{wall}$ surface densities of ~0.1, ~0.2, and ~2 molecule-TF/μm^2, respectively, as estimated by imaging of sorbed FITC-annexin V-stained vesicles (Fig. S1). In all experiments, the PT reagent was incubated with the collagen for 30 min without flow, followed by rinsing and blocking with 20 μL bovine serum albumin (0.1% BSA) buffer.

3.2.3 Blood collection and preparation

Blood was obtained via venipuncture into CTI (4 μg/mL) from healthy donors who self-reported to be free of alcohol use and medication for at least 72 hours prior to blood collection. In some experiments, blood was collected without the use of CTI. All donors provided informed consent under approval of University of Pennsylvania

Institutional Review Board. Blood was treated with anti-FXI antibodies or PPXbd immediately after blood collection. Platelets were labeled with anti-human CD61 antibody (or anti-human CD41a antibody when thrombin was measured with the platelet targeting sensor). Fluorescent fibrinogen was added (1 mg/mL stock solution, 1:80 v/v% in whole blood) for the measurement of fibrin generation. All experiments were initiated within 5 min after phlebotomy.

3.2.4 Microfluidic clotting assay on collagen/±TF surface

An eight channel PDMS (polydimethylsiloxane) flow device was vacuum-mounted perpendicularly to collagen/TF surfaces forming eight parallel spaced prothrombotic patches (250 × 250 μm) as previously described.[20] Treated blood was perfused across the 8 channels by withdraw through a single outlet. Initial wall shear rate was controlled by a syringe pump (Harvard Apparatus PHD 2000, Holliston, MA) connected to the outlet on the flow device. Thrombi were formed either under constant flow rate (constant Q, CTI treated blood in all 8 channels) or under constant pressure drop (constant ΔP) condition.[24] To achieve constant ΔP, EDTA-treated blood was delivered into alternating channels to abolish thrombus formation, thus allowing CTI-treated blood to clot and divert flow into the matched EDTA channels. Experiments with added recombinant tPA were conducted under constant ΔP to avoid clot embolism before acquiring fibrinolysis profiles. Platelet, fibrin and/or thrombin activity were monitored simultaneously by epifluorescence microscopy (IX81, Olympus America Inc., Center Valley, PA, USA). Images were captured with a CCD camera (Hamamatsu, Bridgewater,

NJ, USA) and were analyzed with ImageJ (NIH). To avoid side-wall effects, fluorescence values were only taken from the central 75% of the channel.

3.2.5 Preparation of PPXbd

A synthetic gene containing the AviTag biotin acceptor peptide (Epoch Life Sciences) was cloned into a previously described PPXbd plasmid [97] using NcoI and XbaI. This plasmid was transfected into BL21-D3 cells (New England Biolabs). PPXbd production was induced overnight at 15°C by the addition of 400 μM (final concentration) IPTG to cells growing in NYZ media. The cells were then pelleted and lysed, and PPXbd was purified on amylose resin (New England Biolabs).

3.2.6 Determination of TF surface concentrations

Collagen-adherent relipidated TF (Dade® Innovin® PT reagent) was visualized by annexin V staining (**Figure 3-1**). Surface TF concentration ($[TF]_{wall}$) was estimated by measuring the percent stained surface area and converting it to $[TF]_{wall}$ based on the random packing limit of 200 molec-TF/μm^2 (see detailed calculation below).

Liposome radius (r) was 118 ± 14 nm (measured by dynamic light scattering). The projected area of single liposome is $\pi r^2 \approx 14000\pi$ nm^2. Assume all the liposomes are perfect spheres with radius of 118 nm and are densely packed in a hexagonal packing manner with a packing density of 0.9069, the packing limit was found to be about 21 liposomes/μm^2 (Eqn. 1).

$$1 \times 0.9069 \mu m^2 \times \frac{liposome}{43982 nm^2} \times \frac{10^6 nm^2}{\mu m^2} \approx 21 \frac{liposome}{\mu m^2} \qquad \text{Eqn. 1}$$

We assume on average, 20 TF molecules are incorporated into a single liposome and 50% of the incorporated liposomes are exposing their extracellular domain to the bulk solution.[23, 24] The saturated TF surface concentration was then found to be about 200 TF-molecule/μm^2. Surface coverage (x%) of TF liposomes was measured from annexin V staining. Since the 2D packing limit of the liposomes is known to be 90.69%, the percentage of stained area in packing limit can be calculated (x/90.69 %). This percentage can be used to calculate the corresponded liposome (Eqn. 2) and TF surface concentration (Eqn. 3).

$$\text{liposome surface concentration} = 21\frac{liposome}{\mu m^2}\times\frac{x}{90.69} \qquad \text{Eqn. 2}$$

$$\text{TF surface concentration} = 200\frac{TF-molecule}{\mu m^2}\times\frac{x}{90.69} \qquad \text{Eqn. 3}$$

The estimated concentrations are listed in **Table 3-1**. Based on the estimation, we made nominal estimations that $[TF]_{wall}$ = ~0.1 molec-TF/μm^2, ~0.2 molec-TF/μm^2, and ~2 molec-TF/μm^2 for low, medium and high $[TF]_{wall}$, respectively.

3.2.7 Scanning electronic microscopy

In some experiments, thrombi were fixed under flow *in situ* with 2% Grade I glutaraldehyde in HBS buffer. The glass slides were then removed from the PDMS device and the fixed thrombi were washed 6 times in 0.2 M sodium cacodylate, incubated in sodium cacodylate overnight at 4℃, dehydrated in graded ethanol (with balance of sodium cacodylate), rinsed with hexamethyldisilane, air dried, and sputter coated with gold/palladium. Samples were imaged with Quanta 600 FEG Mark II scanning electron microscope equipped with Schottky field emission electron gun. Thickness of fibrin

fibers was averaged across measurements (Image J, NIH) from 40 random selected fibers in images captured at 3500x magnification.

3.2.8 Statistical analysis

Difference between control and treated groups was analyzed with Student's t-test. The difference was considered significant when p-value is smaller than 0.05.

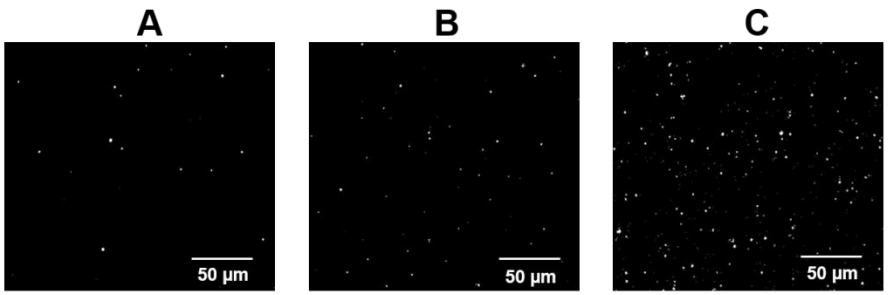

	Low TF	Medium TF	High TF
Surface coverage (%)	0.045 ± 0.017	0.083 ± 0.026	0.797 ± 0.385
Liposome/area (liposome/ μm^2)	0.010 ± 0.004	0.019 ± 0.006	0.185 ± 0.006
TF-molecule/area (TF-molec/ μm^2)	0.099 ± 0.037	0.183 ± 0.057	1.758 ± 0.849
Nominal	**~ 0.1**	**~ 0.2**	**~ 2**

Figure 3-1 Annexin V staining of TF liposomes on collagen surface.

Stained liposomes appear as white dots. Measured surface coverage was used to estimate surface concentration at low, medium and high $[TF]_{wall}$. Nominal $[TF]_{wall}$ were assigned for different TF levels based on the estimations.

	Low (300x dilution)	**Medium (100x dilution)**	**High (5x dilution)**
Measured surface coverage (%)	0.045 ± 0.017	0.083 ± 0.026	0.797 ± 0.385
Liposome/area (liposome/ μm^2)	0.010 ± 0.004	0.019 ± 0.006	0.185 ± 0.006
TF-molecule/area (TF-molec/ μm^2)	**0.099 ± 0.037**	**0.183 ± 0.057**	**1.758 ± 0.849**

Table 3-1 Estimated TF surface concentration.

TF surface concentrations were estimated based on the surface coverage by lipid liposomes measured with annexin V staining.

3.3 Results

3.3.1 Contact pathway was indispensable for thrombin generation on collagen surface

Both anti-FXI antibodies, 14E11 and O1A6, were tested individually in whole blood (20 μg/mL) perfused at a venous wall shear rate of 100 sec^{-1} over a collagen surface (no $[TF]_{wall}$). Perfusion of whole blood (treated only with 4 μg/mL CTI) without antibodies resulted in immediate and rapid platelet accumulation with thrombin and fibrin production detected after 300 sec of perfusion. Both antibodies had minimal effect on platelet deposition, which is driven by the collagen and platelet-derived secondary aggregation mediators ADP and thromboxane.[28] Both antibodies caused complete inhibition of thrombin generation and fibrin formation (**Figure 3-2**). In the presence of low level of CTI, the contact pathway was required as the most proximal trigger of thrombin production as demonstrated by the inhibitory activity of 14E11 and O1A6. This result is consistent with prior observations made with whole blood from a patient with a severe FXI deficiency.[31] Furthermore, in an experiment with raw blood (no CTI) which allows for rapid and massive thrombin and fibrin formation through unrestricted FXIIa generation, 14E11 substantially delayed clotting (**Figure 3-3**). Since addition of CTI and 14E11 together (**Figure 3-2 and Figure 3-3 C-D**) prevented thrombin and fibrin formation, the presence of bloodborne tissue factor can be excluded.

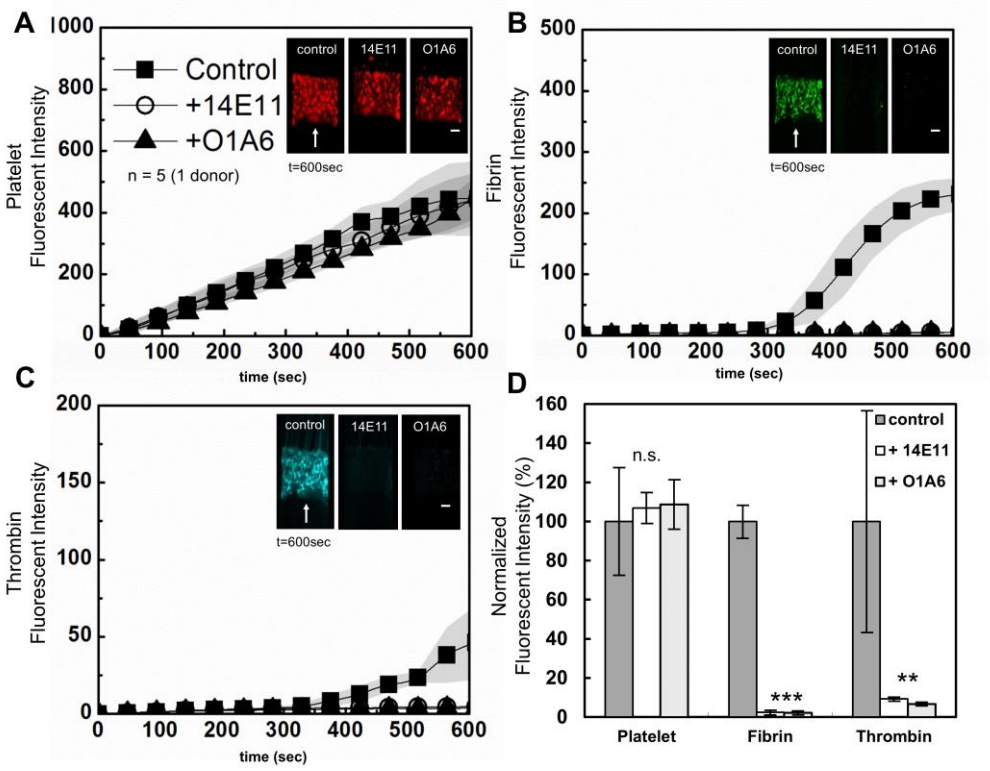

Figure 3-2 14E11 and O1A6 individually block thrombin/fibrin generation on collagen.

Anticoagulated whole blood (CTI, 4 μg/mL) was treated with FXI antibody 14E11 or O1A6 (20 μg/mL) and was perfused over collagen surface at 100 s^{-1} under constant flow rate condition (Q = constant). FXI antibodies efficiently abolished thrombin and fibrin generation on collagen surface without affecting platelet deposition. **A-C,** Dynamics of platelet deposition, and generation of fibrin and thrombin based on 5 clotting events (± SD, shaded). Endpoint images (t = 600 sec) of platelet (red), fibrin (green) and thrombin (cyan) on collagen surface are embedded in corresponded subgraphs (white arrows indicate flow direction, scale bar = 50 μm). **D,** Final platelet, fibrin and thrombin fluorescence (t = 600 sec) was normalized to control. Adding FXI antibodies caused over 90% reduction in final fibrin and thrombin generation. (**, $p < 0.01$; ***, $p < 0.005$)

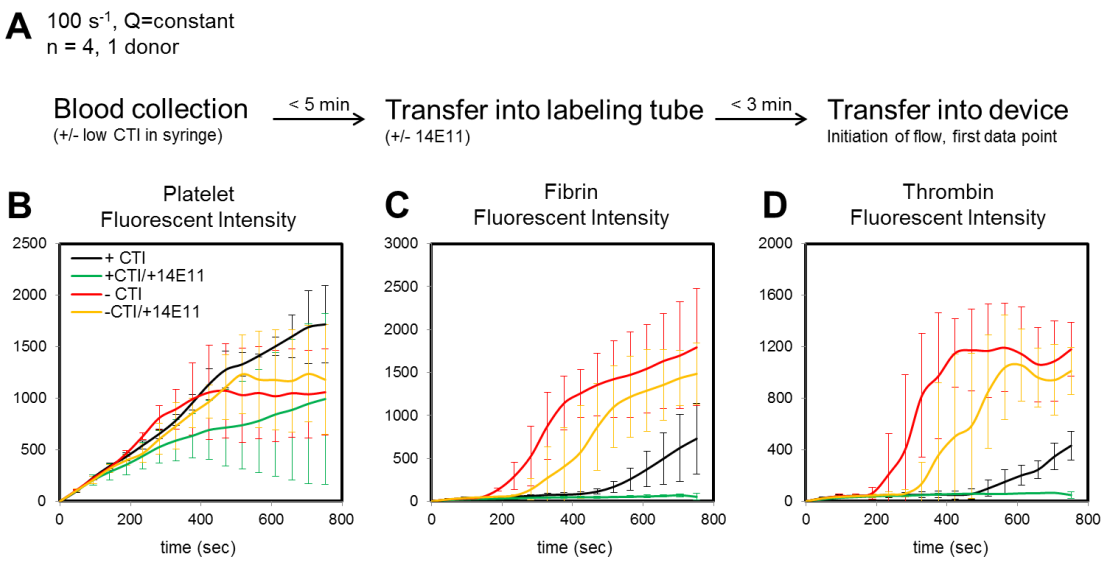

Figure 3-3 Low level of CTI is required for blocking XIIa generation in reservoirs.

A, Blood was collected into syringe with or without CTI (± 4 μg/mL) and was transferred into labeling tubes supplemented with or without 14E11 (± 20 μg/mL) to create 4 anticoagulated conditions. Treated blood was then perfused over collagen surface at 100 s^{-1} (Q = constant). **B-D,** Platelet, fibrin and thrombin dynamic curves were generated based on 4 clotting events. Adding 14E11 to collected non-anticoagulated blood only partially blocked thrombin generation indicating massive and rapid XIIa generation during blood collection. When blood was collected into low CTI, FXIIa generation in reservoir was minimized and the lag-phase before measurable thrombin/fibrin generation was prolonged. 14E11 completely blocked thrombin/fibrin generation in low CTI treated blood.

3.3.2 14E11 and O1A6 inhibited thrombin generation at low $[TF]_{wall}$

Regardless of $[TF]_{wall}$, platelet deposition on collagen/TF surfaces was not affected by 14E11 or O1A6 over the first 420 sec (**Figure 3-4 A-C**). By 500 sec, most of the formed thrombi were partially or fully occlusive and subject to large hemodynamic forces that drove embolization. The lag phase before detectable fibrin formation was < 100 sec on collagen/high $[TF]_{wall}$, and this lag time was prolonged as $[TF]_{wall}$ was decreased (**Figure 3-4 D-F**). As $[TF]_{wall}$ increased, the amount of fibrin produced by 7 min also increased. At low $[TF]_{wall}$ ~0.1 molecule-TF/μm^2, fibrin formation was detectable at ~ 240 sec and was significantly reduced by both 14E11 or O1A6 at times between 300 and 400 sec (**Figure 3-4 D**). O1A6 maintained its ability to inhibit fibrin generation up to medium $[TF]_{wall}$ ~0.2 molecule-TF/μm^2. However, at high $[TF]_{wall}$, fibrin formation was not affected by 14E11 or O1A6.

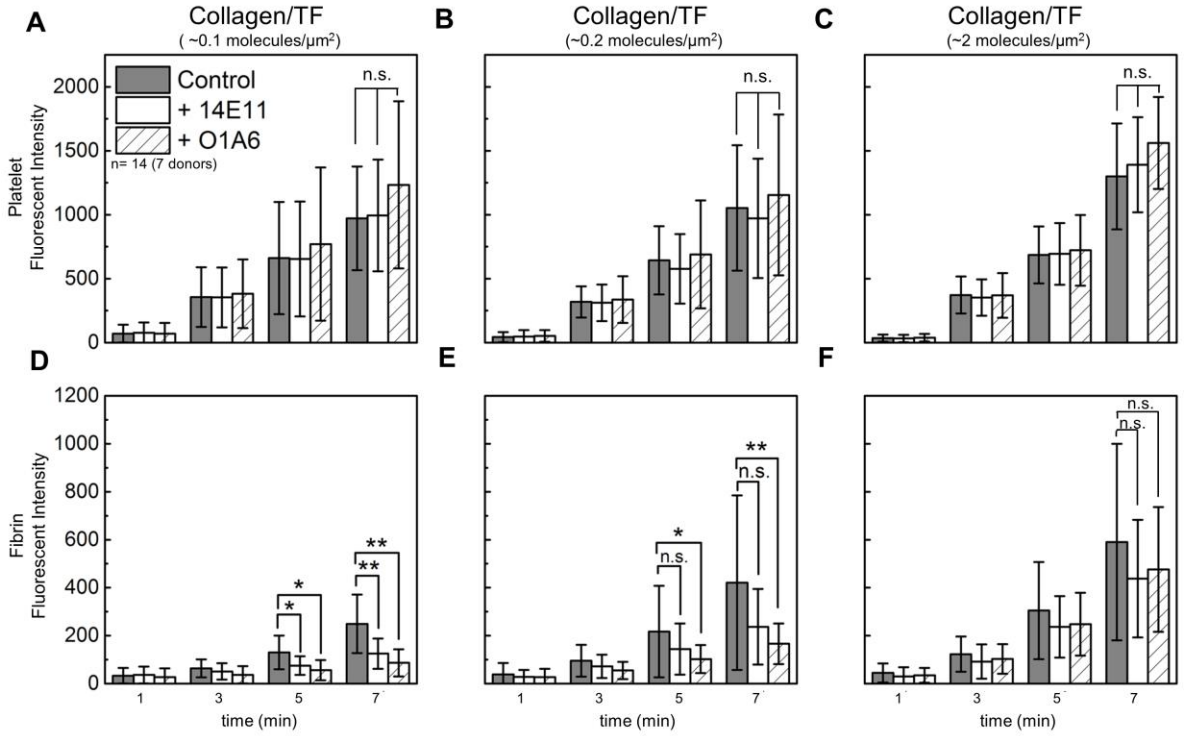

Figure 3-4 Potency of 14E11 and O1A6 varies depending on $[TF]_{wall}$.

Anticoagulated whole blood (CTI, 4 μg/mL) was treated with FXI antibody 14E11 or O1A6 (20 μg/mL) and was perfused over collagen/TF surfaces at 100 s^{-1} (Q = constant). **A-C,** Platelet deposition on collagen was unaffected by FXI antibodies despite the difference in $[TF]_{wall}$. **D, E,** O1A6 showed inhibitory effect on fibrin generation at low and medium $[TF]_{wall}$. 14E11 only reduced fibrin generation at low $[TF]_{wall}$. **F,** Neither of the antibodies caused reduction in fibrin at high $[TF]_{wall}$. (*, $p < 0.05$; **, $p < 0.01$)

3.3.3 PPXbd inhibited fibrin generation on collagen/low $[TF]_{wall}$ surface at venous shear rate

Under conditions of constant flow rate, PPXbd (250 μg/mL) was tested on collagen/TF at the inlet venous shear rate (100 s^{-1}) using whole blood with CTI (4 μg/mL). Platelet aggregation remained unaffected when platelet-derived polyP was inhibited with PPXbd (**Figure 3-5 A-C**), consistent with platelet deposition being largely driven by collagen and released mediators or secondary aggregation. Measurable fibrin accumulation on collagen surface alone (no TF) did not appear until 400 sec (**Figure 3-5 D**) and was less than that observed on collagen/TF surfaces. PPXbd did not reduce fibrin formation on a pure collagen surface, indicating that other triggers were more prominent activators of the contact pathway than platelet-derived polyP. This is consistent with the relatively low activity of small forms of platelet-derived polyP to activate FXII.[98] With TF on the surface, PPXbd reduced fibrin formation at low $[TF]_{wall}$ but this inhibition was not detectable at high $[TF]_{wall}$ (**Figure 3-5 E-F**). This experiment defines a specific condition in which endogenous platelet polyP leads to enhanced fibrin production under a condition of low extrinsic pathway activation. Similarly, for a condition where FXII activation could proceed unimpeded, perfusion of raw blood (no CTI) resulted in rapid and massive platelet and fibrin deposition that was unaffected by PPXbd (**Figure 3-6**).

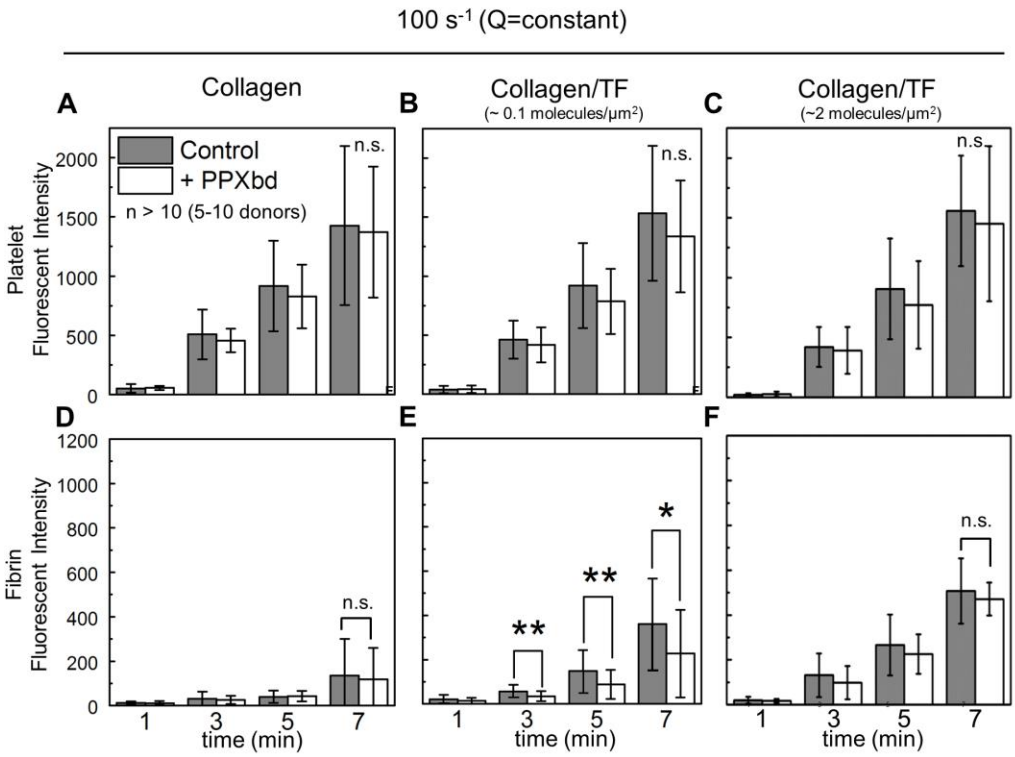

Figure 3-5 PPXbd inhibits fibrin generation at low $[TF]_{wall}$ under venous condition.

Anticoagulated whole blood (CTI, 4 μg/mL) was treated with PPXbd (250 μg/mL) and was perfused over collagen or collagen/TF surface at 100 s^{-1} (Q = constant). **A-C,** Platelet deposition on collagen was unaffected by PPXbd despite the difference in $[TF]_{wall}$. **D-F,** Fibrin generation was only inhibited by PPXbd on collagen/low $[TF]_{wall}$ surface but not on collagen or collagen/high $[TF]_{wall}$ surface. (*, $p < 0.05$; **, $p < 0.01$)

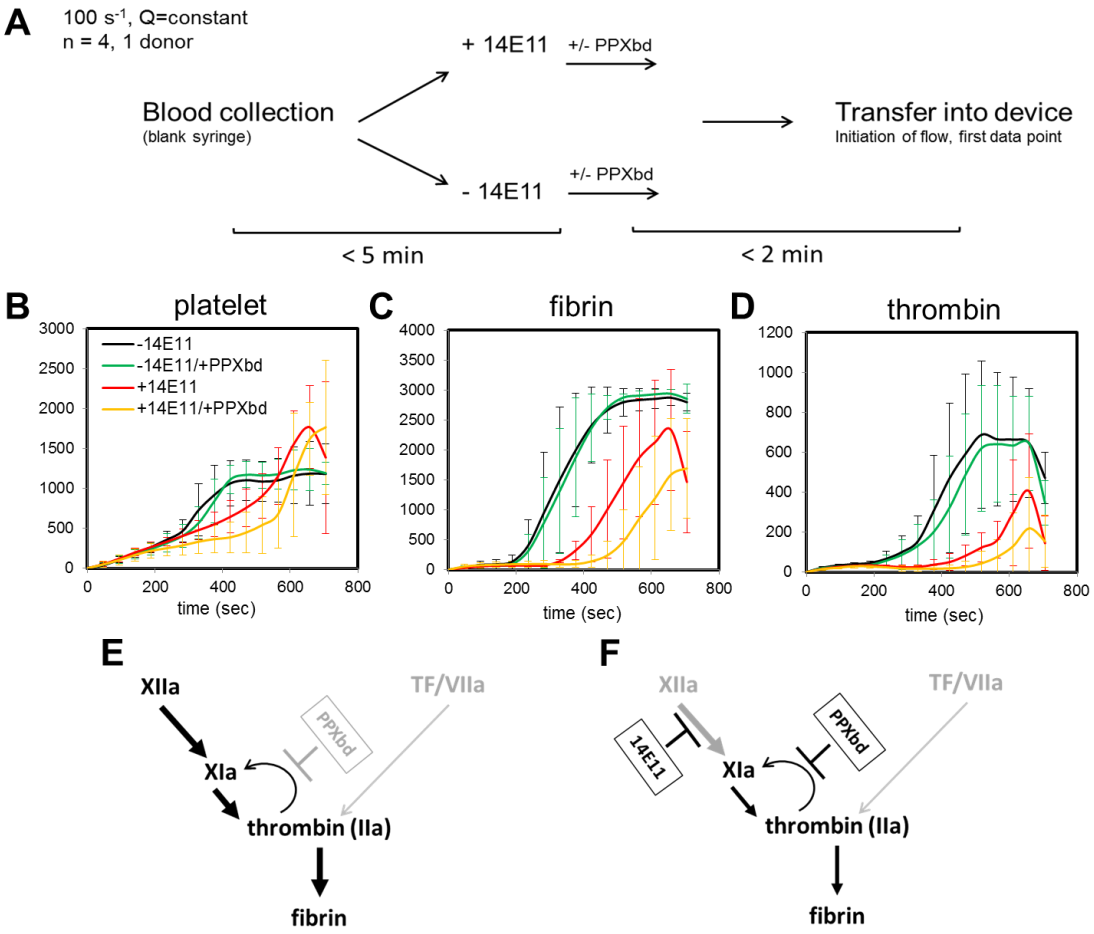

Figure 3-6 Massive XIIa dependent thrombin generation masked the effect of PPXbd.

A, Non-anticoagulated blood was collected and was transferred into labeling tubes in which 14E11 (20 μg/mL) and/or PPXbd (250 μg/mL) were added to create 4 anticoagulated conditions. Treated blood was then perfused over collagen surface at 100 s^{-1} (Q = constant). **B-D,** Platelet, fibrin and thrombin dynamic curves were generated based on 4 clotting events. **E,** Without adding 14E11, XIIa generation during blood collection and in reservoirs lead to fast and massive thrombin/fibrin formation and masked the effect of PPXbd. Adding 14E11 minimized XIIa generation in reservoirs but allowed XIIa generated during blood collection to prime thrombin feedback loop. **F,** The effect of PPXbd was detectable under this condition.

3.3.4 PPXbd inhibited thrombin and fibrin generation on collagen/low $[TF]_{wall}$ surface at arterial shear rate

Since animal studies have supported a role for the contact pathway during arterial thrombosis, we tested PPXbd at arterial shear rate (1000 s^{-1}) under constant pressure drop conditions where occlusive clots can stop flow.[24] Thrombi were formed on collagen or collagen/low $[TF]_{wall}$ in the presence and absence of PPXbd. Consistent with the observation under venous condition, platelet deposition was not significantly altered by polyP inhibition (**Figure 3-7A-B**). As was seen for venous conditions, PPXbd had no significant effect on platelet, thrombin, or fibrin accumulation for clotting of blood on pure collagen (no TF) at an arterial shear rate (**Figure 3-7A, C, E**). PPXbd inhibited thrombin and fibrin by 54% ($p = 0.012$) and 70% ($p = 0.037$) on collagen/low $[TF]_{wall}$ ~0.1 molecule-TF/μm^2 (**Figure 3-7D, F**). The reduction in thrombin signal became significant after 300 sec (**Figure 3-7E, F**). Under this flow condition, occlusive thrombi were observed at around 400 sec into experiment on collagen/low $[TF]_{wall.}$ Simply decreasing $[TF]_{wall}$ to zero did not cause reduction in the time to full channel occlusion. Delayed occlusive thrombi were only observed when polyP was inhibited at no $[TF]_{wall}$ (**Figure 3-8**).

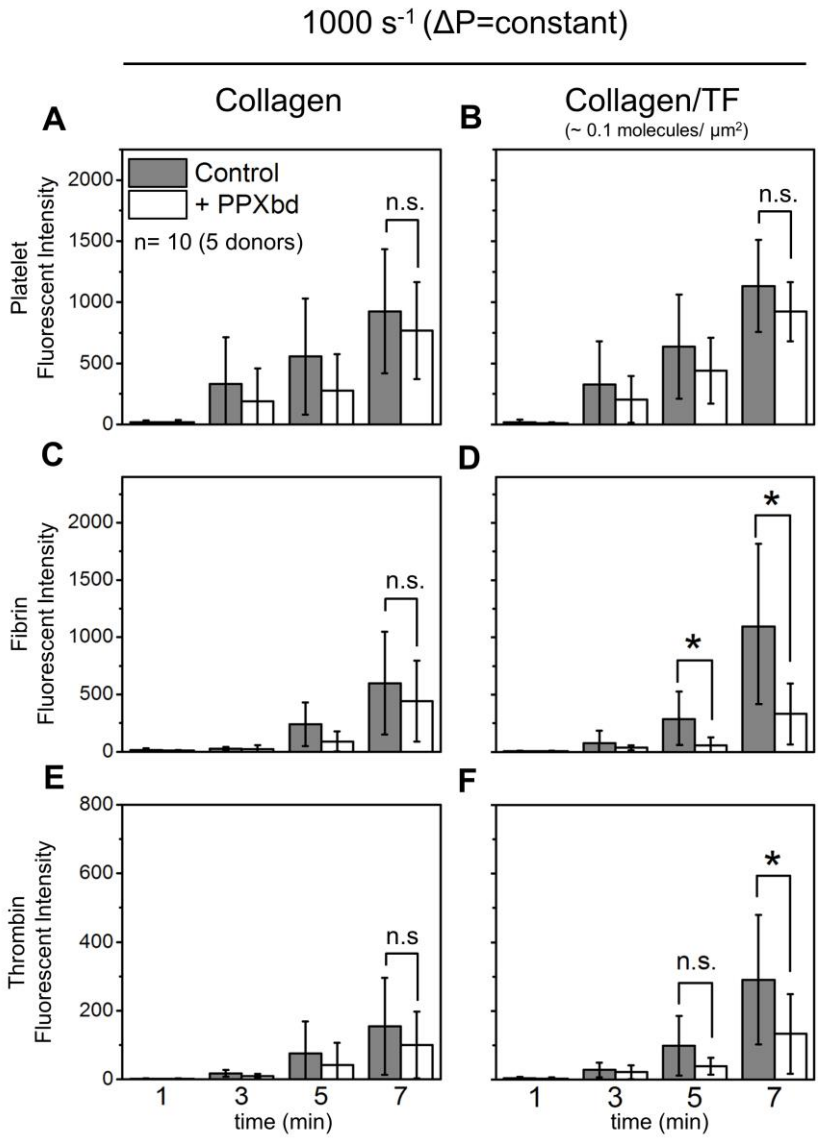

Figure 3-7 PPXbd inhibits fibrin and thrombin generation on collagen/low $[TF]_{wall}$ at arterial shear rate.

Anticoagulated whole blood (CTI, 4 μg/mL) was treated with PPXbd (250 μg/mL) and was perfused over or collagen or collagen/low $[TF]_{wall}$ surface at 1000 s^{-1} under constant pressure drop condition (ΔP = constant). **A, B,** Platelet deposition on collagen was unaffected by PPXbd. **C, D,** Fibrin generation was inhibited by PPXbd on collagen/low $[TF]_{wall}$ surface but not on the collagen-alone surface. **E, F,** Consistent with the reduction in fibrin on collagen/low $[TF]_{wall}$, thrombin generation at low $[TF]_{wall}$ was also lowered by PPXbd after 300 sec. (*, $p < 0.05$; **, $p < 0.01$)

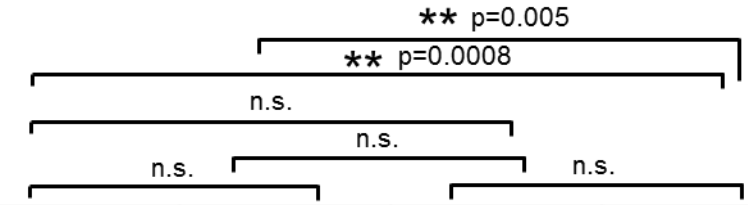

Occlusion time	+ TF/-PPXbd	+TF/+PPXbd	-TF/-PPXbd	- TF/+PPXbd
sec	370±99	408±88	442±106	509±46

Figure 3-8 PPXbd delayed occlusion on collagen surface.

Anticoagulated whole blood (CTI, 4 μg/mL) was treated with PPXbd (250 μg/mL) and was perfused over or collagen or collagen/low $[TF]_{wall}$ surface at 1000 s^{-1} under constant pressure drop condition (ΔP=constant). Full channel occlusion was only significantly delayed when PPXbd treated blood was perfused over collagen surface with no $[TF]_{wall}$ when compare to the occlusion time on surfaces with low $[TF]_{wall}$. t-test results are included (n = 10, 5 donors). (*, $p < 0.05$; **, $p < 0.01$)

3.3.5 PPXbd blocked mechanisms downstream of FXIIa on collagen/low-medium $[TF]_{wall}$

At venous shear, we found the addition of PPXbd to blood, in which FXIIa activation of FXI is blocked by 14E11, caused significant reduction in fibrin formation on collagen/low-medium $[TF]_{wall}$ after the first 200 sec (**Figure 3-9A**). In contrast, adding PPXbd to O1A6 treated blood, in which FIX activation by FXIa is blocked, did not cause further reduction in fibrin formation at the same $[TF]_{wall}$ (**Figure 3-9B**). This suggests the inhibited thrombin/fibrin generation at low-medium but not high or no $[TF]_{wall}$ by PPXbd was associated with its inhibition on mechanisms downstream of FXIIa.

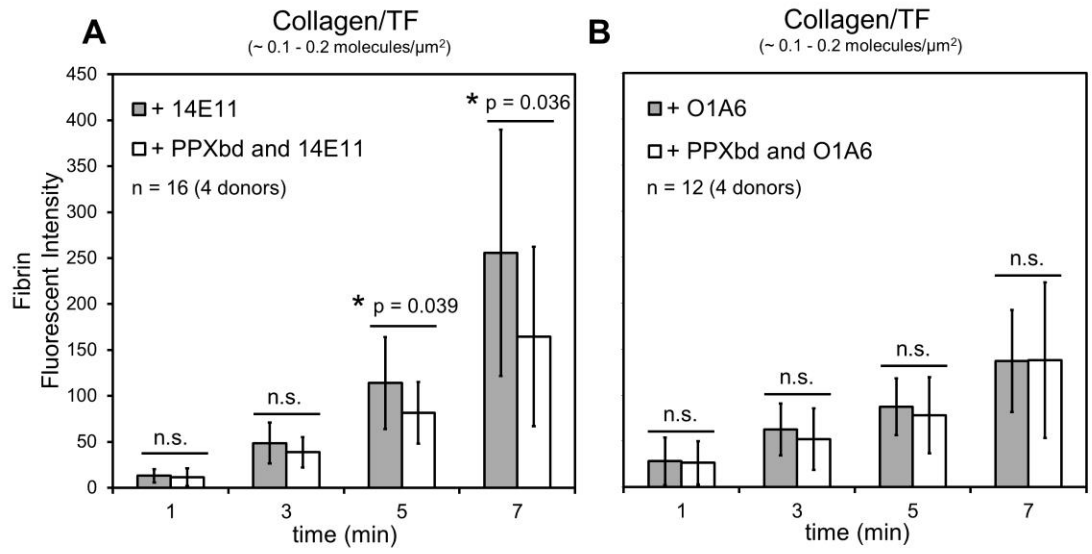

Figure 3-9 PPXbd inhibits pathways downstream of FXIIa.

A, B, Anticoagulated whole blood (CTI, 4 μg/mL) was treated with 14E11 (20 μg/mL) to inhibit FXIIa activation of FXI or with O1A6 to block FIX activation by FXIa and was perfused over collagen/low-medium $[TF]_{wall}$ surface at 100 s^{-1} under constant flow rate mode (Q = constant). Adding PPXbd to 14E11 treated blood caused significant reduction in fibrin signal after the first 200 sec. PPXbd showed no effect on fibrin generation when it was added to O1A6 treated blood. (*, $p < 0.05$; **, $p < 0.01$)

3.3.6 PPXbd altered fibrin structure and promoted clot retraction upon fibrinolysis

Recombinant tPA (30 nM) was added to blood prior to perfusion to initiate fibrinolysis. Degradation of fibrin was observed after occlusion when the platelet mass stopped growing and the fibrin signal started to decline due to lysis. Fibrinolysis initiated earlier and proceeded faster in the presence of PPXbd (**Figure 3-10C, D**) indicating a role for platelet-derived polyP in protecting the fibrin clot from lysis, regardless of the $[TF]_{wall}$. The platelet plateau level was significantly higher in PPXbd-treated clots, which was likely caused by retraction of occlusive thrombi, considering that platelet propagation was unaffected by PPXbd at early time points (**Figure 3-10A, B**). We quantified clot retraction by analyzing the platelet area reduction at the downstream edge which proceeded against the direction of flow (**Figure 3-11A**). The presence of PPXbd caused a larger area reduction at both high and low $[TF]_{wall}$ (**Figure 3-11D**). We further analyzed the retraction under two extreme conditions: (i) preserving all formed fibrin by not adding lytic reagent, and (ii) blocking fibrin polymerization with GPRP. PPXbd had no significant effect on retraction under these two conditions (**Figure 3-11B-C**). We also examined the impact of PPXbd on fibrin physical structure by measuring the fibrin fiber diameter in SEM micrographs of whole blood clots formed under flow condition (100 s^{-1}, Q = constant) on collagen/TF surfaces (**Figure 3-11E-F, H-I**). PPXbd significantly reduced the fiber diameters at both high and low $[TF]_{wall}$ (**Figure 3-11G, J**).

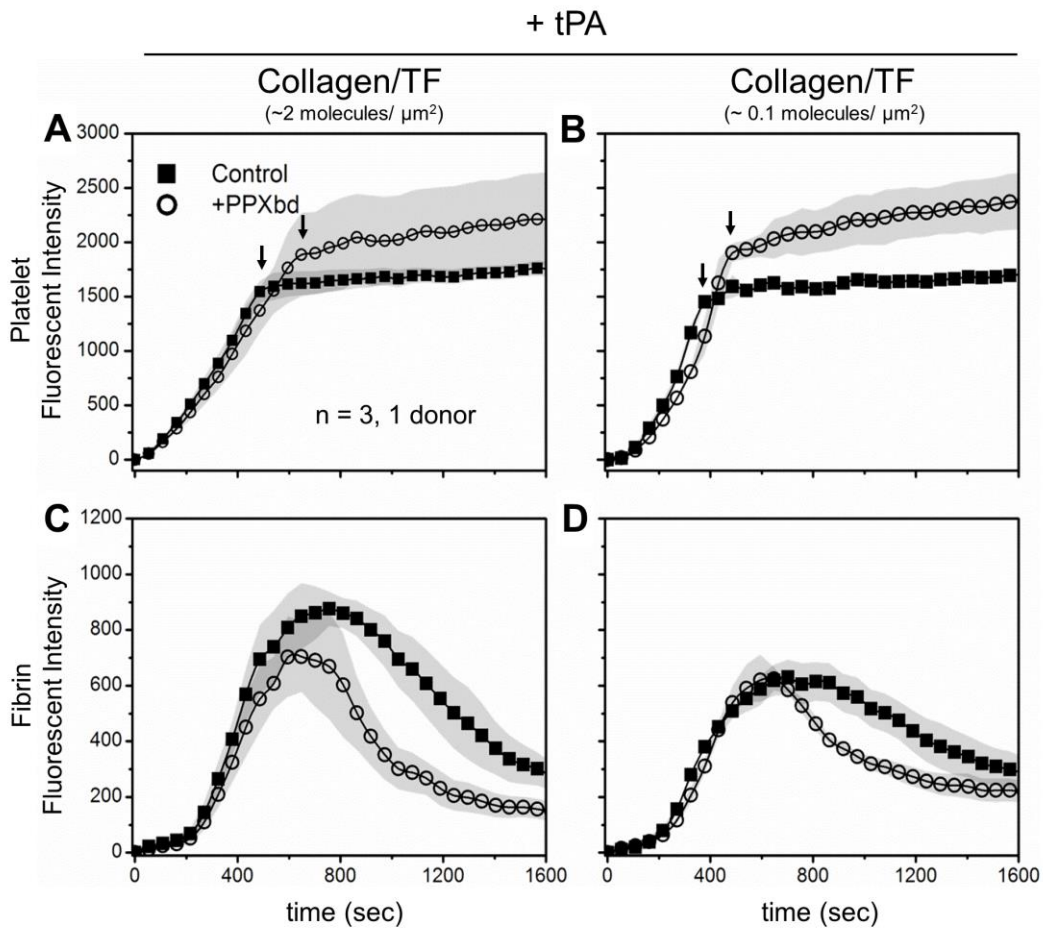

Figure 3-10 PPXbd reduces thrombus resistance to fibrinolysis induced by recombinant tPA.

Recombinant tPA (30 nM) was added to PPXbd-treated whole blood (250 μg/mL) right before flow initiation ($100s^{-1}$, ΔP = constant). **A, B,** Platelet deposition was identical with or without PPXbd during the first 400 sec. However, the platelet signal reached a higher plateau level after occlusion (indicated by black arrows) when treated with PPXbd. **C, D,** Fibrinolysis was initiated after occlusion and proceeded faster in the presence of PPXbd at both high and low $[TF]_{wall}$. Dynamics of platelet and fibrin accumulation were based on three clotting events (± SD, shaded area).

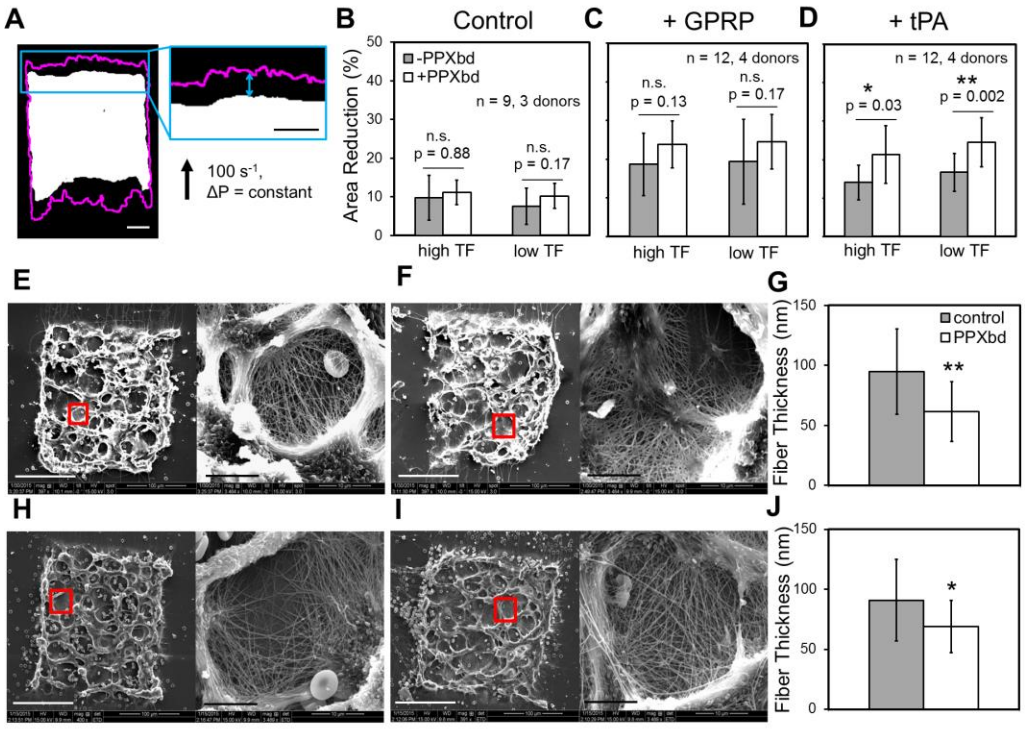

Figure 3-11 PPXbd enhances clot retraction after flow cessation and alters fibrin fiber thickness.

A, Clot retraction was quantified by the reduction in area at the downstream edge, as measured from just prior to occlusion (pink outline) to endpoint of experiment (white area). **B-D,** Scale bars represent 50 μm. Anticoagulated WB (4 μg/mL CTI) was either untreated or treated with 5 mM GPRP or 30 nM recombinant tPA and was perfused over collagen surface with high or low $[TF]_{wall}$. Area change was averaged across multiple donors. **E, F, H, I,** Representative scanning electron micrographs of thrombi formed under flow (100 s^{-1}, Q = constant) on collagen/high $[TF]_{wall}$ surface with or without PPXbd or on collagen/low $[TF]_{wall}$ surface with or without PPXbd. Left subgraphs (scale bar = 100 μm) of **E, F, H, I** show the structure of whole thrombi while right subgraphs (scale bar = 10 μm) are zoomed in images of the areas outlined by red boxes. **G, J,** Flow direction was from right to left. Average fiber thickness was smaller in PPXbd treated thrombi at both high and low $[TF]_{wall}$. (*, $p < 0.05$; **, p , 0.01)

3.4 Discussion and Conclusions

In this study, we investigated the role of FXI in contact activation and in promoting thrombin amplification by selectively targeting FXIIa-dependent FXI activation and FXIa-dependent activation of FIX and FV using FXI antibodies 14E11 and O1A6, respectively. The extrinsic pathway was left intact but its relative contribution was tuned by varying wall TF concentration. Based on our observations, we propose a model showing relative contributions of the three major mechanisms of thrombin generation: FXIIa dependent thrombin generation, FXIa mediated thrombin amplification, and TF induced thrombin generation (**Figure 3-12**). The contact pathway was required for thrombin generation on collagen surfaces since 14E11 and O1A6 robustly blocked thrombin and fibrin generation. At low $[TF]_{wall}$, contributions of the contact pathway and the extrinsic pathway were comparable. 14E11 and O1A6 individually caused partial inhibition of fibrin generation. As $[TF]_{wall}$ was increased, FXIIa dependent contact activation became less significant. Thrombin feedback mechanism became more detectable since O1A6 but not 14E11 caused significant reduction in fibrin generation. Finally, when $[TF]_{wall}$ exceeded 2 molec-TF/μm^2, neither of the FXI antibodies reduced fibrin formation, indicating thrombin was generated primarily via the extrinsic pathway. The activity of the two antibodies, especially at low $[TF]_{wall}$, in reducing fibrin formation was essentially due to the inhibition of contact activation, as was observed in **Figure 3-2**, although the identity of the most proximal activators of FXII and FXI was not resolved.

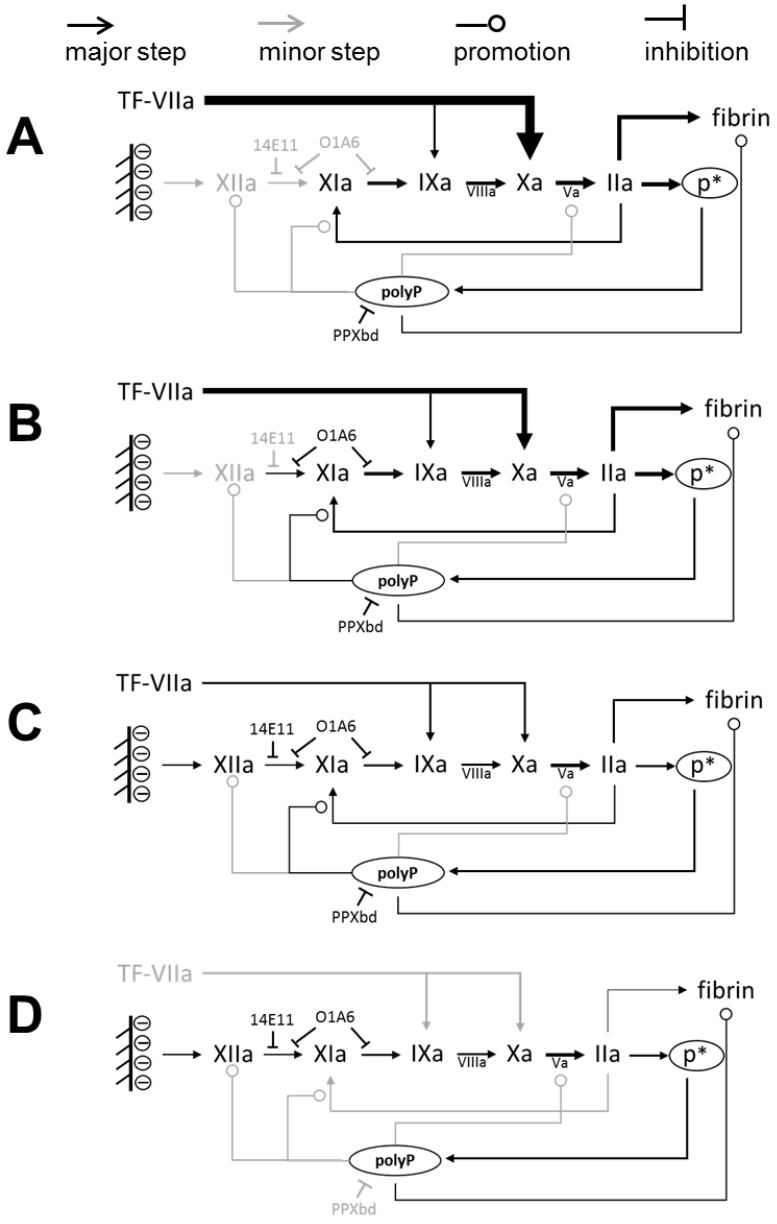

Figure 3-12 Role of XIIa, XIa, and polyP in thrombus formation on collagen/TF surfaces.

Proposed schematic showing the role of activated coagulation factors and platelet secreted polyP in thrombin generation at high (**A**), medium (**B**), low (**C**) and null (**D**) $[TF]_{wall}$. Weight and shade of arrows represent the relative contribution of the indicated mechanism. Activated platelets are indicated by "p*".

Platelet-derived polyP has been proposed as a mediator for coagulation and clot structure. However, the masking effect of TF has caused discrepancy in reported data regarding platelet-derived polyP as endogenous activator of FXII[81, 99-101], which raises the question whether polyP is physiologically important, as TF is usually present at injury sites. Our microfluidic data supports a role for platelet polyP as an enhancer of clotting under specific venous flow conditions with low (but not high) levels of wall derived TF, consistent with the role of thrombin-feedback activation of FXI implicated in the FXI-ASO study of DVT prevention.[90] The fact that adding PPXbd to FXIIa inhibited blood caused further reduction in fibrin at low-medium $[TF]_{wall}$ suggests that polyP potentiating pathway(s) downstream of FXIIa activation of FXI that requires low participation of the extrinsic pathway. Insignificant thrombin feedback caused by insufficient thrombin generation on collagen or overwhelmed thrombin generation by high $[TF]_{wall}$ made the potentiating effect of polyP on thrombin feedback mechanism negligible. Interestingly, reduction in thrombin was seen with PPXbd on collagen (no $[TF]_{wall}$) when 14E11 was added to raw blood (no CTI) shortly after blood collection. In this case, 14E11 only partially blocked thrombin generation indicating thrombin leakage from surface-induced contact activation during blood collection, which was probably sufficient for initiating the thrombin feedback loop. As expected, the effect of PPXbd was completely masked by massive FXIIa dependent thrombin generation in raw blood when 14E11 was excluded. Thus, we hypothesize that the contribution of polyP is only detectable when the thrombin feedback loop is primed with adequate, but not excessive amounts, of thrombin generated via either the contact or extrinsic pathway. The sensitivity of thrombin and fibrin production to the inhibitory effect of PPXbd under

arterial shear condition at low (but not no) $[TF]_{wall}$ suggests a similar promoting role of polyP in arterial thrombosis. However, we found the role of polyP as FXII activator in this microfluidic model was less important as surface-immobilized long chain polyP (700mer), which was shown in well plate as a much more potent FXII activator than platelet-derived short chain polyP [98], failed to promote fibrin generation on a collagen (no $[TF]_{wall}$) surface (**Figure 3-13**). In this assay, platelet aggregation is primarily mediated by collagen signaling and endogenous secondary aggregation agonists, and thus was not sensitive to the reduction in thrombin generation caused by PPXbd. Delayed full channel occlusion only occurred when TF and polyP were both absent even though total platelet fluorescence was not affected, indicating factor(s) other than total deposited platelet mass (i.e. spatial distribution of platelet mass) could be affected by polyP and cause the change in occlusion time.

PolyP also exerts effects on clot structure by enhancing fibrin polymerization [85, 98] and attenuating binding of fibrinolytic proteins to fibrin.[86] But these effects have not been validated in human whole blood under flow conditions in the presence of TF. We were able to show the reduced diameter of fibrin fibers formed in polyP-deficient thrombi regardless of the wall TF concentration. As a result, polyP-deficient thrombi were more prone to tPA-induced lysis. We also noticed polyP attenuated retraction of occlusive thrombi during fibrinolysis. We speculate that polyP modulated contraction by enhancing fibrin structure based on the observation that thrombi contracted to the same degree with or without polyP when fibrin polymerization was abolished. Furthermore, the attenuating effect of polyP on clot retraction was only significant upon fibrinolysis. Platelets are known to generate heterogeneous contractile force based on the stiffness of

surrounding environment.[102] It is possible that polyP incorporated into fibrin fibers caused the fibers to exhibit better retention of stiffness upon fibrinolysis, thus limiting clot retraction. The effect of polyP on clot stiffness is probably thrombin-independent and directly caused by the incorporation of polyP into fibrin fibers[85] since similar attenuating effect was observed at both low and high $[TF]_{wall}$. When fibrinolysis was excluded, the stall force generated by the dense and stiff fibrin network prevented platelets from contracting despite the difference in fibrin structure caused by polyP.

In this study, we demonstrated that the role of FXIIa, FXIa and platelet-derived polyP in thrombus formation on collagen may vary depending upon $[TF]_{wall}$. To our knowledge, this is the first study to show the effect of polyP on thrombin generation and fibrin structure with human whole blood under controlled flow condition with the presence of surface immobilized TF.

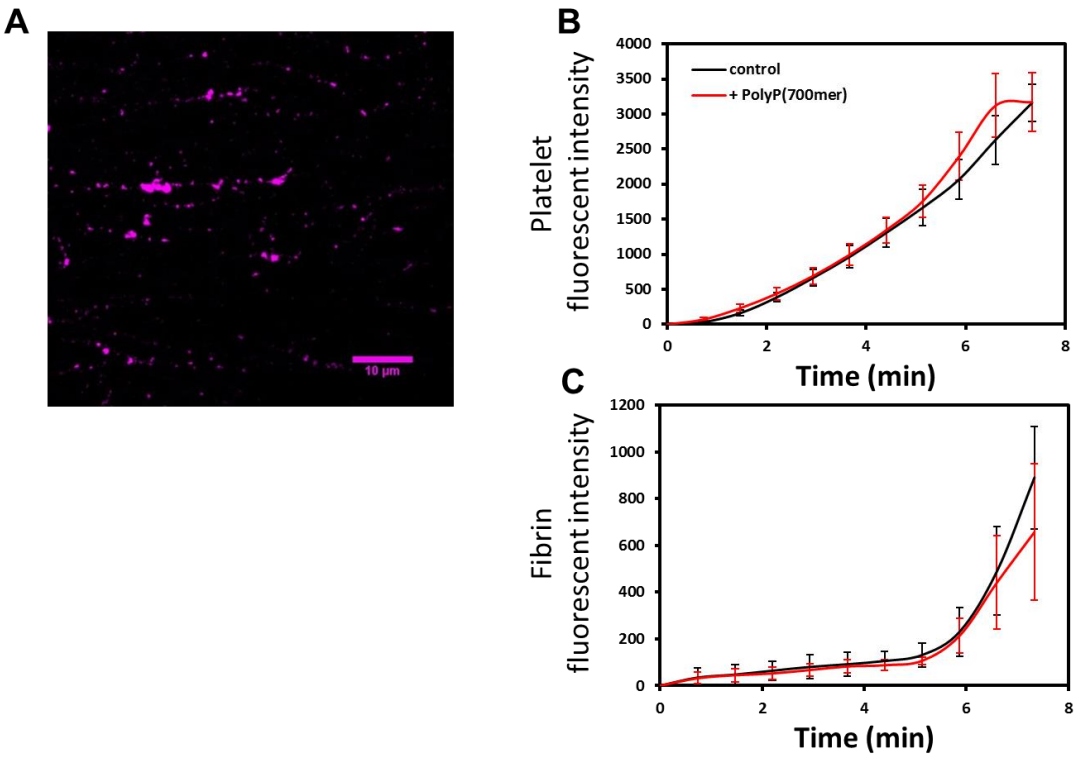

Figure 3-13 Platelet and fibrin deposition on collagen/polyP surface.

A, DAPI (4',6-diamidino-2-phenylindole) stained long chain polyP (700mer, Kerafast, Boston, MA, USA) on collagen surface (scale bar = 10 µm). **B, C,** Platelet deposition and fibrin generation on collagen surface was not affected by polyP.

Chapter 4 : Platelet-targeting thiol reduction sensor detects protein disulfide isomerase activity on activated platelets in mouse and human blood under flow

4.1 Introduction

Thiol isomerases constitute a family of enzymes that are commonly found in endoplasmic reticulum (ER). These enzymes mediate disulfide bond formation, reduction, and rearrangement which are essential for protein folding. Platelets do not have an ER, but store and secrete protein disulfide isomerase (PDI) and other thiol isomerases upon activation [103-106]. Among the family of thiol isomerases, PDI, ERp57, and ERp5 have been implicated in thrombus formation [107-113]. Thiol isomerases have two catalytically active thioredoxin-like domains which can be in either a reduced (dithiol) or oxidized (disulfide) form depending upon surrounding redox condition. Activated platelets primarily express PDI in dithiol form, which catalyzes reduction or isomerization of disulfide bonds and has been proposed to induce free thiol exposure on activated platelet surface and conformational changes in GP1bα [114]. PDI expression upon platelet activation facilitates redox remodeling of $\alpha_{IIb}\beta_3$ and promotes platelet aggregation [115-118]. Once secreted, PDI likely accumulates in the thrombus by directly interacting with β_3 integrin [116]. $\alpha_2\beta_1$ is also a potential substrate for PDI since disulfide exchange is necessary for $\alpha_2\beta_1$ but not GPVI mediated platelet adhesion [119]. With the promising antithrombotic efficacy of PDI inhibition both *in vitro* and *in vivo*, PDI inhibitors like quercetin-3-rutinoside (rutin) have been tested as potential antithrombotic reagent [120-122]. PDI has also been hypothesized as a mediator of tissue factor decryption [123, 124]. The source of PDI activity in a clot is also poorly understood. Endothelium may serve as the primary source of PDI required for thrombus

formation [125], although mouse platelet-derived PDI was also essential for thrombus formation on a collagen-coated surface [126].

Common reductase activity assays [127] are not easily adapted for detection under hemodynamic conditions in whole blood due to instantaneous dilution of signal by flow and distinctive redox condition in whole blood as compare to assay buffers. Fluorescent-conjugated PDI antibodies have been used to detect PDI *in vivo* but have not been able to detect PDI activity within thrombi [107, 125, 128]. In the present study, we developed a platelet targeting sensor for measuring total platelet-derived thiol reductase activity under flow conditions. The sensor contains a disulfide linked glutathione (GSSG) mimicking peptide conjugated to a CD61 antibody that is able to bind to platelets (**Figure 4-1**). The peptide fluoresces upon disulfide bond breakage and the antibody localizes the fluorescent signal on the platelet surface. We characterized and used this sensor to detect thiol reductase activity in a microfluidic thrombosis model and in an *in vivo* laser injury model, acquiring new information about the role of platelet-derived PDI in thrombus formation and spatial gradient of thiol reductase activity *in vivo*.

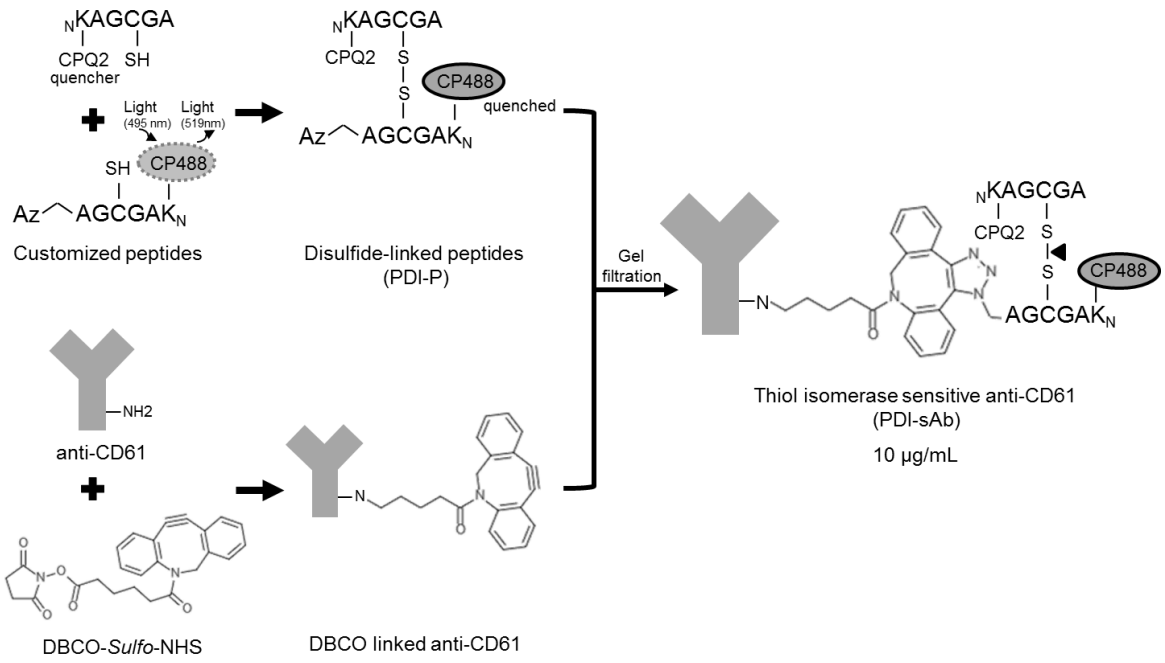

Figure 4-1 Platelet-targeting thiol isomerase sensitive fluorogenic sensor (PDI-sAb).

Customized thiol containing peptides have either a quencher (CPQ2) attached at N-terminus and or a fluorophore (CP488) and an azido group attached at N-terminus and C-terminus, respectively. The fluorophore is quenched due to close proximity to quencher once the peptides were bridged correctly by disulfide bond. Dibenzylcyclooctyne-NHS ester (DBCO) labels primary amine groups on anti-CD61 antibody and reacts with azide-labeled peptide thus serving as a connector linking disulfide bridged peptides (PDI-sP) to antibody. Fluorescence increases (at 519 nm) upon disulfide bond breakage by thiol isomerase.

4.2 Materials and Methods

4.2.1 Materials

Customized peptides *AGCGAK(CPQ2)* and *azidoacetyl-AGCGAK(CP488)* (CPC scientific, Sunnyale, CA, USA) are conjugated with a quencher (CPQ2, peptide Q) or a fluorophore (CP488, peptide F) (M.W. 996.1 and 944.9, respectively, purity > 90%). Reagents and antibodies used in this study are listed as follows: DBCO-*Sulfo*-NHS Ester (Click Chemistry Tools, Scottsdale, AZ, USA), azide-free anti-human CD61 antibody (BioLegend, San Diego, CA, USA), anti-human CD41a, antibody anti-human CD62P antibody (BD Biosciences, San Jose, CA, USA), Alexa Fluor® 647 conjugated human fibrinogen (Life Technologies, Grand Island, NY, USA), human recombinant protein disulfide isomerase (rhPDI, Biovision, Milpitas, CA, USA), 5,5'-dithiobis-(2-nitrobenzoic acid) (DTNB), dithiothreitol (DTT), glutathione (GSH), oxidized glutathione (GSSG), sodium phosphate, disodium ethylenediaminetetraacetic acid (EDTA), acetic acid, sodium citrate (Sigma-Aldrich, St. Louis, MO, USA), H-Gly-Pro-Arg-Pro-OH (GPRP, EMD Chemicals, San Diego, CA, USA), corn trypsin inhibitor (CTI, Haematologc Technologies, Essex Junction ,VT, USA), D-Phe-Pro-Arg-CMK (PPACK, Santa Cruz Biotechnology, Dallas, Texas, USA), apixaban (Selleck Chemicals, Houston, TX, USA), Dade® Innovin® PT reagent (Siemens, Malvern, PA, USA), Bradford protein assay kit, HEPES (Fisher Scientific, Pittsburg, PA, USA) and BioGel P-6 gel (Bio-Rad, Hercules, CA, USA).

4.2.2 Production of disulfide-linked thiol isomerase sensitive hetero-peptide dimers (PDI-sP)

Hetero-peptide dimers were synthesized according to a previously developed method (**Figure 4-2**) [129]. Briefly, peptide Q (quencher) and peptide F (fluorophore) were dissolved separately in 0.1 % (v/v) acetic acid to a concentration of 10 µg/µL. Ellman's buffer was prepared with 100 mM sodium phosphate, 5 mM EDTA and 7.5 mM DTNB in H_2O (pH = 7.4). Reaction buffer was prepared with 100 mM sodium phosphate and 5 mM EDTA in H_2O (pH = 7.4). Peptide Q (10 µL) was mixed with 80 µL of reaction buffer and 10 µL of Ellman's buffer. The reaction mixture was blanketed with N_2 and incubated for 2 hours at room temperature before peptide F (10 µL) was added to the reaction, followed by another 2 hours of N_2 blanketed incubation in the dark. Formation of heterodimers (PDI-sP) was verified by adding reducing reagent DTT and measuring the fluorescence increase. Addition of DTT on average caused a 10-fold increase in fluorescence (**Table 4-1**).

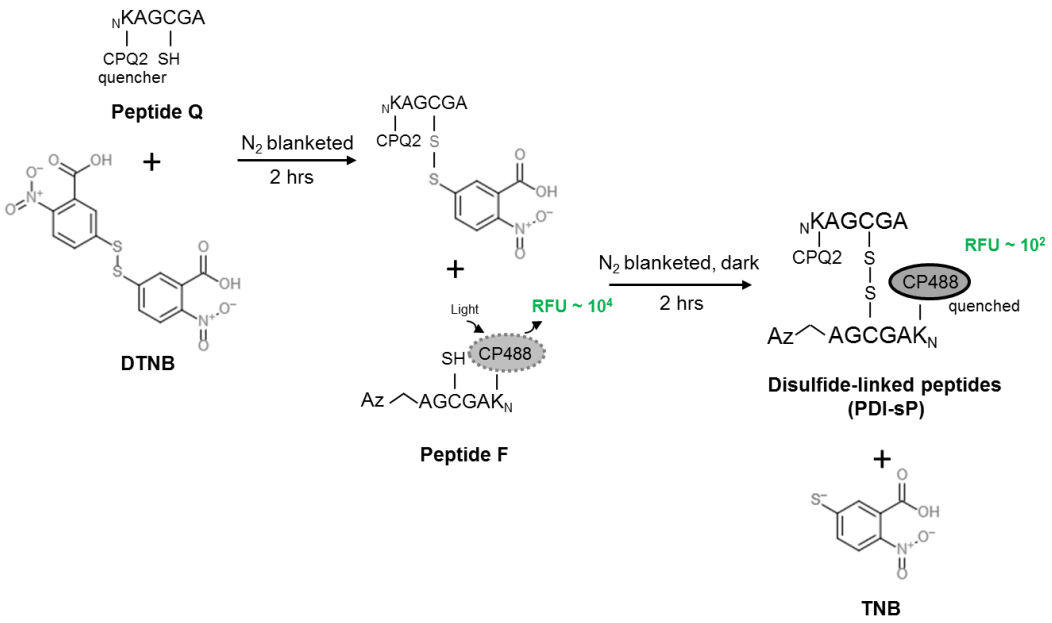

Figure 4-2 Two step reaction for producing disulfide-linked thiol isomerase sensitive hetero-peptide dimers (PDI-sP).

Thiol group on the quencher conjugated peptide (peptide Q) is firstly protected by adding 5,5'-dithiobis-(2-nitrobenzoic acid (DTNB) into the reaction and incubating under N_2 blanket for 2 hr. The fluorophore conjugated peptide (peptide F) was then added into the reaction to replace the protective group. After 2 hr incubation under N_2 blanket in the dark, peptide Q and F were linked by a disulfide bond forming PDI-sP and causing dramatic reduction in measured fluorescence in the reaction. 2-nitro-5-thiobenzoate (TNB) as byproduct of the reaction will be eliminated in subsequent purification steps.

	- DTT	+ DTT (30 mM)	Fold increase
0x dilution	402	5476	13.6
10x dilution	679	8541	12.6
100x dilution	363	3476	9.58

Table 4-1 PDI-P fluorescence change after addition of reducing reagent DTT.

Adding 30 mM DTT caused a greater than 10 fold increase in fluorescent signal. The high sensitivity of disulfide-bridged peptide to thiol reductase activity was maintained even when PDI-P was highly diluted.

4.2.3 Synthesis of thiol isomerase sensitive antibody (PDI-sAb)

DBCO-*Sulfo*-NHS Ester was dissolved in 1% DMSO to a final concentration of 900 μM and was mixed with anti-human CD61 antibody and HEPES-buffered saline (HBS buffer, 20 mM HEPES, 150 mM NaCl, pH = 7.4) in 2:1:7 volume ratio. The DBCO linking reaction was quenched by addition of Tris-HCl buffer (1 M, pH = 8.0) after 30 min incubation at room temperature. PDI-sP was added to the reaction in a 1:1 volume ratio. The reaction was incubated in the dark at room temperature for 4 hours and was then purified on BioGel P-6 gel column yielding purified PDI-sAb in HBS buffer (10 μg/ml measured by Bradford protein assay). Sensitivity of PDI-Ab to reducing reagents was measured in a Flex station microplate reader (495 nm ex/519 nm em, Molecular Devices, Sunnyvale, CA, USA) by directly mixing reducing reagents with PDI-sAb. PDI-sAb fluorescence on platelets was measured by flow cytometry (Accuri C6). A mouse specific version of the sensor was generated using an anti-mCD41 antibody.

4.2.4 Microfluidic clotting assay on collagen surface

PDI-sAb was tested in human whole blood (WB) in a previously developed microfluidic assay [20]. Briefly, a 250 μm wide collagen strip was generated by perfusing collagen type I fibrils through a PDMS patterning device that was vacuum-bonded on ethanol cleaned glass slides. The patterning device was then replaced by an eight-channel flow device which was perpendicularly vacuum-bonded on the collagen surface, generating 8 evenly spaced prothrombotic patches (250 μm×250 μm). Human WB was anticoagulated with a low level of CTI (4 μg/mL WB) or PPACK (100 μM) and was

perfused over collagen surface at venous shear rate (100 s^{-1}). The shear rate was controlled by a syringe pump (Harvard Apparatus, Holliston, MA, USA). The dynamic change of platelet (CD41a), fibrin(ogen), and PDI-sAb (1:9 WB) signal was monitored with IX81 fluorescent microscope (Olympus, Center Valley, PA, USA).

4.2.5 Blood collection and preparation

Blood was collected via venipuncture from healthy donors (free of alcohol and medication 72hrs prior to donation) in accordance with the University of Pennsylvania IRB approval. Blood was collected directly into CTI (4 μg/mL) or PPACK (100 μM) for microfluidic experiment or into sodium citrate (1:9 WB) or PPACK for platelet rich plasma preparation (300×g, 10 min).

4.2.6 Mouse intravital microscopy

Intravital imaging was done as previously described [130]. Briefly, male mice 8-12 weeks of age were anesthetized with an intraperitoneal injection of sodium pentobarbital (90 mg/kg), and their jugular vein was cannulated for the introduction of PDI-Ab and anti-CD62P AF-647. The mouse cremaster muscle was prepared for viewing, and maintained under a constant flow of bicarbonate buffer (37 °C) bubbled with 95%/5% N2/CO2. Mouse arterioles of 30-50 μm diameter were visualized with a BX61WI microscope (Olympus, St. Louis, MO, USA) with a 60X (0.9 NA) water immersion objective, and a CSUX1 spinning disk confocal scanner (Yokogawa, Sugar Land, TX, USA). Fluorescence imaging was done using diode pumped solid state lasers (405 nm, 488 nm, 561 nm, 647 nm) with acousto-optic tunable filter control as an

excitation source (LaserStack, Intelligent Imaging Innovations, Denver, CO, USA). Images were captured using an Evolve digital camera (Photometrics, Tucson, AZ, USA).

Penetrating injuries were produced with a pulsed nitrogen dye laser (SRS NL100, 440 nm) focused on the vessel wall through the microscope objective. The laser was fired 1-10 times until red blood cells either escaped into the extravascular space or became trapped within the layers of the vessel wall. The University of Pennsylvania Institutional Animal Care and Use Committee approved all procedures. After injury, platelet deposition was monitored using brightfield imaging, core development with anti-CD62P, and PDI activity with PDI-sAb. Background fluorescence was measured within the vessel for both PDI-sAb and anti-CD62P, and subtracted from the images to determine positive signal. In representative images, the core is shown as binary based on the background fluorescence and PDI-sAb signal is shown as the indicated gradient. Microscope control, image capture, and analysis were performed by Slidebook 5.0 (Intelligent Imaging Innovations, Denver, CO, USA).

4.3 Results

4.3.1 Sensitivity of PDI-sAb to reducing reagents

Rapid disulfide cleavage of PDI-sAb was observed upon addition of high dosages of DTT (**Figure 4-3A**) or GSH (**Figure 4-3B)**. Peak fluorescence was quickly achieved within 30 sec. PDI-sAb exhibited a threshold response to DTT cleavage. It remained in disulfide form at low DTT concentrations (5 and 50 μM) but was robustly cleaved by higher concentrations of DTT and reached 8-fold increase in fluorescence with the highest tested DTT concentration (30 mM). Compared to DTT, GSH was more potent in

cleaving PDI-Ab at 50 μM. However, GSH exhibited much lower reductive activity at higher dosages (5 and 30 mM), indicating the different electron transfer potentials of the two reducing reagents.

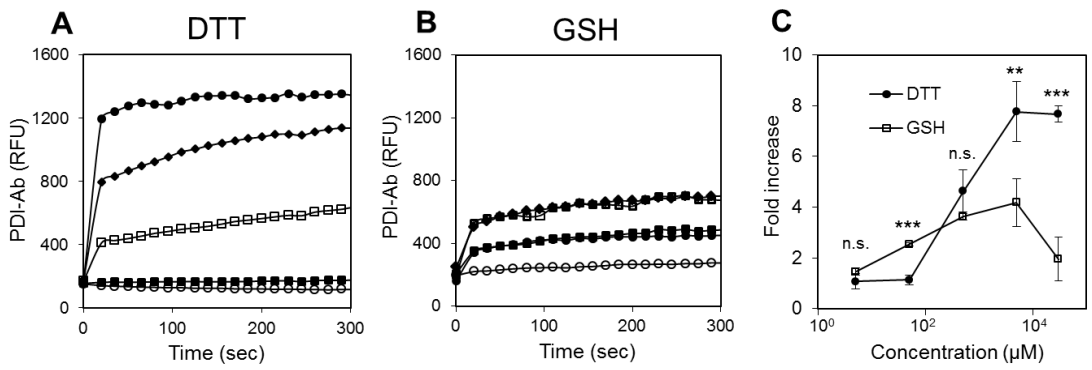

Figure 4-3 PDI-sAb sensitivity to reducing reagents.

A, B, To determine the sensitivity of synthesized PDI-sAb to reducing reagents, various concentrations of DTT or GSH were added to PDI-Ab (○ 5 μM, ■ 50 μM, □ 500 μM, ♦ 5 mM, ● 30 mM). Fluorescence increased immediately after the addition of reducing reagents and reached peak value within the first 30 seconds. **C,** Fold increase in RFU at 300 sec reveals a difference in potency of reducing reagents. (*, $p < 0.05$; **, $p < 0.01$, ***, $p < 0.005$)

4.3.2 Sensitivity of PDI-sAb to rhPDI and psPDI

Platelet-rich plasma was isolated from citrated human whole blood and was incubated with PDI-sAb (2 μg/ml) for 5 min before dilution to 2% PRP in HBS buffer. Human recombinant PDI (0, 70, or 700 nM rhPDI) was then added to initiate PDI-sAb cleavage. The time and dose-dependent to the increase in PDI-sAb signal indicated sensitivity to reductase activity of nanomolar concentrations of rhPDI (**Figure 4-4A**). In these measurements, a low concentration of 50 μM DTT was added to provide a favored redox condition and to prevent dithiol reformation before sampling. Such low DTT concentration did not lead to appreciable increase in fluorescent signal (**Figure 4-3A and Figure 4-4**) indicating the shift in PDI-sAb signal was solely dependent on the thiol reductase activity provided by rhPDI (**Figure 4-4B**).

The sensitivity of PDI-sAb to endogenous platelet reductase activity was also measured by flow cytometry with citrated 2% PRP. PRP was incubated with PDI-sAb in HBS buffer for 5 minutes before recalcification (5 mM Ca^{2+}) and addition of agonists (60 μM TRAP and 2 nM convulxin). Unstimulated platelets did not express significant reductase activity within the first 300 sec. A slight increase in PDI-sAb signal was observed at later times, which was probably caused by platelet activation and granule release indicated by slight increase in P-selectin expression after 400 sec post recalcification (**Figure 4-5A, C, D**). Stimulated platelets rapidly expressed massive reductase activity. The dynamics of the PDI-sAb signal were similar to that of P-selectin expression suggesting expression of reductase activity on platelet surface occurred at the same time as granule release (**Figure 4-5B, C, D**).

With the observation of concurrent expression of P-selectin and PDI activity on the platelet surface, correlation between PDI activity expression and phosphatidylserine (PS) exposure was also tested. A total of 10^4 events were collected after incubating 2% PRP (isolated from PPACK treated whole blood) with PDI-sAb (5 μg/ml) and agonists (60 μM TRAP and 2 nM convulxin) for 15 minutes. Baseline activity was measured in PDI-sAb labeled non-stimulated PRP (**Figure 4-6A, C**). By the end of 15 minutes incubation, a majority (90.1%) of the stimulated platelets expressed P-selectin on their surfaces (**Figure 4-6B**). About half of the P-selectin expressing population exhibited cell surface-associated thiol reductase activity (94.8% of the total reductase activity). There was a clear linear dependence of thiol reductase activity with P-selectin expression. Only slightly over than half (59.6%) of the stimulated platelets became PS positive, but over 80% of the reductase activity was expressed on PS positive platelets (**Figure 4-6D**). Our data indicates the expression of thiol reductase activity was directly associated with the level of platelet activation and granule release.

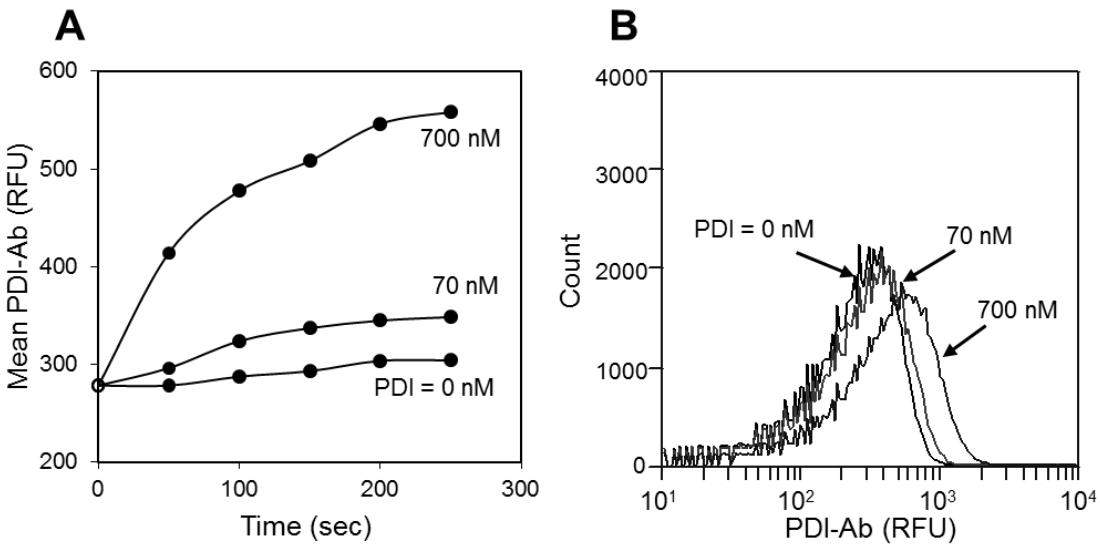

Figure 4-4 PDI-sAb sensitivity to exogenously added rhPDI.

A, Real time flow cytometry of unstimulated platelets labeled with PDI-sAb. Recombinant human PDI (rhPDI) was added to initiate sensor cleavage. Mean fluorescence increased rapidly and reached maximum value by 300 sec at [rhPDI] = 700 nM. **B,** A histogram of all collected events shows a significant shift in mean PDI-sAb fluorescence by 700 nM rhPDI.

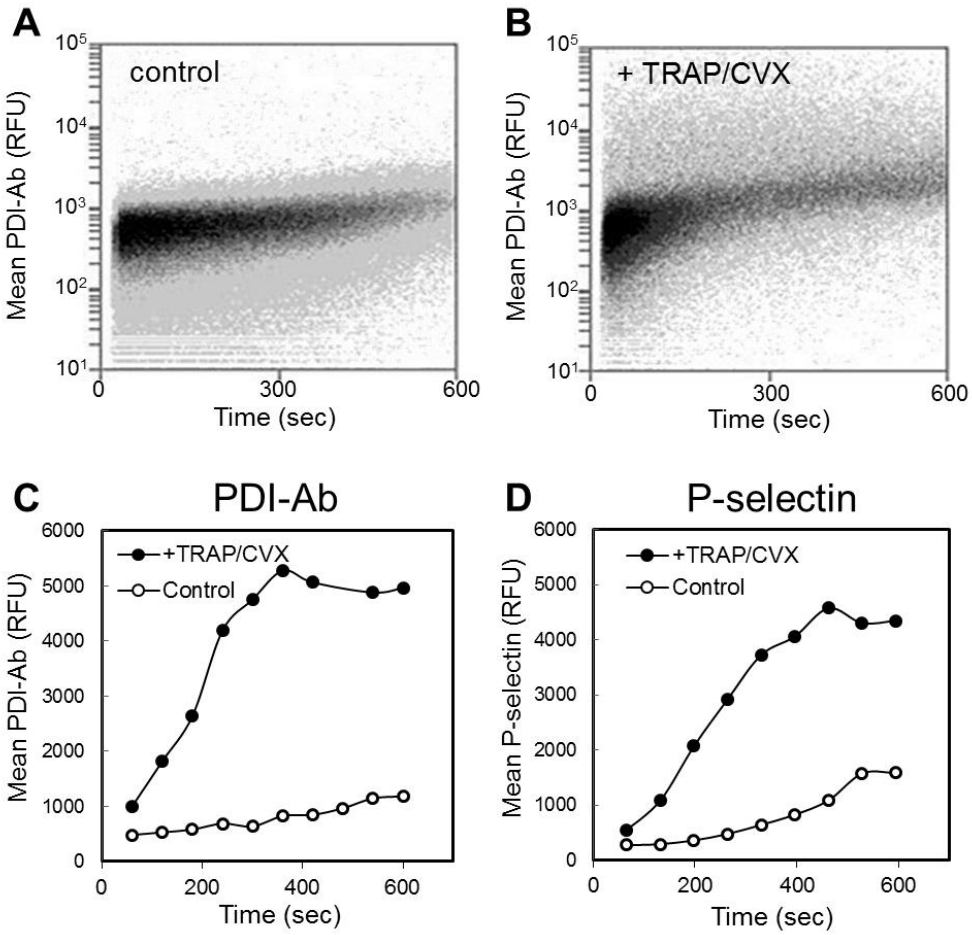

Figure 4-5 Sensitivity of PDI-sAb to platelet-derived thiol reductase activity.

A, B, Real-time flow cytometry of PDI-sAb labeled resting (**A**) or stimulated platelets (**B**). A rapid increase in PDI-sAb mean fluorescence was only observed when platelets were stimulated by TRAP and convulxin. **C, D,** A dynamic increase of PDI-sAb mean fluorescence is consistent with that of P-selectin expression on stimulated platelet surface.

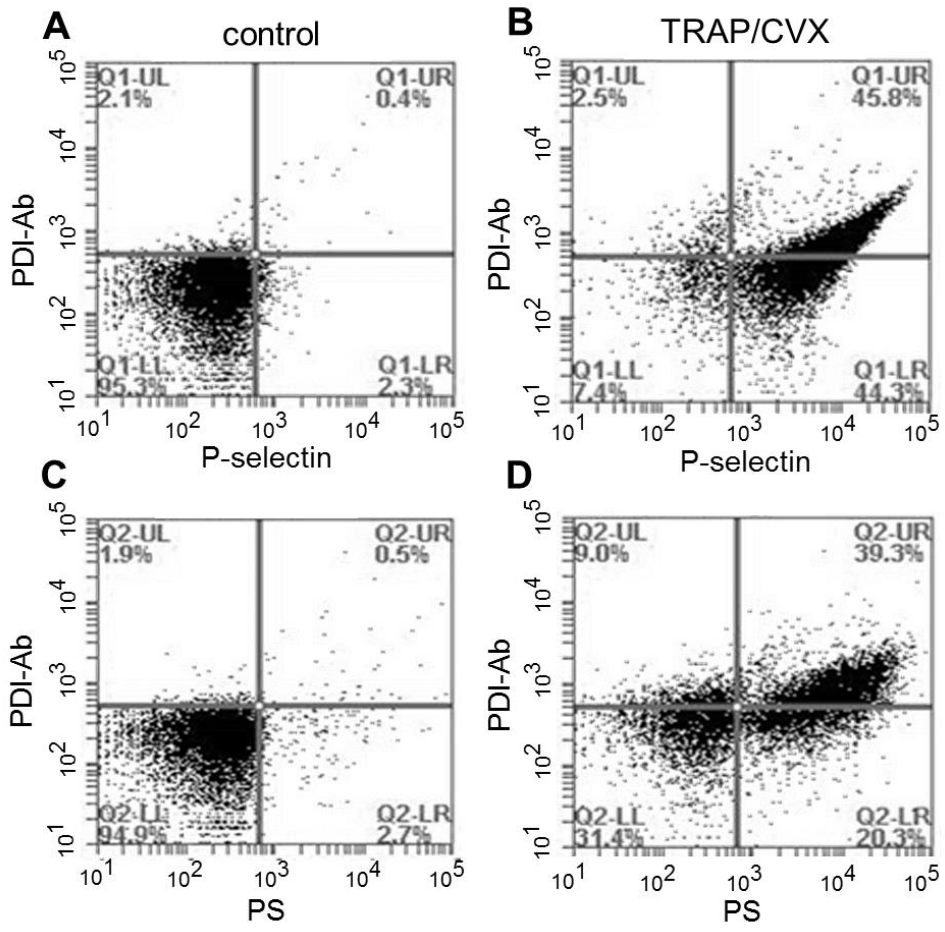

Figure 4-6 Platelet expression of thiol reductase activity is associated with granule release and PS expression.

A-D, Two dimensional dot profiles show the relationship between thiol reductase activity expression and granule release on resting or stimulated platelets and the relationship between thiol reductase activity expression and PS expression on resting or stimulated platelets. The vertical axis represents PDI-sAb fluorescence while the horizontal axis represents P-selectin (**A, B**) or PS (**C, D**) fluorescence.

4.3.3 Sensitivity of PDI-sAb to PDI inhibition

To test the sensitivity of PDI-sAb to PDI inhibition, 2% PRP (isolated from PPACK treated whole blood) was incubated with the PDI inhibitors rutin (740 μM, IC_{50} = 6.1 μM)[121] or PACMA 31(420 μM, IC_{50} = 10 μM)[131] along with platelet agonists (60 μM TRAP and 2 nM convulxin) and PDI-sAb (5 μg/ml). A total of 10^4 events were collected after a 15 min incubation. Maximum thiol reductase activity was collected on stimulated platelets without inhibitor addition. Rutin is a selective inhibitor of PDI [121] but only caused partial reduction in reductase activity on stimulated platelets suggesting other platelet-derived thiol isomerases are also important sources of platelet surface reductase activity (**Figure 4-7A**). PDI-null platelets display normal P-selectin exposure [126]. A slight reduction in P-selectin exposure on rutin-treated platelets suggesting off-target effects of rutin at the high dosage levels [126]. Complete inhibition of PDI-sAb signal was observed when stimulated platelets were treated with PACMA31 (**Figure 4-7C**). This dramatic inhibitory effect of PACMA31 was probably caused by its cell permeability, which probably also contributed to the severely disturbed P-selectin expression (**Figure 4-7D**). We also found when platelets were treated with rutin or PACMA31, much less reductase activity was observed even in the P-selectin positive population, which indicates that the decreased PDI-sAb signal on rutin or PACMA31 treated platelets was not simply due to reduced thiol isomerase expression caused by disturbed granule release (**Figure 4-8**). It has also been reported PDI inhibition upregulates PS exposure on endothelial cells [132], but we failed to detect an effect of rutin on platelets PS exposure (**Figure 4-9**).

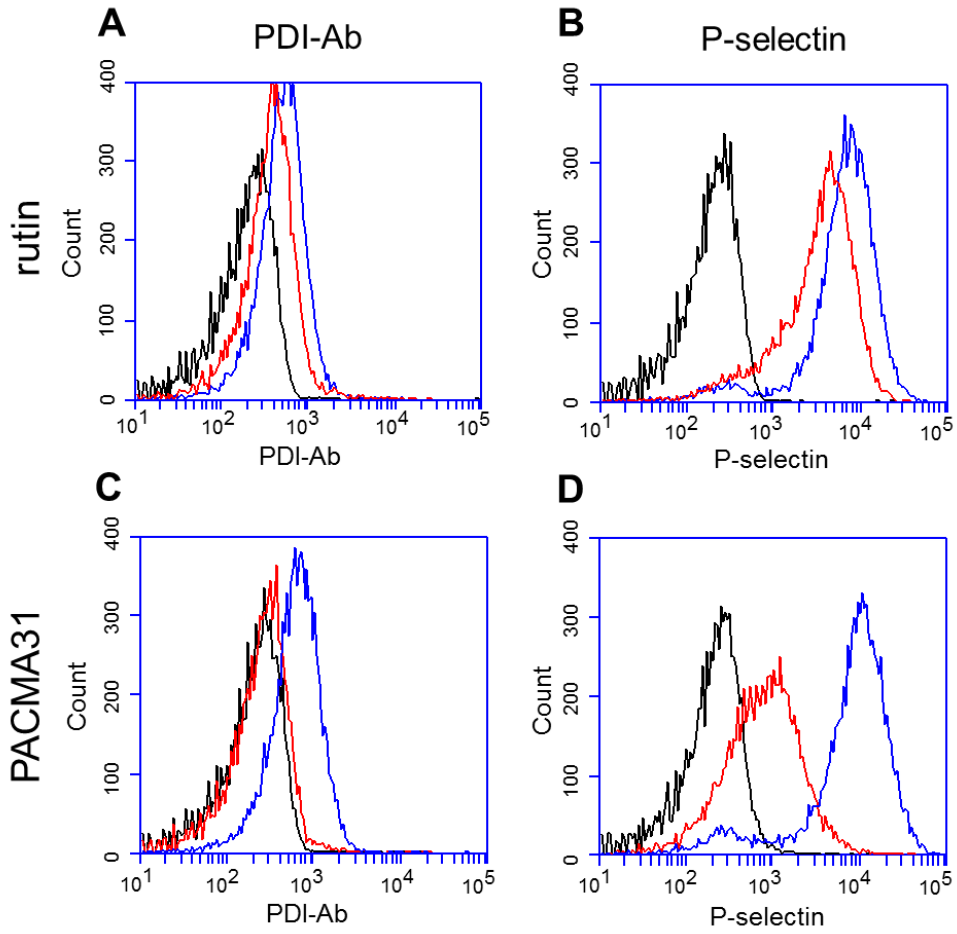

Figure 4-7 PDI-sAb sensitivity to PDI inhibitors.

Histograms show thiol reductase activity and P-selectin expression on resting (black), stimulated (blue) or inhibitor-treated stimulated (red) platelets. Rutin (740 μM) partially inhibited reductase activity (**A**) and had mild inhibitory effect on P-selectin expression (**B**) while PACMA31 (420 μM) resulted in a complete knock-out of reductase activity (**C**) and a large reduction in P-selectin expression (**D**).

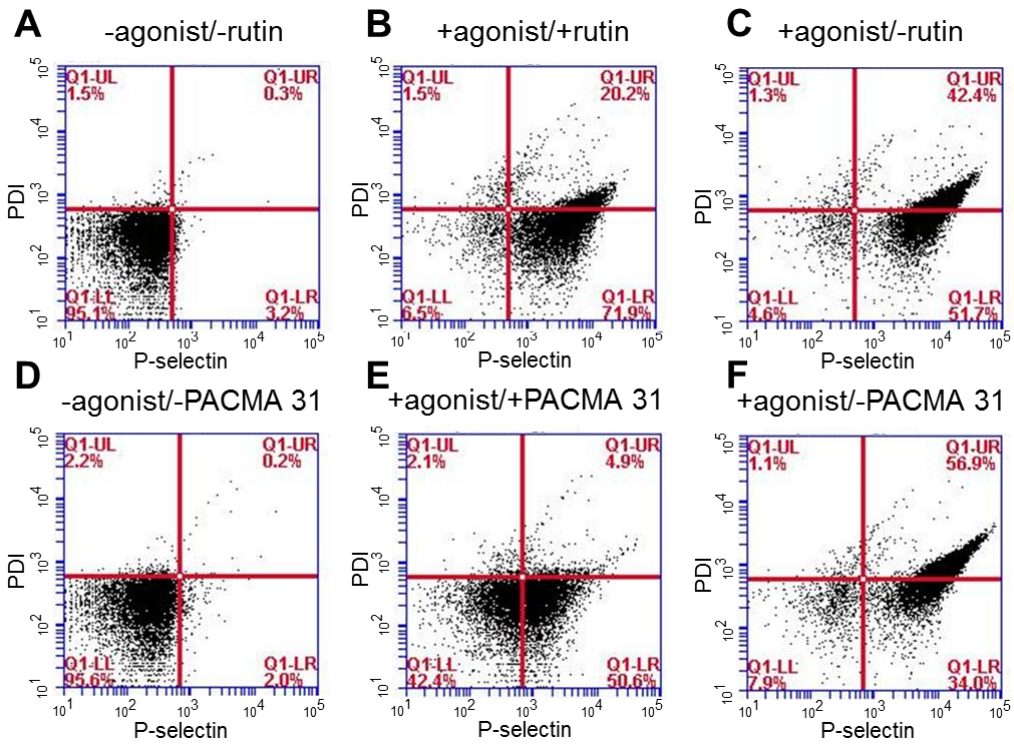

Figure 4-8 PDI inhibitors cause reduction in thiol reductase activity expression on platelet surface.

Two dimensional dot profile shows the relationship between thiol reductase activity expression (vertical axis) and P-selectin expression (horizontal axis) on resting platelet surfaces (**A, D**), stimulated but inhibited platelet surfaces (**B, E**), or on stimulated platelet surfaces (**C, F**). PDI specific inhibitors rutin (**B**) or PACMA 31 (**E**) was used to inhibit platelet-derived PDI activity. Both rutin and PACMA 31 caused significant reduction in platelet surface-associated thiol reductase activity even in P-selectin positive population.

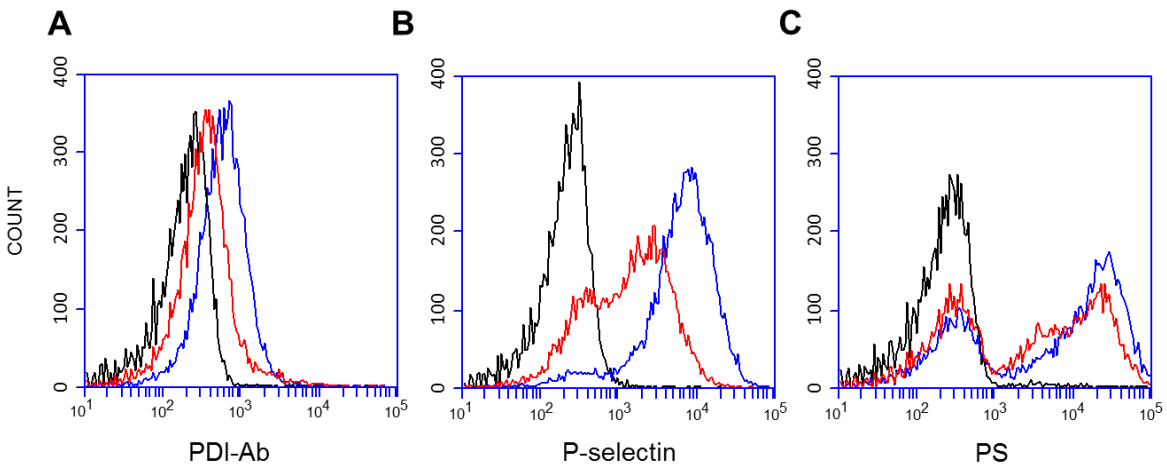

Figure 4-9 Rutin does not cause reduction in platelet PS exposure.

The histograms show thiol reductase activity (**A**), P-selectin expression (B) or PS exposure (**C**) on resting (black), stimulated (blue) or rutin-treated stimulated (red) platelets. Rutin caused significant reduction in mean PDI-sAb fluorescence indicating its inhibitory effect on PDI activity (**A**). Rutin also caused impaired P-selectin expression compare to stimulated but non-inhibited platelets (**B**). However, rutin did not cause reduction in PS exposure (**C**).

4.3.4 Detection of PDI reductase activity in a microfluidic thrombosis model

CTI- (4 μg/ml) or PPACK- (100 μM) treated human whole blood was labeled with PDI-sAb (1:10 WB, 1 μg/ml) before it was perfused over a patterned collagen surface at 100 s^{-1} initial wall shear rate. Platelet deposition and reductase activity in growing thrombi were monitored simultaneously. The rapid increase of PDI-sAb signal was predominately observed over the first 200 sec whereas platelets continued to accumulate for over 500 sec (**Figure 4-10**). In the presence of thrombin, adding rutin (82 μM) did not cause reduction in platelet aggregation or in PDI-sAb cleavage (**Figure 4-10 A-C**). A similar effect was observed with a monoclonal function-blocking PDI antibody (RL90, 20 μg/mL); platelet aggregation on collagen was only affected by PDI inhibition when thrombin was inhibited by PPACK (**Figure 4-11**). Interestingly, rutin and RL90 only caused reduction in PDI-sAb and CD41 fluorescence after 60 sec, which is when primary aggregation of platelets on collagen occurred.

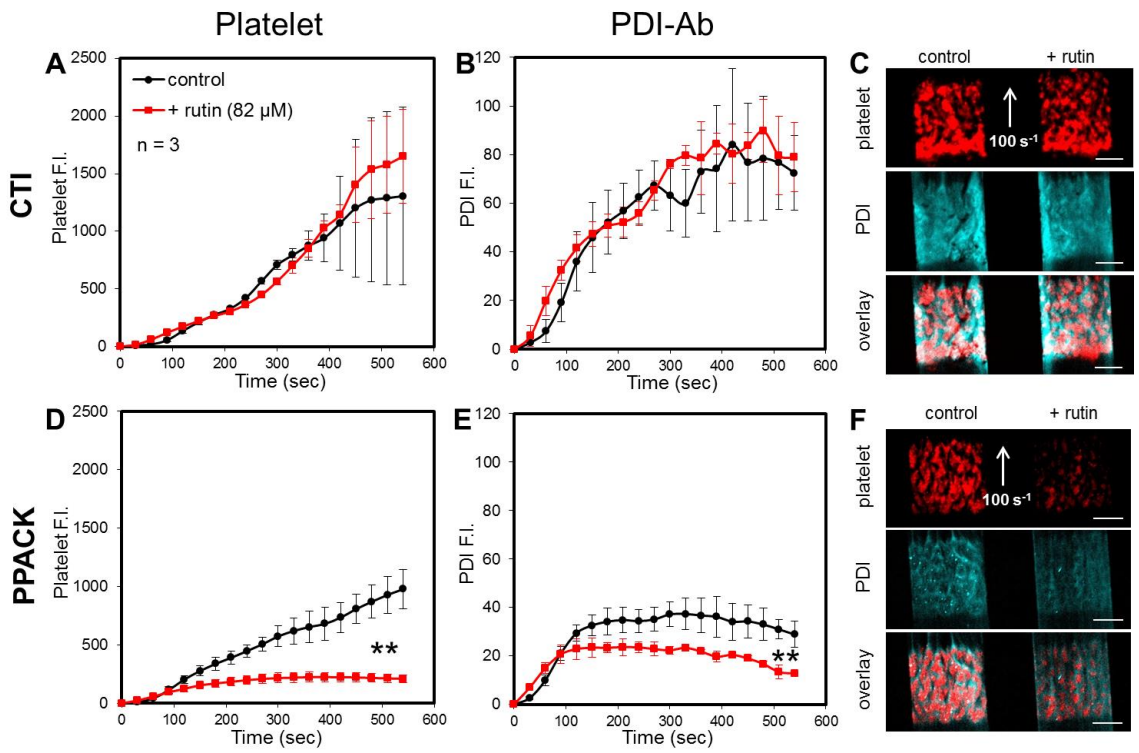

Figure 4-10 Detection of thiol reductase activity *in vitro*.

Low level of CTI (4 μg/ml, **A-C**) or PPACK (100 μM, **D-F**) treated whole blood was perfused over collagen at venous shear rate (100 s^{-1}). **A, B,** Platelet deposition and thiol reductase activity were unaffected by rutin (82 μM) in the presence of thrombin. **C,** Images of platelet and PDI-sAb signals on collagen at 500 seconds show no distinguishable difference between control and rutin treated thrombi. **D, E,** Rutin caused significant reduction in platelet deposition and detected thiol reductase activity when thrombin was inhibited by PPACK. **F,** Real time images at 500 seconds show a severe reduction in platelet and PDI-sAb signals in rutin treated thrombus. Scale bars represent 100 μm.

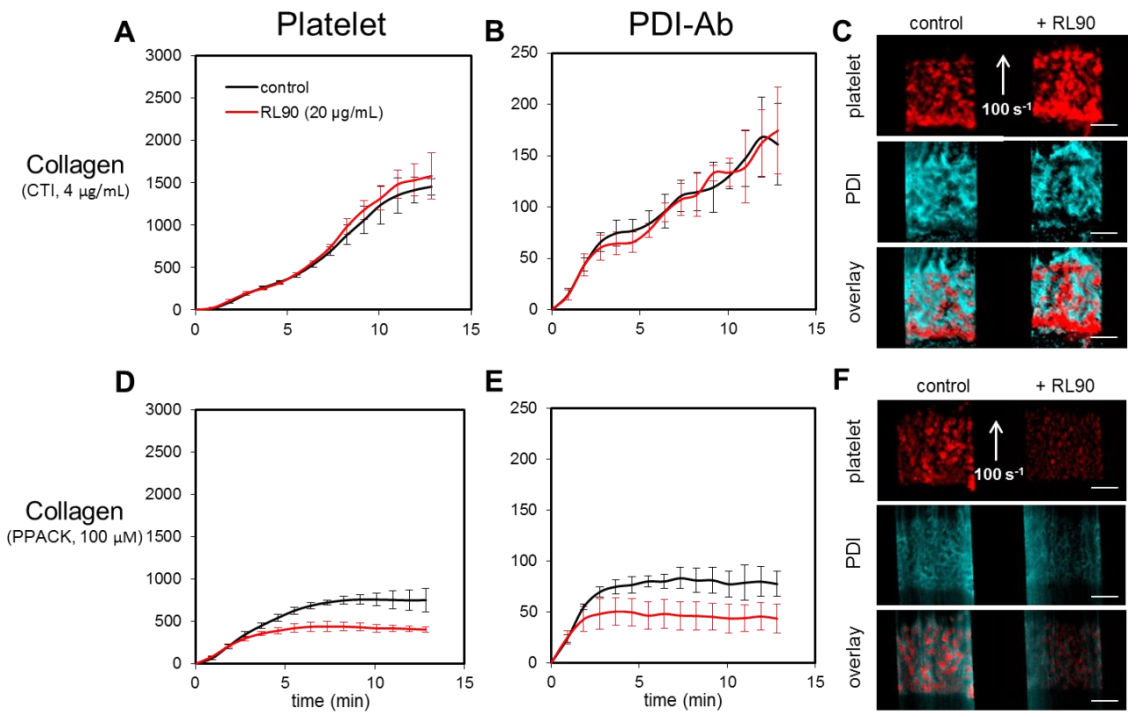

Figure 4-11 Rutin causes severe reduction in platelet deposition on collagen in the absence of thombin.

Low level of CTI- (4 µg/mL) treated (**A, B**) or PPACK- (100 µM) treated whole blood (**C, D**) was perfused over a collagen surface at venous shear rate (100 s^{-1}). **A, B,** Platelet deposition and thiol reductase activity were unaffected by RL90 (20 µg/mL) in the presence of thrombin. **C,** Images of platelet and PDI-sAb signals on collagen at 500 seconds show no distinguishable difference between control and RL90 treated thrombi. **D, E,** RL90 caused significant reduction in platelet deposition and detected thiol reductase activity when thrombin was inhibited by PPACK. **F,** Real time images at 500 seconds show a severe reduction in platelet and PDI-sAb signals in RL90 treated thrombus. Scale bars represent 100 µm.

4.3.5 Detection of PDI reductase activity in vivo

Laser injury of mouse cremaster arterioles consistently produces a hemostatic thrombus that prevents continued red cell loss, and develops a characteristic architecture consisting of a core of highly activated platelets covered by a shell of loosely-packed and less activated platelets [133]. Using a mouse anti-platelet scaffold we produced a mouse PDI-sAb to investigate PDI reductase activity in the context of this injury model. We consistently observed a gradient of PDI-sAb signal within the thrombus, which was strongest in the core region proximal to the injury site (**Figure 4-12**). These results are consistent with our *in vitro* results showing increased PDI reductase activity associated with highly activated, P-selectin positive platelets.

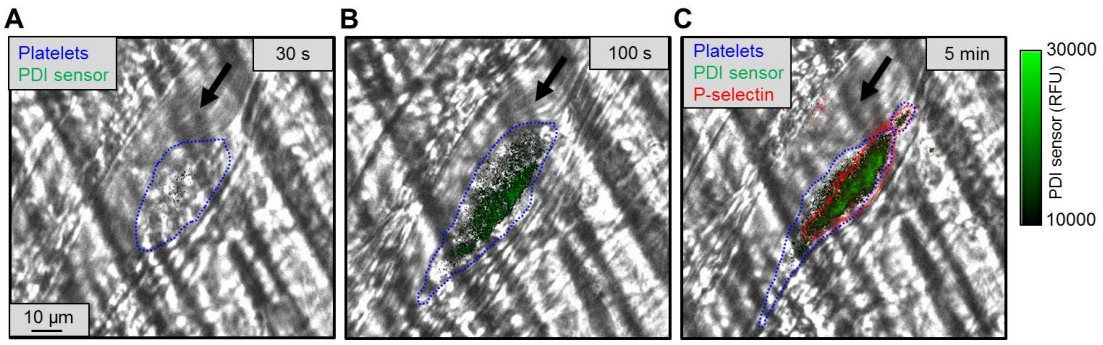

Figure 4-12 Detection of thiol reductase activity *in vivo*.

Thiol reductase activity was detected in thrombus formed after laser-induced arteriolar wall injury in mouse. The site of the injury was observed using confocal fluorescence microscopy. Black arrow indicates flow direction. **A,** Platelets (blue) were outlined with bright field images. **B, C,** Thiol reductase activity (green) was more concentrated in the core area and co-localized with P-selectin positive (outlined in red) area (**C**).

4.4 Discussion and Conclusions

In vivo studies have suggested that endothelial PDI plays a role in thrombus formation. [125], but the importance of platelet-derived PDI has been questioned. To address this issue, in this study we have developed a platelet-targeted PDI sensor (PDI-sAb) that is suitable for sensing thiol reductase activity on or near the surface of human platelets in a microfluidic thrombosis model that does not include endothelial cells. Additionally, we generated a version of the sensor that targets mouse platelets and used it to visualize sensor fluorescence dynamics within a growing thrombus in an *in vivo* laser injury model.

In flow cytometry, we found that PDI-sAb was a sensitive marker for thiol reductase activity and was capable of detecting the activity of nanomolar levels of rhPDI. Upon activation, platelets displayed rapidly increasing PDI-sAb signal, which was consistent with the dynamics of P-selectin expression on platelet surface, suggesting the endogenous source of detected reductase activity. We subsequently found the majority of the detectable activity was localized on PS positive platelets, suggesting that expression of the reductase activity is dependent on the level of platelet activation.

In a microfluidic clotting assay, we were able to visualize the development of PDI-sAb signal in growing thrombi on collagen surface. Most of the PDI-sAb signal increase was detected during the first 200 sec suggesting initial platelet deposition on collagen and proximity to the surface, instead of secondary platelet aggregation during clot buildup, was correlated with platelet thiol reductase activity expression. Despite the high micromolar levels of GSH contained in whole blood [134], we found neither

anticoagulated whole blood nor thrombin (concentrated pure enzyme) exhibited appreciable reductase activity for at least 15 minutes (**Figure 4-13**), which confirms the thrombus incorporated PDI-sAb signal was caused by endogenous thiol reductase activity instead of non-specific cleavage by blood enzymes. Several *in vitro* studies have shown the importance of thiol isomerase activity for normal platelet aggregation [108, 110, 112, 121, 125]. However, neither PDI inhibitor rutin nor PDI antibody RL90 caused reduction in platelet accumulation on collagen surface in the presence of thrombin in our hands. A previous study has shown PDI-null platelets exhibit normal aggregation and granule release when stimulated by high dosages of agonists [126]. In our microfluidic assay, the abundant surface-immobilized collagen and locally-generated secondary aggregation agonists (i.e. thrombin, ADP, and thromboxane) were probably sufficient to overcome PDI inhibition by rutin or RL90. Thus, we attribute the lack of efficacy of PDI inhibition to high level of both primary and secondary agonists for platelet aggregation and the compensating effect from other platelet-expressed thiol isomerases. We also found that when thrombin is inhibited, PDI inhibition only disturbed platelet aggregation after the initiation phase (~60 sec). In this assay, immobilized collagen vigorously and rapidly activates and recruits platelets during the initiation phase. It is unlikely PDI can further promote this process given both of the potency and surface density of collagen is high. In this microfluidic system, PDI was most likely taking part in platelet secondary aggregation by either facilitating $\alpha_{2b}\beta_3$ remodeling or other unknown mechanisms and its effect is only detectable in the absence of thrombin. However, we cannot tell if this was because PPACK neutralized the masking effect of thrombin on PDI function or thrombin

inhibition caused deficient expression of other endogenous thiol isomerases as alternative sources of thiol isomerase activity.

We have also presented, to our knowledge, the first sensor capable of measuring the spatiotemporal distribution of PDI reductase activity *in vivo*. We observed a gradient of PDI-sAb signal emanating away from the *in vivo* injury site. PDI reductase activity was predominately associated with highly activated P-selectin positive platelets which were localized in the core of thrombus. Both endothelium and platelets are sources of extracellular PDI *in vivo* [107, 108, 125]. Endothelium- and platelet-derived PDI may differ in function in that endothelium PDI may be more critical for initial platelet recruitment while platelet PDI may be more important for continued thrombus propagation [107, 121, 135]. The finding that PDI inhibition had no effect on initial platelet aggregation on collagen in the microfluidic thrombosis model lacking endothelium is in agreement with this scenario. Sequential PDI secretion by endothelium and then activated platelets would introduce a time dependency of PDI availability from different cellular sources [107, 125], which could also contribute to a less dominant role of platelet PDI on initial platelet adhesion *in vivo*.

The mouse PDI-sAb can detect endogenous platelet reductase activity as well as reductase activity derived from other cellular sources but the sensor is clearly sensing the platelet surface. The fact that PDI-sAb signal accumulated near endothelium before the appearance of the P-selectin positive core area also suggests endothelium as the initial source of PDI. After the core-shell structure of thrombus was fully developed, PDI-sAb signal was still well retained in the P-selectin positive core area, consistent with flow

cytometry results that reductase activity was most localized on the most activated platelets.

In summary, we used a novel approach to visualize extracellular reductase activity during thrombus formation both *in vitro* and *in vivo*. We found the distribution of reductase activity was strongly correlated with P-selectin display and somewhat less correlated with PS exposure even though most of reductase activity was localized on PS exposed platelets. Expression of thiol isomerase activity was mostly correlated with initial platelet aggregation on collagen in the microfluidic thrombosis model. PDI inhibition showed limited effect in the present of thrombin suggesting dependency of platelet PDI function on the combination and level of triggers for platelet activation. Reductase activity was concentrated in the thrombus core area *in vivo* and was co-localized with P-selectin display, which could be a result of more platelet activation in the core and physical proximity of the core to endothelium, an alternative cellular source of reductase activity.

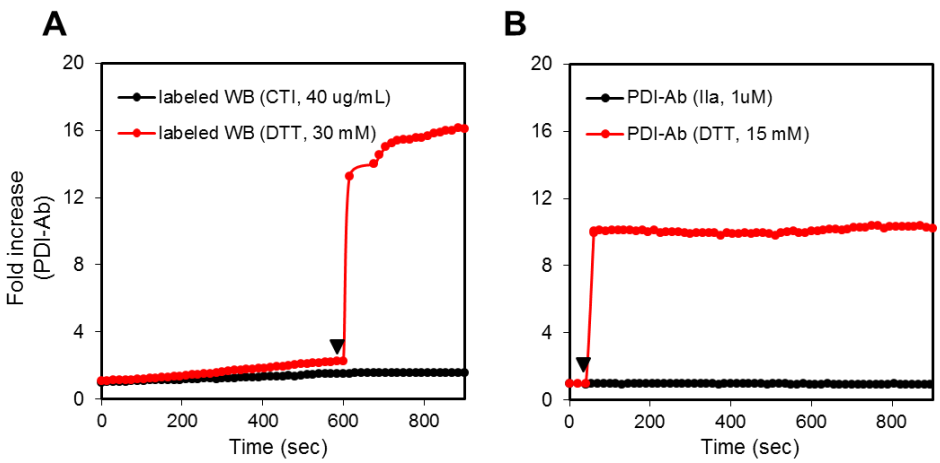

Figure 4-13 PDI-sAb specifically detects thiol isomerase activities in blood.

A, High CTI- (40 μg/mL) treated whole blood was labeled with the PDI-sAb and rested in wells for 15 minutes. No fluorescence change was detected by the end of 15 minutes in resting blood (black). In contrast, adding DTT (30 mM, red) at t = 600 seconds (indicated by black inverted triangle) caused over 10-fold change in fluorescence. **B,** Thrombin (IIa, 1 μM, black) or DTT (15 mM, red) was added to PDI-sAb (indicated by black inverted triangle) in well-plate. The fluorescence change in the wells was recorded for up 15 minutes. IIa did not cleave PDI-sAb, while DTT caused rapid cleavage of PDI-sAb, indicated by the 10-fold increase in fluorescence.

Chapter 5 : Minimum wound size for clotting: flowing blood coagulates on a single collagen fiber presenting tissue factor and von Willebrand factor

5.1 Introduction

Blood coagulation in healthy humans is tightly regulated such that hemostatic clot formation is rapid but self-limiting at sites of vascular injury. Vascular damage involves exposure of flowing blood to collagen and tissue factor (TF), components that platelets and plasma do not normally encounter in healthy vessels. TF binds Factor VIIa to generate Factor Xa (FXa) and Factor IXa (FIXa), leading to amplified thrombin generation and consequent fibrin polymerization. Platelet deposition is driven by collagen and thrombin and autocrinic release of ADP and thromboxane. The extracellular triggers, platelet receptors, and intracellular signaling events of platelet activation as well as the TF-triggered extrinsic pathway of coagulation are well defined in terms of molecular components.

However, it is unknown if a lower size limit of a surface defect exists for human blood coagulation under flow. Prior experimental determinations of the smallest sized surface stimuli necessary for clotting of human blood, defined as the *patch size threshold*, have not deployed the combination of whole blood, hemodynamic flow, and a platelet adhesive stimulus. Observations with plasma indicate that a surface trigger may be small enough to escape hemostatic responses because diffusible and rapidly inhibited species might not reach a local critical concentration. Thus, transport effects may sufficiently damp the amplification reactions of the coagulation cascade. Plasma incubated under static conditions has great difficulty in generating fibrin when placed on lipid/TF features smaller than 50 μm in diameter, but rapidly generates fibrin on features larger than 100

μm in diameter.[136] In such measurements, the rate of generation of active FXa and Factor Va, thrombin, and fibrin monomer in proximity to the discrete lipid surface must overcome (i) diffusion that dilutes local concentrations and (ii) inhibitors such as tissue factor pathway inhibitor and antithrombin that quench active species. A similarly sized patch threshold was detected with static incubation of platelet rich plasma over lipid-TF features smaller than 100 μm in diameter,[137] but a strong patch size threshold was less apparent when whole blood was incubated on such features. Convective flow adds an additional transport mechanism to remove reactive species from a discrete triggering zone. Perfusion of plasma through a capillary with a 200-μm long zone of lipid/TF displayed difficulty in clotting at even sub-physiological wall shear rates above 30 s^{-1}.[138] Similarly, capillary perfusion of platelet rich plasma over 200-μm long zones of lipid/TF displayed difficulty in clotting at a venous wall shear rates of 80 to 120 s^{-1}. However, a platelet adhesive and stimulatory surface such as collagen was not part of that measurement. In contrast, human whole blood readily clots on 250-μm diameter spots of microprinted collagen/TF [25] or 250-μm long zones of collagen/TF in microfluidic channels [13, 24] at venous and arterial flow conditions.

In the present microfluidic study of human blood, surface feature size was reduced to one of the smallest possible physiological procoagulant trigger, a single collagen fiber. Lipidated TF and von Willebrand factor (VWF) were used to decorate collagen fibers to mimic the surface stimuli expected *in vivo*.[139, 140] Human whole blood was minimally perturbed with 4 μg/mL corn trysin inhibitor (CTI, a βFXIIa inhibitor) and was immediately perfused over patterned small patches after phlebotomy

within 5 min in order to minimize contact-pathway triggered clotting while maintaining normal blood responsiveness of the extrinsic pathway of TF initiated coagulation.[12, 13] By taking this microfluidic approach, we determined if a patch size threshold exists for human blood. We determined under what biochemical and hemodynamic conditions a single collagen fiber can support a clotting response of platelet deposition, platelet-localized thrombin generation,[55] and fibrin polymerization.

5.2 Materials and Methods

5.2.1 PDMS patterning and flow devices

Poly(dimethylsiloxane) (PDMS, Ellsworth Adhesives, Germantown, WI) microfluidic devices were fabricated as previous described.[22] Single channel (10 or 20 μm in width, 60 μm in height) devices were used for protein patterning on glass slides. The device used for microfluidic thrombosis assay has 8 evenly spaced flow channels (250 μm in width, 60 μm in height) that connect individual cylindrical reservoirs to a single outlet. Both devices can be reversibly mounted on glass slides by vacuum bonding.

5.2.2 Preparation of small collagen patches

Glass slides were treated with Sigmacote® (Sigma-Aldrich, St. Louis, MO) to impede blood clotting outside the patterned prothrombotic surfaces before they were rinsed with DI water and were dried with compressed filtered air. Perfusion of 5 μL of collagen type I (1 mg/mL, Chronolog Corp, Havertown, PA) followed by 20 μL of bovine serum albumin (0.5% BSA in HBS) through the main channel on the patterning device that was mounted on a glass slide resulted in immobilized patches of aligned collagen fibers on the glass slide.[20, 22] In order to capture single collagen fibers,

collagen type I was diluted (10x dilution, 100 µg/mL) in isotonic glucose buffer before being perfused through 10 µm wide channels. Lipidated TF was added by incubating Dade® Innovin® recombinant human TF (VWR Corp, Radnor, PA) over patterned collagen for at least 30 min before a BSA rinse. VWF was added by incubating collagen fibers with human plasma VWF (30 µg/mL, FVIII free, Haematologic Technologies, Essex Junction, VT) prior to perfusion and an immediate rinse with BSA. Both bright field imaging and fluorescent post-staining were used to ensure the precision of the patterning technique (**Figure 5-1**). For collagen staining, micropatterned zones were stained with biotinylated anti-collagen I antibody (Abcam, Cambridge, MA), which was then detected with Alexa Fluor 488 streptavidin (Life Technologies, Grand Island, NY) before a buffer wash. Annexin V-PE (1% in 5mM $CaCl_2$ buffer, BD Bioscience, San Jose, California) and anti-VWF (0.5% in HBS buffer, Abcam, Cambridge, MA) were subsequently added for fluorescent staining when collagen fibers were precoated with TF liposomes and VWF, respectively.

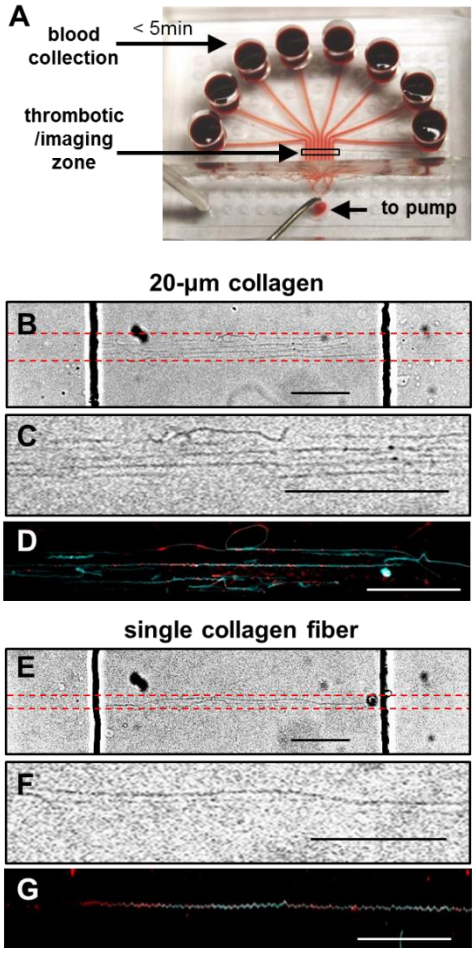

Figure 5-1 Microfluidic perfusion and micropatterned collagen fiber surfaces.

A, An 8-channel microfluidic device (each channel: 250-µm wide x 60-µm high) for perfusion of whole blood over a patterned collagen feature. CTI (4 µg/ml)-treated whole blood was transferred to each reservoir within 5 min of phlebotomy and was immediately perfused over the collagen zone at venous or arterial wall shear rates (100 or 1000 s^{-1}) controlled by a syringe pump connected at the outlet. **B, E,** Red dashed lines indicate location of patterned collagen. Collagen fibers were oriented perpendicularly to the flow channels (dark vertical lines are channel side walls). **B, C,** A 20-µm collagen zone was typically composed of 4 to 8 aligned collagen fibers. **E, F,** Single collagen fibers were confined within the 250-µm wide zone and no upstream or downstream collagen deposition was detected. Annexin V staining demonstrated TF liposomes (red) absorbed on fibers in the 20-µm collagen zone (**D**, cyan) or on a single collagen fiber (**G**, cyan). All scale bars: 50 µm in **B-G**.

5.2.3 Blood collection and preparation

Blood was collected via venipuncture from health donors (who were self-claimed to be free of alcohol and medication for at least 72 hr prior to donation) into D-Phe-Pro-Arg-CMA (PPACK, 100 μM, Haemtech, Essex Junction, VT) and apixaban (1 μM, Selleckchem, Houston, TX) or into CTI (4 or 40 μg/mL WB, Haematologic Technologies, Essex Junction, VT). Informed consent was obtained for each donor and performed in accordance with the University of Pennsylvania's IRB approval and the Declaration of Helsinki. Minimal amount of CTI (4 μg/mL) was used to block surface induced clotting during blood collection while still allowing thrombin generation through both the contact and/or the extrinsic pathways depending on TF surface concentration in patterned prothrombotic patches.[12, 13] The combination of 100 μM PPACK (irreversible thrombin inhibitor) and 1 μM apixaban (direct Xa inhibitor) was used to achieve complete thrombin inhibition.

Blood was treated with anti-human CD61 antibody (BD Biosciences, San Jose, California) and Alexa Fluor 647 fluorescent fibrinogen (Life Technologies, Grand Island, NY) for platelet and fibrin(ogen) detection, respectively. All experiments were initiated within 5 min after venous phlebotomy. Platelet thrombin biosensor was added into blood in a 1:9 ratio for the observation of thrombin generation in some experiments [55]. In these experiments, anti-human CD41a antibody was used for platelet detection.

5.2.4 Microfluidic thrombosis model

The 8-channel flow device was mounted perpendicularly to patterned collagen patches. Blood was perfused over collagen patches at either venous (100 s^{-1}) or arterial initial wall shear rates (1000 s^{-1}). Initial wall shear rate in flow channels was controlled with a syringe pump withdrawal at constant volumetric flow rate at the outlet on the device. Platelet accumulation, fibrin formation, and thrombin generation were monitored with a fluorescence microscope (IX81, Olympus America Inc., Center Valley, PA). Images were captured with a CCD camera (Hamamatsu, Bridgewater, NJ) and were analyzed with ImageJ (NIH, Bethesda, DC). To avoid edge-wall effects, average fluorescence after background subtraction in the center 65% region of the collagen patches were collected and recorded for data analysis.

5.2.5 Scanning electronic microscopy

Thrombi formed on single collagen/TF/VWF fibers were fixed under flow in situ with 2% glutaraldehyde in 0.1 M sodium cacodylate buffer for at least 3 hr at room temperature before they were removed from the PDMS microfluidic devices. The fixed thrombi were then incubated in the same buffer overnight at 4 °C, dehydrated in graded ethanol (with balance of sodium cacodylate buffer), finalized with hexamethyldisilane, air dried and stored under vacuum before sputter coating with gold/palladium and imaged by scanning electron microscopy.

5.2.6 Statistical analysis

Data were compared to controls using two-tail Student's t-test. P-value < 0.05 was considered statistical significant.

5.3 Results

5.3.1 Micropatterned zones of collagen fibers

Using a micropatterning microfluidic device, a 20-μm long zone of multiple collagen fibers was deposited on glass, followed by placement perpendicular to the fiber orientation of the 8-channel microfluidic blood perfusion device with 8 independent 250-μm wide flow channels for blood perfusion (**Figure 5-1A**). Typically, 4 to 8 individual collagen fibers were present in this 20-μm long zone (**Figure 5-1B, C**) which were then coated with lipidated TF (**Figure 5-1D**) and/or VWF in some experiments. No fibers were detected outside the 250-μm wide × 20-μm long patterning region. Similarly, a single collagen fiber was deposited across the confined 250-μm wide region (**Figure 5-1 E-G**). Annexin V staining confirmed that collagen fibers were able to bind by physisorption the TF liposomes containing phosphatidylserine (**Figure 5-1G)**. TF liposomes covered 30.4 ± 4.1 % (n = 11) of total collagen fiber surface, which corresponded to a relatively high TF surface concentration of ~1-10 TF molecules/μm^2 [13]. This TF surface concentration is comparable to that expected in adventitial regions of vessels or in human atherosclerotic carotid artery plaques.[139, 141]

5.3.2 A single collagen fiber with tissue factor triggers coagulation at venous wall shear rate

The combination of TF-coated collagen fibers, CTI-treated whole blood, and a venous shear rate (100 s^{-1}) resulted in a favorable condition for thrombin generation. Under this condition, platelets were able to adhere and form a substantial clot buildup of platelets and fibrin on either a 20-μm long collagen/TF zone (20-μm collagen/TF) or on a single collagen/TF fiber (**Figure 5-2A**). For the 20-μm collagen/TF, platelet

accumulation began in the first 100 sec of flow and continued over the entire 600 sec experiment, resulting in a clot mass that essentially filled the channel (60 μm high) over the collagen surface (**Figure 5-2C**). Within the clot formed on the 20-μm collagen/TF, thrombin was robustly detected using the thrombin activity biosensor bound to the deposited platelets (**Figure 5-2A**), while fibrin polymerization proceeded over the entire course of the experiment (**Figure 5-2C**) within the platelet deposit. For zones mimicking the defect size of a single endothelial cell (~20 μm), human blood robustly clots under venous flow conditions when presented the essential triggers of collagen and tissue factor. On a single collagen/TF fiber, platelets were able to adhere and accumulate, generate thrombin and fibrin under a venous flow condition (**Figure 5-2A, C**). For a single collagen fiber, the platelet deposits did not grow across the entire channel height, but reached a height of about 30 microns by 600 sec. This reduction in platelet accumulation (per unit area) on the single collagen/TF fiber was apparent throughout the entire time course of the experiment (**Figure 5-2C**). However, fibrin generation per unit area was not significantly affected by the reduction of stimulus size to the limit of a single collagen fiber that captured platelets (**Figure 5-2C**). Consistent with prior studies with lipid coated surfaces presenting TF, the use of lipidated TF alone without collagen was not able to trigger or support a clotting response in the wall shear rate range of 100 to 1000 s^{-1} [136, 137].

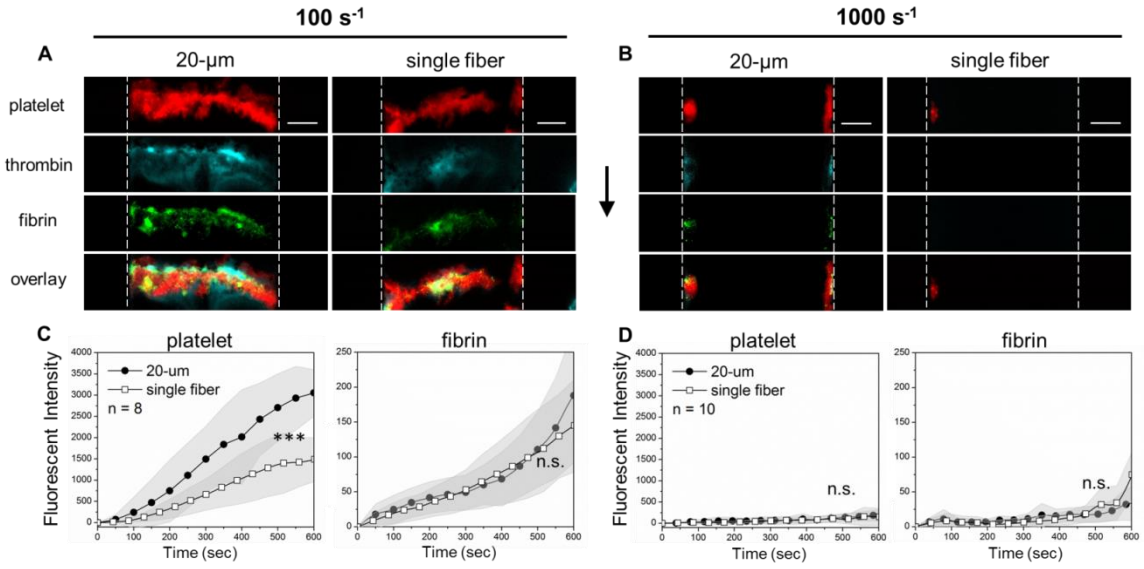

Figure 5-2 Thrombus formation on collagen/TF at venous and arterial flows conditions.

A, B, CTI-treated (4 μg/ml) whole blood was perfused over collagen/TF at venous wall shear rate (100 s^{-1}) or arterial wall shear rate (1000 s^{-1}). Blood coagulation occurred on the 20-μm long collagen/TF zone and the single collagen fiber at 100 s^{-1}, but not at 1000 s^{-1} (excluding side-wall accumulation where shear rates are reduced). **B, D,** For the center two-thirds of the channel (excluding the side-wall), platelet and fibrin fluorescence were imaged dynamically for 8 replicate clots at each condition. Vertical dashed lines represent flow channel side walls. Flow direction: top to bottom. Scale bar: 50 μm. (***$p < 0.005$; ns, not significant).

The production of thrombin and fibrin in this experiment was highly dependent on the lipidated TF bound to the collagen fibers. Fibrin generation was not detected on a 20-μm collagen zone or the single collagen fiber lacking TF (**Figure 5-3B,E and Figure 5-4**). In the absence of TF, thrombin generation in minimally perturbed blood (4 μg/mL CTI) requires a Factor XIIa/Factor XIa-dependent mechanism via the contact pathway, which is substantially inhibited by CTI during the short duration of the 600-sec experiment. Also, contact activation is generally slower and less efficient than the extrinsic pathway under flow condition.[12] Even with a low level of CTI (4 μg/mL), a small amount of thrombin likely was generated to enhance platelet activation and deposition on the 20-μm collagen zone lsacking TF, but was insufficient to generate any fibrin (**Figure 5-3E**). Relative to CTI-treated blood, complete inhibition of thrombin generation using PPACK/apixaban caused a significant reduction of platelet deposition on the 20-μm collagen lacking TF (**Figure 5-3D**). For perfusion of CTI-treated whole blood at venous shear rate, there was substantial platelet deposition on 20-μm collagen lacking TF, but much smaller deposits were seen on a single collagen fiber lacking TF (**Figure 5-4**). Platelet deposition on a single collagen fiber (no TF) was essentially negligible upon thrombin inhibition with PPACK/apixaban (**Figure 5-4C**). Thus, the combination of a platelet adhesive and stimulatory surface along with local thrombin generation triggered by TF (or much less potently by contact activation in CTI-treated blood) was required for platelet deposition on a trigger as small as a single collagen fiber.

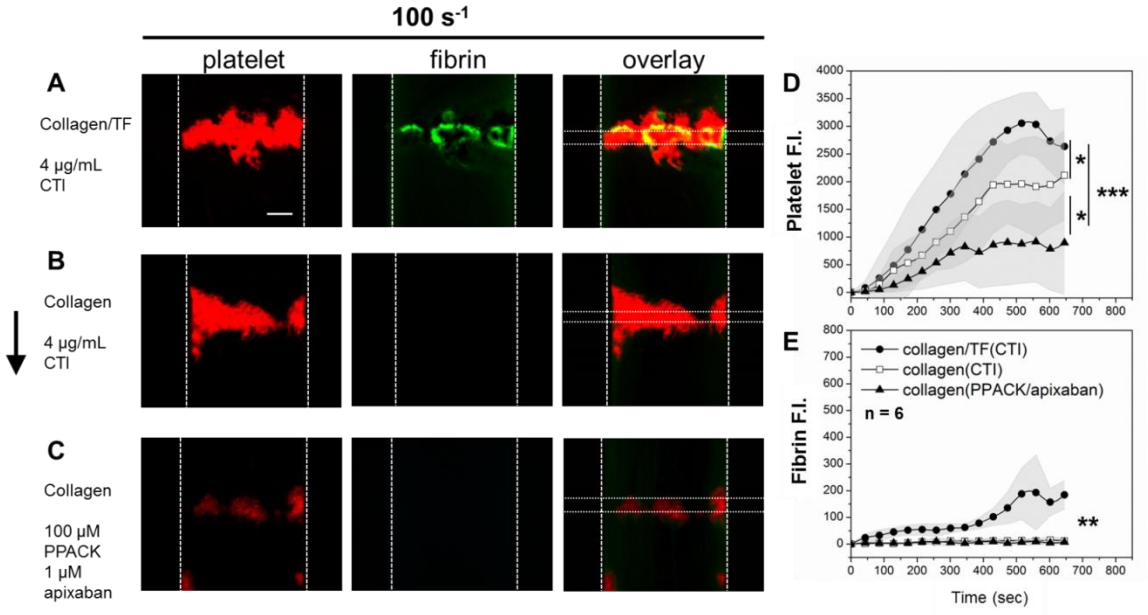

Figure 5-3 Thrombus formation on 20-µm collagen at venous flow condition.

Both platelet deposition (red) and fibrin formation (green) was observed when CTI-treated (4 µg/ml) whole blood was perfused over 20-µm collagen/TF at 100 s^{-1}. **B, C,** No fibrin deposition was observed when CTI or PPACK (100 µM) and apixaban (1 µM) treated blood was perfused over 20-µm collagen at venous flow condition. Horizontal dashed lines indicate the location of collagen strips (determined by bright field imaging) while vertical dashed lines outline flow channels. Flow direction: top to bottom. **D, E,** The presence of TF significantly promoted endpoint platelet and fibrin deposition. Scale bar: 50 µm. (* $p< 0.05$; ** $p< 0.01$; **** $p < 0.001$).

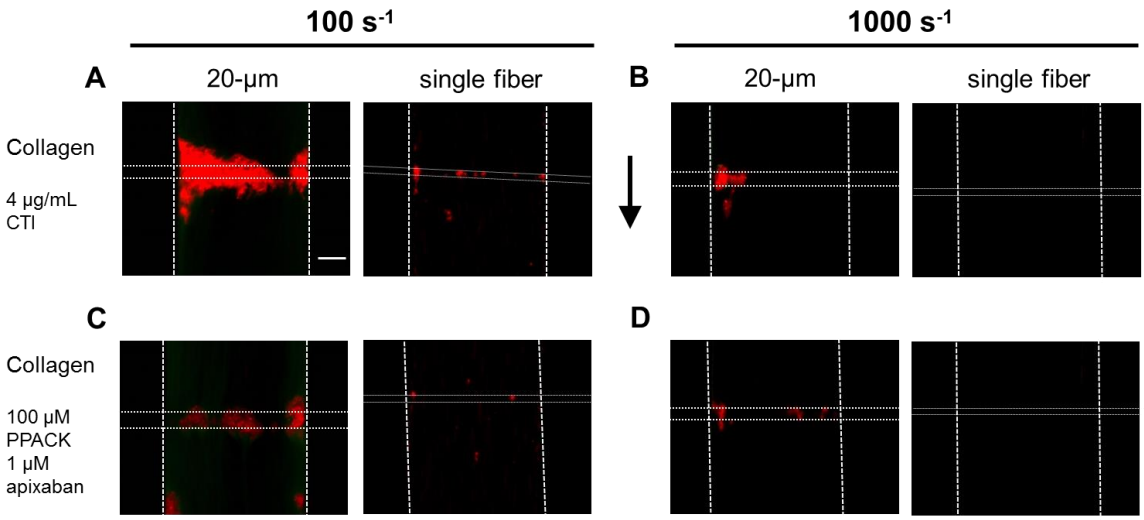

Figure 5-4 Thrombus formation on small patches of collagen (no TF) at venous and arterial flow conditions.

CTI (4 µg/ml **A, B**) or PPACK (100 µM) and apixaban (1 µM) treated whole blood (**C, D**) was perfused over a single collagen fiber or over 20-µm collage at venous (100 s^{-1}, **A, C**) or arterial (1000 s^{-1}, **B, D**) wall shear rate. Fibrin was not detected on collagen surfaces under these shear conditions. Without thrombin inhibition, substantial platelet accumulation was observed on 20-µm collagen. Reduction in platelet accumulation was a result of thrombin inhibition by PPACK and apixaban. Vertical dashed lines outline flow channels. Horizontal dashed lines indicate the location of collagen patches. Flow direction: top to bottom. Scale bar: 50 µm.

5.3.3 Patch threshold on collagen/TF at arterial flows when von Willebrand Factor is absent

Under arterial flow with wall shear rate of 1000 s^{-1}, reactive species washout in the boundary layer is greater (Péclet number > 10^3), platelet collision times are shorter (<5 msec) and shear forces per platelet are substantially greater (>1000 pN).[142, 143] Severely impaired thrombus formation was consistently observed on both 20-μm long zones of collagen and single collagen fibers, even in the presence of TF coating the collagen (**Figure 5-2B, D**). On the 20-μm collagen/TF zone, some platelets deposited near the channel side wall where the no-slip condition applies and the flow velocities were lower. However, in the center two-thirds of the rectangular channel (neglecting the side walls) where the wall shear rate was 1000 s^{-1}, platelet and fibrin deposition was negligible (**Figure 5-2B,D and Figure 5-3B**). Even with immobilized TF, a single collagen fiber was neither able to capture platelets nor able to support thrombin generation at 1000 s^{-1} (**Figure 5-2B,D and Figure 5-4**). This result was fully consistent with the essential role of VWF required for platelet GPIbα-dependent capture to collagen at arterial shear rates[144] that proceeds firm arrest mediated by GPVI-engagement and subsequent $\alpha_2\beta_1$ integrin activation. In the absence of VWF pre-adsorbed to collagen, a patch size threshold existed on 20-□m collagen/TF and on a single collagen fiber/TF due to a fundamental defect in platelet attachment at arterial wall shear rates, even with TF present. The level of wall shear stress (10 dyne/cm^2) at this arterial condition was insufficient to cause plasma vWF to unfold and form fiber aggregates on the collagen, as previously observed at pathological wall shear stresses of >300 dyne/cm^2 (at wall shear rate of >30,000 s^{-1}) typical of stenosis.[145]

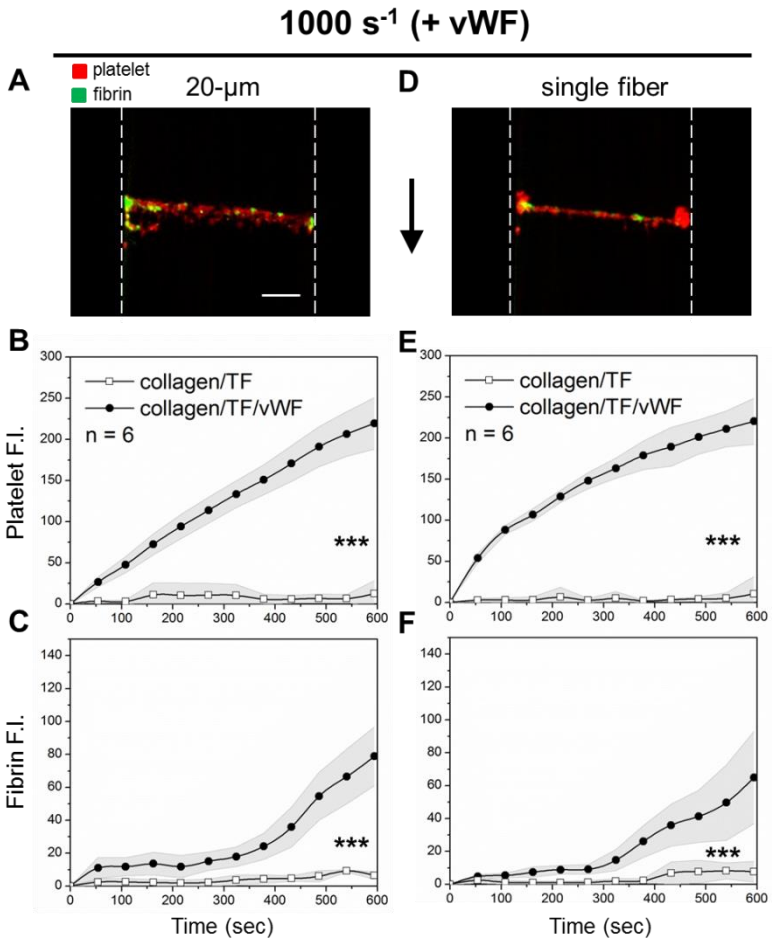

Figure 5-5 For arterial flow, coagulation on collagen/TF fibers requires pre-adsorbed VWF.

A, D, CTI-treated whole blood was perfused at arterial wall shear rate 1000 s^{-1} over 20-µm collagen/TF zone plus VWF or over a single collagen/TF fiber plus VWF. With VWF, the collagen/TF accumulated platelets (red) and fibrin (green) for the 20-µm zone or the single fiber by 600 sec. **B, E,** Onset of platelet deposition on collagen/TF/VWF fibers was instantaneous after flow initiation. **C, F,** There was ~ 300 sec delay in fibrin production on both 20-µm zone and a single collagen/TF/VWF. **B-E,** In comparison, both platelet deposition and fibrin formation were essentially absent on collagen/TF lacking VWF. Vertical dashed lines represent flow channel side walls. Flow direction: top to bottom. Scale bar: 50 µm. (***$p < 0.005$).

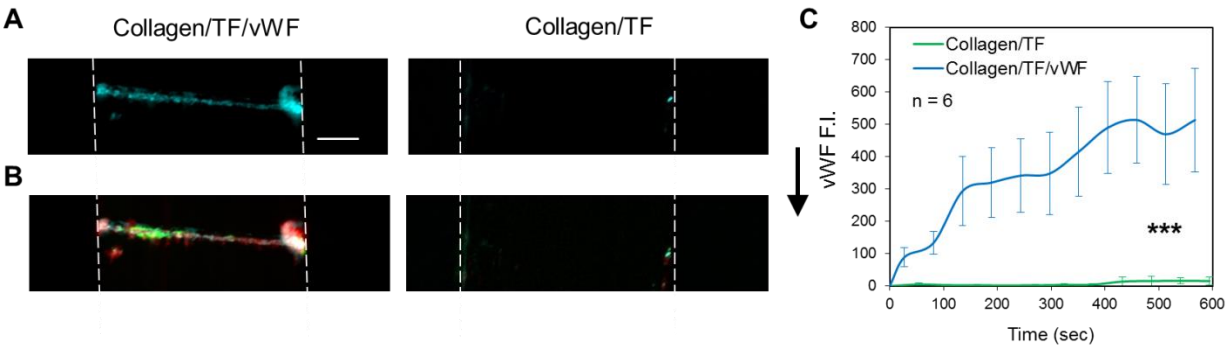

Figure 5-6 Incorporation of plasma vWF into formed thrombus on single collagen/TF/VWF fibers.

A, B, Detected VWF (cyan) on a single collagen/TF/VWF fiber is co-localized with platelet (red). **C,** VWF signal on single collagen/TF/VWF increased significantly over time. Negative control images confirm that a single collagen/TF fiber lacking pre-adsorped VWF is not able to capture VWF from plasma. All images were taken at the end of flow experiments (t = 600 sec). Vertical dashed lines outline flow channels. Flow direction: top to bottom. Scale bar: 50 μm. (*** $p < 0.005$).

5.3.4 Single collagen fiber with TF and VWF supports coagulation at arterial shear rate

At an arterial wall shear rate of 1000 s^{-1}, pre-adsorption of VWF to collagen eliminated the patch size threshold and promoted platelet and fibrin deposition on both the 20-μm collagen/TF/VWF and the single collagen fiber/TF/VWF feature (**Figure 5-5**). On collagen/TF/VWF, platelet deposition began immediately after flow initiation. The rate of platelet deposition on the 20-μm collagen/TF/VWF was relatively constant over the 600 sec experiment while a gradual slowing in platelet deposition was observed on a single collagen/TF/VWF fiber after the first 100 sec (**Figure 5-5B,E**). Under arterial flow, fibrin generation was less abundant than that observed for venous flow conditions (**Figure 5-5C**), consistent with previously observations for 250-μm collagen/TF features lacking pre-adsorbed VWF.[24] Fibrin generation was however no longer confined near the side walls of the device with reduced flow, as was seen for collagen/TF (no VWF). Fluorescent staining revealed that the captured platelets also released platelet VWF and the clot localized VWF signal increased with time (**Figure 5-6**). In contrast, the single collagen/TF fiber lacking pre-adsorbed VWF did not exhibit the ability to capture either flowing platelets or sufficient plasma VWF from blood (**Figure 5-6 and Figure 5-7C**). Clearly, pre-adsorbed VWF mediated more efficient platelet deposition than collagen alone, as expected for high shear conditions [146]. Furthermore, the presence of TF significantly promoted the probability of platelet deposition on a single VWF coated collagen fiber. Unlike the complete coverage of the single collagen/TF/VWF fiber by platelets and fibrin (**Figure 5-7A**), scattered platelet microaggregation but not fibrin deposition was observed on the single collagen/VWF fiber without immobilized TF

(**Figure 5-7B**). The maximum height of the formed clot on a single collagen/TF/VWF fiber was limited to ~10 μm over the collagen fiber on the surface (**Figure 5-8**), considerably smaller than the nearly occlusive clot heights seen over the 20-μm collagen/TF/VWF zone under venous flow conditions. Scanning electron microscopy (SEM) images show only three to four layers of platelet deposition on the single collagen/TF/VWF fiber (**Figure 5-7D, E**). The bottom layer platelets were fully spread and adherent to the surface, whereas the top layers platelets displayed an activated and rounded morphology with pseudopods.

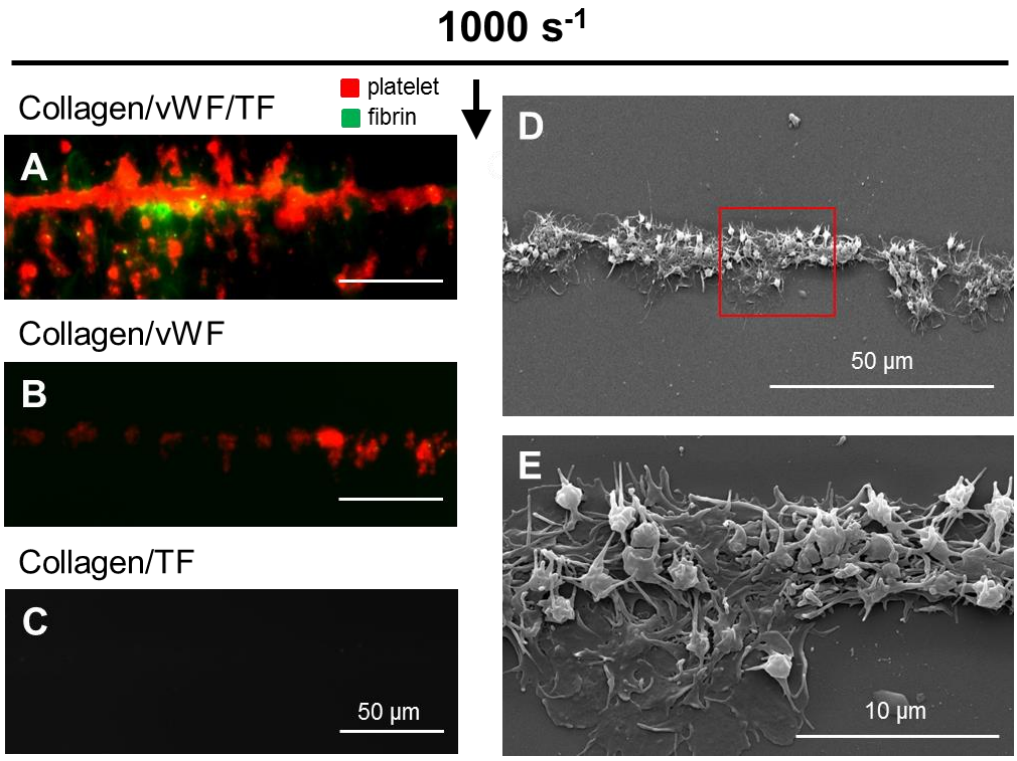

Figure 5-7 VWF and TF synergistically promote coagulation on single collagen fiber at arterial flow.

A, CTI-treated whole blood was perfused at arterial wall shear rate 1000 s^{-1} over single collagen fibers. Platelets (red) and fibrin (green) coated the single collagen/vWF/TF fiber by the end of 400 sec. **B,** Scattered small platelet aggregates but not fibrin deposited on the single collagen/vWF fiber. **C,** No platelet or fibrin was captured on the single collagen/TF fiber lacking VWF. Scale bars represent 50 µm in A-C. **D,** SEM image showing the structure of a thrombus formed on a single collage/vWF/TF fiber. **E,** Closer view of the area enclosed in the red box showing three to four layers of platelet deposition on the collagen/vWF/TF fiber. Bottom layer platelets were flat and fully adherent to the surface, whereas top layer platelets were activated but unspread. Flow direction: top to bottom.

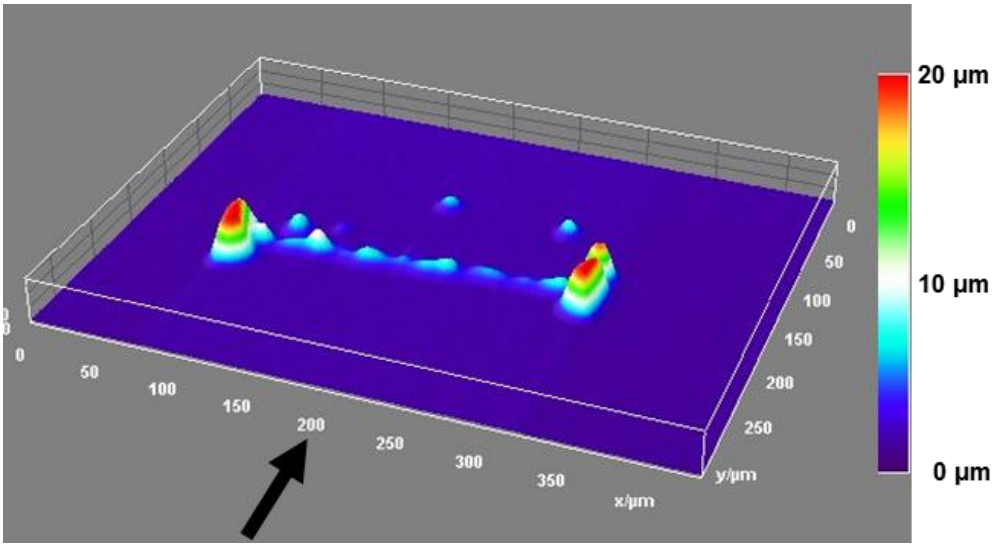

Figure 5-8 Surface plot of platelet deposits on a single collagen/TF/VWF fiber.

Surface plots of platelet deposits on single/TF/vWF fibrils were constructed in Image J with stacks of confocal images taken at the end of the experiments (t = 600 sec, z-step size = 2 µm). More platelets tend to accumulate along the wall due to edge-wall effect. However, the maximum height of platelet mass is 8-10 µm in the center two-thirds of the channel where all the dynamic fluorescence data was collected.

5.4 Discussion

In this microfluidic study with human blood, we define the conditions for flowing blood to clot on features as small as a single collagen fiber. At venous whole blood flow, a single TF-coated collagen fiber promotes robust coagulation in the absence of any apparent patch size threshold. For arterial blood flow over collagen/TF lacking VWF (and platelets), the convective removal of FXa and FIXa from the TF liposomes quenched any observable thrombin production and subsequent fibrin polymerization. To overcome patch size thresholding at arterial flows, human blood exploits VWF to initiate a full coagulation response on a biological unit as small as a single collagen fiber.

Numerous mouse studies,[130, 133, 147] ex vivo studies with human blood in microfluidic assays,[55, 148, 149] and multiscale numerical modeling [62, 150-152] have quantified the complex hemodynamic and transport interactions during coagulation.[153] Beyond the highly regulated biochemical networks associated with platelet signal transduction and the coagulation protease cascade, relevant physical processes during hemostasis include: (i) platelet margination to the wall due to red blood cell motions, (ii) the diffusivity of reactive species and their enhanced removal by convection or intraclot permeation, (iii) modulation of intraclot diffusion and permeation by platelet retraction, and (iv) the effect of flow on the rate and adhesive success of platelet encounters with the surface.[130, 147, 149, 154-156] Importantly, the structural and kinetic properties of VWF facilitate platelet capture at high shear conditions [144] and VWF deficiency is strongly linked to bleeding phenotypes.[157]

A plasma or platelet rich plasma (PRP)-based static experimental system does not fully reflect the complexity of whole blood clotting under hemodynamic conditions. With flow, red blood cells drive elevated platelet levels near the wall and this phenomenon does not occur in flowing platelet rich plasma. With flowing blood, the platelet deposition density greatly exceeds that expected under static conditions. Platelet surface area in the dense retracted core of a clot can reach levels as high as 100 $cm^2/\mu L$ of clot.[153] With platelet deposition, the membrane surface area is greatly increased for accumulation of coagulation factors (such as FXa), a process absent in plasma studies of patch size thresholding. Deposited platelets can also create restricted transport zones to facilitate assembly of coagulation components in the core of the hemostatic thrombus [55, 130, 133, 147] as well as offering $\alpha_{2b}\beta_3$ binding sites to anchor fibrin polymerization under flow.

These studies address the minimum length scale and biochemical criteria necessary for a hemostatic response and are fully consistent with the known bleeding risks linked to deficiencies in platelets, thrombin generation, or VWF. Consistent with our findings with human whole blood, in vivo laser injury of the mouse cremaster arteriole causes a micron-scale wall defect [158] to drive platelet deposition, thrombin generation,[55, 130] and fibrin polymerization, especially in the core of the clot.[133, 147] Clot production under flow is also highly relevant to dangerous thrombotic events of coronary artery occlusion. An important issue related to the patch size threshold is whether a surface defect is of sufficient size and potency to cause vessel occlusion at a given prevailing flow condition. In coronary stenosis, pathological shear rates are many

fold greater than the physiological levels of the current study. Collagen triggers plasma VWF fiber formation upon acute exposure of platelet free plasma to a pathological shear of over 30,000 s^{-1}.[145] Also, these large insoluble fibers can capture and support shear induced platelet activation.[159] The observation of a single collagen fiber coated with TF and VWF supporting clotting is also consistent with an earlier study of whole blood perfused over VWF pre-coated microspheres (2-μm diameter) at a pathological shear rate of 10,000 s^{-1} with platelet aggregation extending over 5 bead diameters downstream of the initial platelet-bead adhesion.[160]

The maximum height of microthrombi on single collagen/TF/VWF fibers was ~10 μm with three to four layers of platelets, indicating a self-limiting response at arterial flow condition. The rapid flow-enhanced elution of platelet agonists may be a cause of self-limited clot growth on a single collagen fiber. Even though endothelium was not included in this study, evidence for microthrombi formation at extremely small sites of endothelial erosion on developing coronary plaque is also consistent with our findings.[161, 162] Spatial heterogeneity of platelet activation is well documented in laser injury of mouse cremaster arterioles [133] where thrombin [55] and fibrin are localized in the platelet P-selectin positive core. SEM images (**Figure 5-7**) show platelets in individual layers exhibit different morphologies, even for a single fiber triggering event, suggesting heterogeneity in the level of platelet activation along the height of the deposit. Furthermore, we found TF and VWF synergistically promoted thrombus formation on single collagen fibers at arterial flow condition. By capturing platelets with VWF at flow arterial conditions to a single fiber presenting TF, the generated FXa and

FIXa were kinetically significant and sufficiently localized to promote continued platelet capture, thrombin generation, and fibrin polymerization. For defects as small as a single collagen fiber, the molecular components of the extrinsic pathway function at arterial flow conditions because of local VWF-dependent platelet deposition. For exceedingly small arterial defects, platelets are particle-based sensors that allow engagement of the coagulation protease cascade under high flow.

5.5 Conclusions

In conclusion, we demonstrated in a microfluidic system that initiation of clotting of flowing human whole blood overcomes a patch threshold response to stimuli patch size when TF and VWF are present. At venous shear rate, the presence of tissue factor can trigger a full clotting response with platelet deposition, thrombin generation, and fibrin polymerization on a single collagen fiber. Pre-adsorbed VWF and TF enabled clotting on a single collagen fiber at arterial shear rate. Blood coagulates on surface triggers as small as a single collagen fiber to obviate any physiological patch size threshold.

Chapter 6 : Dynamics of thrombin generation and flux from clots during whole human blood flow over collagen/tissue factor surfaces

6.1 Introduction

Human thrombin is a multifunctional protease central to coagulation by its enzymatic cleavage of platelet PAR1 and PAR4 receptors [163], cleavage of fibrinogen to fibrin monomer [164], generation of Factor XIIIa (FXIIIa) [165, 166], and feedback activation of Factor XIa (FXIa) [13, 18]. The extrinsic coagulation pathway is triggered by tissue factor/Factor VIIa (TF/FVIIa) which generates Factor Xa (FXa) and Factor IXa (FIXa) and is essential for hemostasis. In contrast, deficiencies in the contact pathway (Factor XII [FXII] and FXI) are not linked to strong bleeding phenotypes.

The kinetics of the extrinsic tenase (TF/FVIIa), the intrinsic tenase (FIXa/FVIIIa), and prothrombinase (FXa/FVa) have been extensively measured [167-169] and kinetically modeled for plasma [170-173] or purified enzymes with added lipid [174-176], and platelet rich plasma [51, 177-179]. These prior kinetic studies explore rate processes in a closed and isotropic context (i.e. a tube). However, clotting under hemodynamic flow is an open system, involving platelet adhesion and activation on a surface as well as rapid build-up of a dense platelet core surrounded by less activated platelets in surrounding shell of the clot. The core of the clot is highly contracted with P-selectin positive platelets [133, 147], localized thrombin and fibrin [55, 130], and localized disulfide reductase activity [180]. The kinetics of thrombin generation are less well understood in this hierarchical structure where intrathrombus transport and binding effects may control reactions [150, 181-184]. For example, fibrin is known to inhibit

thrombin via its antithrombin-I activity [185-187]. Under venous flow, γ'-fibrin has been shown to limit thrombin transport, fibrin production, and clot size [188].

Direct thrombin or Factor Xa (FXa) inhibitors are orally available and clinically approved and do not requiring frequent coagulation monitoring in patients [189]. The reduction of thrombotic risk, while still allowing for sufficient hemostasis to prevent undesired bleeding, is central to therapeutic potency and dosing. Calibrated automated thrombinography (CAT) is a calibrated thrombin generation assay that reports thrombin concentration in activated plasma samples as a function of time [190]. CAT measurement determines the coagulability of plasma, potentially helpful for clinical diagnosis and drug monitoring. However, the CAT assay provides limited information on the actual dynamics of thrombin generation in platelet-rich clots formed under flow. By recreating hemodynamic flow over procoagulant surfaces, the dynamics and pharmacology of thrombin generation can be studied with human blood ex vivo. In microfluidic clotting assays, fibrin generation is often used as an indirect indicator for thrombin activity [12, 13, 23, 24, 31]. Our lab previously developed a peptide-based platelet targeting biosensor to report platelet associated thrombin activity in both microfluidic and animal thrombosis models [55, 130]. To our knowledge, there has been no direct quantitative measurement of thrombin flux from a growing thrombus under hemodynamic flow. This lack of measurement may be due to the limited sensitivity of immunoassays to detect released thrombin in the stable complex of thrombin-antithrombin (TAT) since released thrombin would be severely diluted in macroscopic flow systems with mL/min-scale perfusion. In contrast, microfluidics allows detection of clot-released species by limiting their dilution through use of μL/min-scale perfusion.

Theoretical and experimental studies have suggested thrombin generation is sensitive to prevailing shear rate and surface tissue factor (TF) levels [25, 191, 192]. At a venous shear rate condition, thrombin flux is predicted to be within a range of 10^{-13}-10^{-11} nmole/μm^2-sec [191-193]. Using plasma perfusion, our group previously demonstrated in a membrane microfluidic system that both wall shear rate and thrombin flux regulate physical structure of deposited fibrin fibers. Under venous shear condition, a wall thrombin flux of 10^{-11} nmole/μm^2-sec is required for platelet-free plasma to form a 3-dimensional fibrin network [193], which is the fibrin structure that is usually observed in whole blood thrombi formed on the surface with collagen and TF at venous shear rates [13]. In blood, antithrombin (AT) is a potent and rapid thrombin inhibitor [194]. Thrombin half-life is less than a minute in the presence of AT [195], a reaction accelerated by heparin. Thrombin-antithrombin (TAT) complex measurement has been routinely used to estimate thrombin level in plasma samples [51, 196, 197]. Here we measure thrombin flux from TF bearing collagen surface and aggregated platelets at a venous shear rate in a human whole blood microfluidic thrombosis assay by collecting effluent at the outlet of the microfluidic system and subsequently measuring TAT complex concentration with enzyme linked immunosorbent assay (ELISA).

6.2 Materials and Methods

6.2.1 Materials

Anti-human CD61 (BD Biosciences, San Jose, CA), Alexa Fluor®647 conjugated human fibrinogen (Life Technologies, Grand Island, NY), H-Gly-Pro-Arg-Pro-OH (GPRP, EMD Chemicals, San Diego, CA), corn trypsin inhibitor (CTI, Haematologic

Technologies, Essex Junction, VT), GR144053 trihydrochloride (Tocris Bioscience, Minneapolis, MN), Ethylenediaminetetraacetic acid (EDTA, Sigma, St. Louis, MO), Sigmacote® siliconizing reagent (Sigma, St. Louis, MO), Human Thrombin-Antithrombin Complex ELISA Kit (Abcam, Cambridge, MA), Dade® Innovin® PT reagent (Siemens, Malvern, PA), Collagen Type I Chrono-Par^{TM} aggregation reagent (Chrono-log, Havertown, PA), and Sylgard® 184 Silicone Elastomer kit (Dow Corning, Auburn, MI). O1A6 FXI antibody was a gift from Dr. Andras Gruber (Department of Biomedical Engineering, Oregon Health and Science University).

6.2.2 PDMS patterning and flow device

Polydimethylsiloxane (PDMS) devices were fabricated as previously described [20, 22]. Protein patches with defined dimensions were patterned on glass slides with single channel devices (250 or 1000 μm in width, 60 μm in height). Multi-channel flow chambers with 8 evenly spaced flow channels (250 μm in width, 10000 μm in length, and 60 μm in height) diverging from a single inlet and converging into a single outlet were used for microfluidic thrombosis assay. All PDMS devices have features on their bottom allowing them to be reversibly vacuum bonded onto glass slides.

6.2.3 Analysis of system response time

A model microfluidic system was characterized in COMSOL Multiphysics® Modeling Software (COMSOL Inc., Burlington, MA). A rectangular domain (10000 μm by 60 μm) with created to represent one lane of the actual microfluidic device. The local wall shear rate was maintained at $200s^{-1}$, consistent with the experiments. The thrombin

flux was imposed between 100 μm and 350 μm and the transport was mainly governed by the convection and diffusion assuming no hindrance from the developing clot. To calibrate the system response time, a rectangular flux signal with amplitude of 10^{-11} nmol/μm-sec was applied for duration of 1 second. The system was propagated with a constant timestep of 0.05 sec to obtain the average thrombin concentration at the outlet. Similarly, an empirical thrombin flux fitted with the experimental measures was applied to obtain the resultant mixing-cup average concentration at the outlet.

6.2.4 Preparation of thrombotic patches

Glass slides were treated with Sigmacote® to retard surface triggered clotting. To generate collagen patches on glass slides, collagen type I (1mg/mL, 5 μL) followed by bovine serum albumin (0.5% BSA in Hepes Buffered Saline, 20 μL) was perfused through the main channel on a single channel patterning device [20]. The length of a collagen patch (250 μm or 1000 μm) is defined by the dimension of the main channel. Tissue factor can be added by subsequent perfusion of 10 μL of Dade Innovin® PT reagent through the main channel and incubation over patterned collagen for 30 min before a BSA wash. The 23 nM PT reagent stock [96] was diluted 10-fold and 200-fold to achieve high and low surface TF surface densities of ~1, and ~0.1 TF molecule/μm^2, respectively. Sorbed TF lipid vesicles were stained with FITC-annexin V. TF surface densities were estimated by fluorescent imaging of stained vesicles, as previously described [13, 23].

6.2.5 Blood collection and sample preparation

Blood was collected via venipuncture from healthy donors who provided consent under approval of University of Pennsylvania Institutional Review Board and were free of any medication or alcohol for at least 72 hr prior to donation. Blood was collected into syringes with high dosage of CTI (40 μg/mL) and was transferred into Eppendorf tubes where it was labeled by CD61 antibody (2 %v/v) and fluorescent fibrinogen (1.3% v/v) for platelet and fibrin epifluoresence detection, respectively. In some of the microfluidic experiments, additional treatments that were added to blood sample prior to perfusion to block platelet aggregation or fibrin polymerization. These additional treatments are indicated in the Results.

6.2.6 Microfluidic thrombosis assay

After protein patterning, the single channel patterning device was replaced with the multichannel flow device. The flow channels were placed perpendicularly to patterned TF bearing collagen patches. Labeled whole blood was transferred to syringes which were then mounted on a PHD 2000 syringe pump (Harvard Apparatus, Holliston, MA) operating on an infusing mode. Blood was infused into the flow device at a constant flow rate of 16 μL/min which corresponds to an initial wall shear rate of 200 s^{-1}. Platelet aggregation and fibrin formation were simultaneously monitored with a fluorescence microscope (IX81, Olympus America Inc., Center Valley, PA). Images were captured with a CCD camera (Hamamasu, Bridgewater, NJ) and were analyzed with ImageJ (NIH, Bethesda, DC). The outlet of the flow deivce was blocked with 10 μL of EDTA. Calcium dependent thrombin generation in blood was immediately quenched by

EDTA once blood exits the device. Blood sample was collected from the outlet every other minute. Another 10 μL of EDTA was added to block the outlet immediately after sample collection. Collected blood samples were allowed to sit for at least 10 minutes for TAT complex formation before subsequent steps.

6.2.7 TAT-ELISA assay

Collected blood samples were centrifuged at 1300 g for 15 min. TAT complex concentration in isolated platelet poor plasma was detected in a sandwich TAT-ELISA assay. Background TAT level was determined by measuring TAT concentration in plasma sample isolated from blood that was quenched with EDTA right after phlebotomy. Since AT reacts with thrombin in a 1:1 stoichiometric ratio, measured average TAT concentration ($\bar{C}$) within the 2 min time interval between sample collections was converted to an average thrombin flux ($\bar{J}$) using the following equation:

$$\bar{J} = \frac{\bar{C}Q}{A} \qquad \text{Equation 1}$$

where Q is flow rate (16 μL/min) and A is total thrombotic area in each device.

6.3 Results

6.3.1 Device response time

Release of a diffusible species from a surface into a flow stream is a classic concentration boundary layer phenomenon that can influence the dynamics of measurement of the species at the system outlet. Additionally, for sampling parabolic flows at the system outlet, the faster streamlines at and near the center of the flow contribute more volume per unit time than the slower streamlines at the wall boundary.

The discrete sampling of volume at the system exit flow where the species concentration may be nonuniform is defined as the "mixing-cup" concentration and involves weighting the concentration profile by the velocity profile [198]. In order to calculate the lag time of the microfluidic device and exit line and thus relate surface events to remotely sampled volumes at the exit, a computational model with a rectangular domain was created and the transport of thrombin was calculated by standard Finite Element Method in COMSOL (**Figure 6-1**). A flux with constant amplitude of 10^{-11} nmol/μm-sec and duration of 1 second was applied at the bottom of the channel near the entrance. Within 1 second, the thrombin concentration was high over the entrance (where collagen/TF resides in the experiment) due to the release of soluble thrombin from the bottom boundary; there was no significant thrombin yet reaching the outlet. After 1.6 seconds, the outlet (mixing-cup average) thrombin concentration begins to rise as thrombin is transported advectively by the flow and also by molecular diffusion. By 5 seconds, there was essentially no thrombin left near the entrance since the imposed thrombin flux only lasted for 1 second, indicating complete and rapid washout at a wall shear rate of 200 s^{-1}. By 7 seconds, the concentration of thrombin collected at the outlet reached a maximum. It took almost 20 seconds for the concentration of thrombin to decay back to zero at the outlet (**Figure 6-1B-C**). Overall, the simulation demonstrated that the microfluidic assay (**Figure 6-1A**) allows the detection of locally generated thrombin at the collagen site with only a minor lag time of ~ 10 sec. Also, dilution of thrombin (or TAT) in the prevailing microfluidic flow was predicted to allow detection of nM-levels of TAT in the effluent.

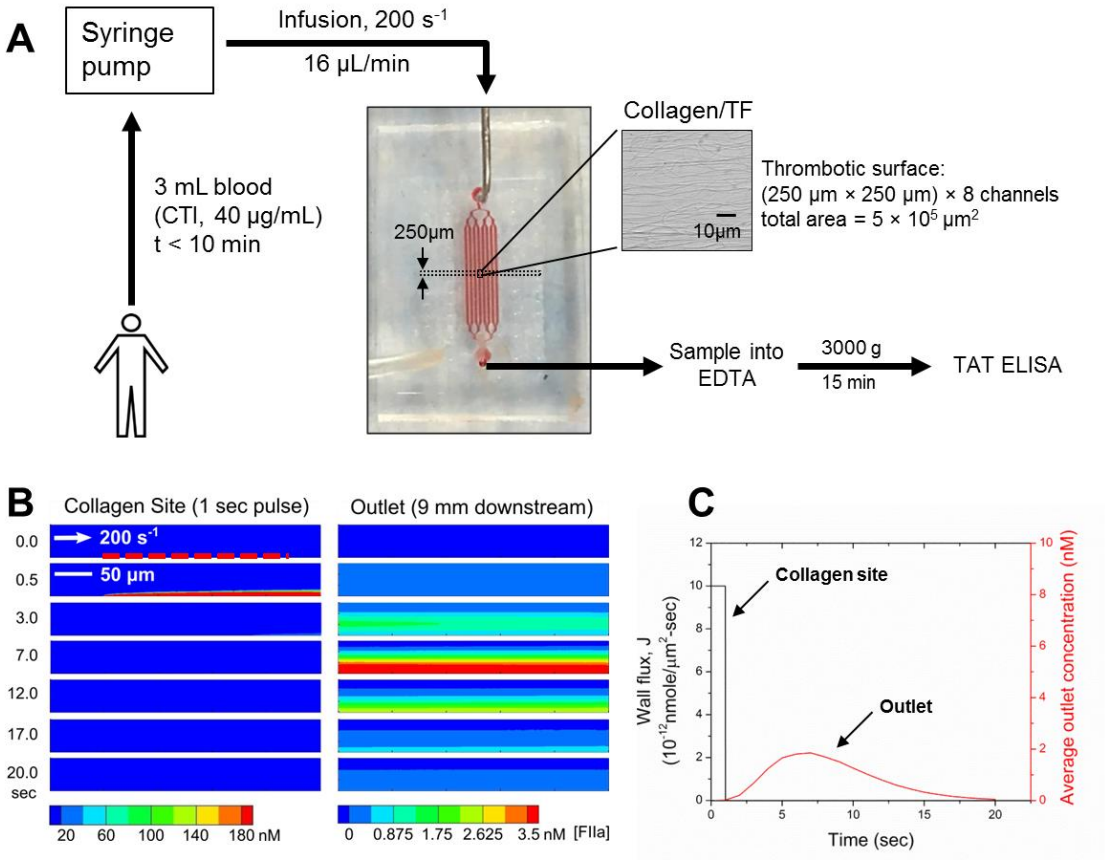

Figure 6-1 Microfluidic setup for measuring thrombin flux during whole blood thrombosis on collagen/TF surface.

A, A microfluidic device with 8 channels (each channel: 250-µm in width and 60-µm in height) diverging from a single inlet and converging into a single outlet was used for whole blood perfusion over collagen/TF surface. Blood was collected into CTI (40 µg/mL) and was loaded into syringes which were subsequently mounted on a syringe pump. Blood infusion was initiated within 10 min of phlebotomy at a constant flow rate of 16 µL/min (initial wall shear rate = 200 s^{-1}). Device outlet flow was collected into EDTA to quench thrombin generation with EDTA and allow for TAT formation. Blood samples (collected every 120 sec) were subsequently centrifuged and analyzed by TAT ELISA. **B,** The microfluidic system was characterized with a COMSOL convection-diffusion model. To calculate the device response time, thrombin flux signal from a 250-µm long surface domain with amplitude of 10^{-11} nmole/µm^2-sec was imposed as a boundary condition for duration of 1 sec. Location of the surface domain is indicated by a red dashed line. **C,** Average thrombin concentration at the outlet peaked after a delay of 7 sec and leveled off to zero by 20 sec.

6.3.2 Clotting under flow: Fibrin rapidly captures thrombin

Platelets immediately adhered and accumulated on collagen/TF surface (~1 TF molecule/μm^2) after initiation of whole blood flow initiation, whereas fibrin generation was detected after a 250 second lag followed by a nearly linear increase until the end of the experiment at 800 sec (**Figure 6-2 and Figure 6-3**). Under these conditions of platelet deposition and fibrin generation on the collagen/TF surface, very little TAT was detected over the 800 sec experiment unless Gly-Pro-Arg-Pro (GPRP, 5 mM) was used to prevent fibrin polymerization (**Figure 6-2B**). Collection of effluent into benzamidine (instead of EDTA) to inhibit thrombin prevented the immunodetection of TAT (*not shown*), indicating that free thrombin was eluted off the clot in the presence of 5 mM GPRP, that then complexed with antithrombin to form TAT in the EDTA-treated sample. Fibrin captured >85% of locally generated thrombin (**Figure 6-2B**). Thus, the fibrin polymerization inhibitor GPRP was added to all subsequent experiments to eliminate fibrin capture of thrombin and allow detection of TAT in the effluent. Prior studies have shown that GPRP has a minor effect on platelet deposition at the low forces of venous flow conditions [24]. Also, the contribution of the contact pathway in this microfluidic assay has been shown to be minimal for 40 μg/mL CTI-treated whole blood when compared to the contribution of the TF-driven extrinsic pathway [26].

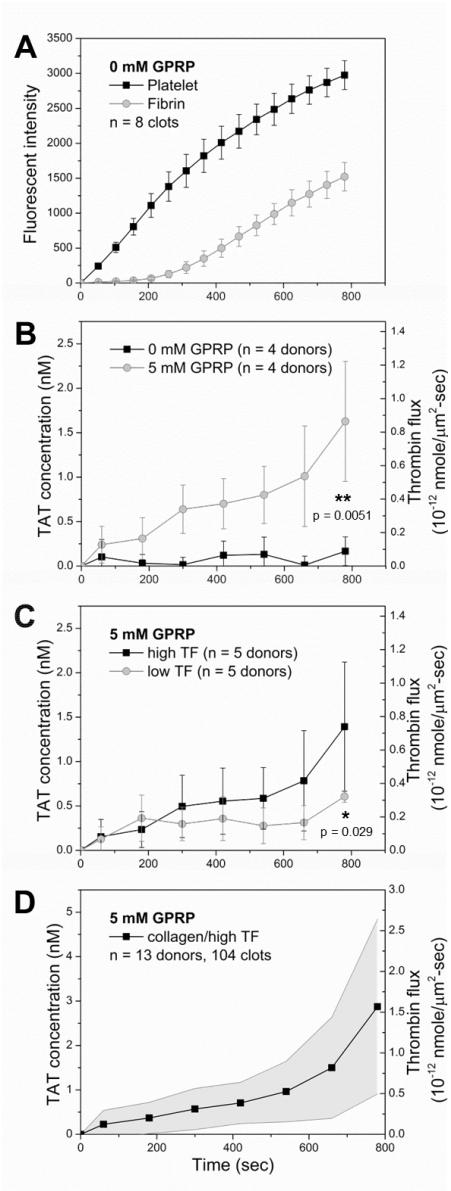

Figure 6-2 Thrombin flux from clots growing on collagen/TF.

A, Dynamics of platelet aggregation (■) and fibrin formation (○) during CTI-treated (40 μg/mL) whole blood perfusion over collagen/high TF (1 molec/μm^2) at initial wall shear rate of 200 s^{-1}. **B,** Measured TAT concentration and thrombin flux during blood perfusion over collagen/high TF in the presence (○) and absence (■) of GPRP. **C,** TAT concentration and thrombin flux for TF surface concentration from 1 molec/μm^2 (■) to 0.1 molec/μm^2 (○). **D,** Averaged TAT concentration and thrombin flux from 13 healthy donors for blood perfusion (40 μg/mL CTI and 5 mM GPRP) over collagen/high TF at 200 s^{-1}. * $p < 0.05$, ** $p < 0.01$.

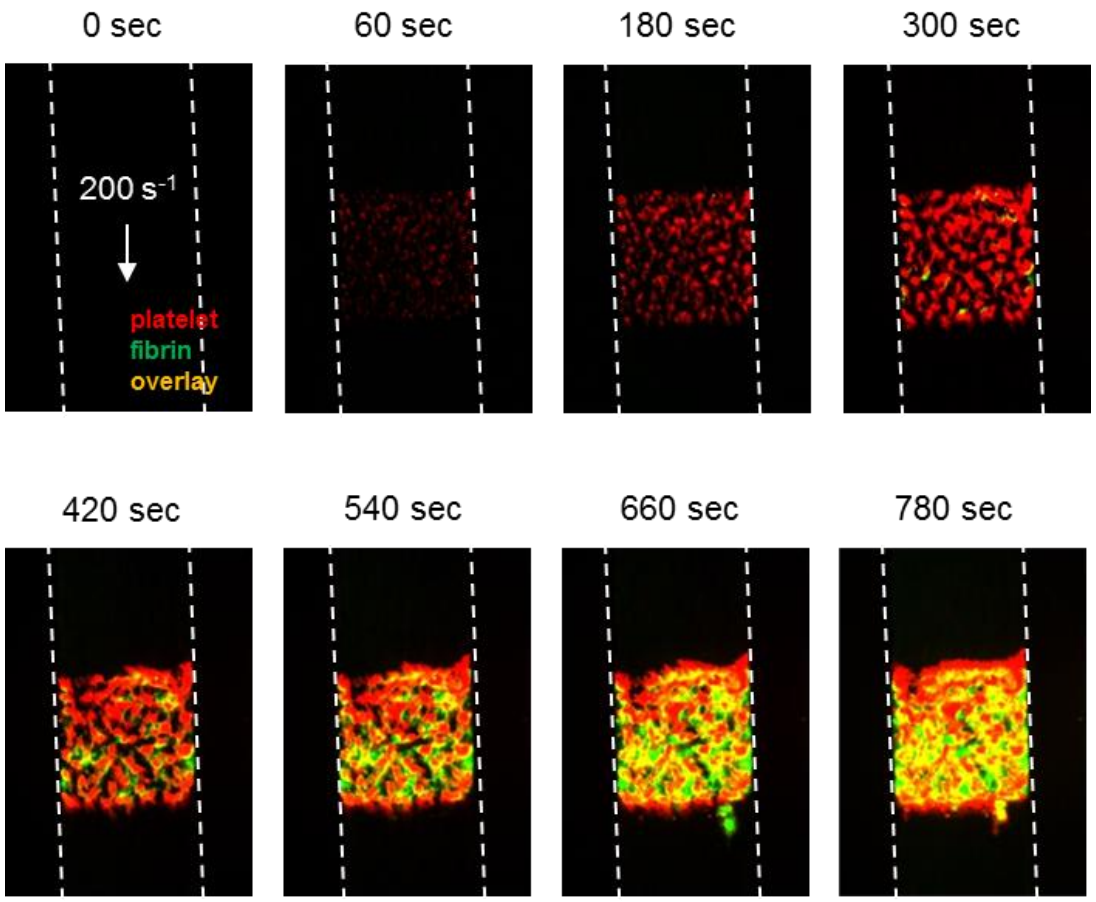

Figure 6-3 Platelet aggregation and fibrin formation on collagen/TF.

Platelet deposition (red) and fibrin formation (green) at indicated time points during blood perfusion (40 μg/mL CTI) over collagen/TF (1 molec/μm^2). Initial wall shear rate = 200 s^{-1}. Flow direction: top to bottom. Dashed lines outline flow channels.

6.3.3 Increased surface TF concentration promotes thrombin flux

Since fibrin formation requires a threshold concentration of surface TF [25], we tested if the amount of immunodetected TAT complex in the effluent was dependent on TF concentration on the collagen surface. At ~1 TF molec/μm^2 (collagen/high TF), the TAT concentration displayed a slow increase during the first 500 sec and then an accelerated increase during the following 300 sec. By 800 sec, the thrombin flux reached ~ 0.8×10^{-12} nmole/μm^2-sec (**Figure 6-2C**). At ~ 0.1 TF molec/μm^2 (collagen/low TF), there was a brief initial increase of TAT concentration within the first 200 sec. Between 200 and 600 sec, TAT concentration remained largely constant. After 600 sec, accelerated increase of the TAT concentration was observed. By 800 sec, thrombin flux from collagen/low TF surface reached ~ 0.4×10^{-12} nmole/μm^2-sec, which was only half of the thrombin flux from collagen/high TF surface (**Figure 6-2C**).

The collagen/high TF surface was used as the test surface for all subsequent experiments. A master thrombin generation curve (**Figure 6-2D**) was developed from 13 individual experiments with blood from 13 donors, representing the average dynamics of human thrombin generation from clots formed on collagen/high TF surface (~1 molecule TF/ μm^2, 5 mM GPRP, 40 μg/mL CTI): a slow increase in thrombin flux during the first 500 sec to 0.5 x 10^{-12} nmole/μm^2-sec, followed by an accelerated increase (~4x higher than the rate of increase during the first 500 sec), reaching a thrombin flux of ~1.5 x 10^{-12} nmole/μm^2-sec by 800 sec at the endpoint of the experiment. The standard error was attributed to interdonor variation in thrombin generation of about ± 50 %, as has been previously observed with measurements of thrombin generation by the CAT assay [196].

Given this observed variation, subsequent experiments were conducted with at least 4 donors under matched conditions.

6.3.4 Thrombin flux amplification via thrombin feedback activation of FXI

The large and late stage increase in thrombin flux detected between 500 and 800 sec was consistent with the late stage fibrin and thrombin activity previously detected as a result of platelet polyphosphate enhancement of the thrombin-mediated FXIa feedback pathway [13, 82, 84, 98]. This late stage participation of thrombin-mediated activation of FXIa has also been theoretically predicted [89]. The FXI antibody O1A6 inhibits FXIIa activation of FXI and disrupts the FXI dependent thrombin amplification loop by inhibiting FXIa generation of FIXa and subsequent FXa activation (**Figure 6-4**). Adding O1A6 (20 μg/mL) into the blood sample abolished the accelerated increase of thrombin flux from the collagen/TF surface after 500 sec (**Figure 6-4B**). Thrombin flux increased to 0.2×10^{-12} nmole/μm^2-sec during the first 400 sec, and remained relatively constant after that.

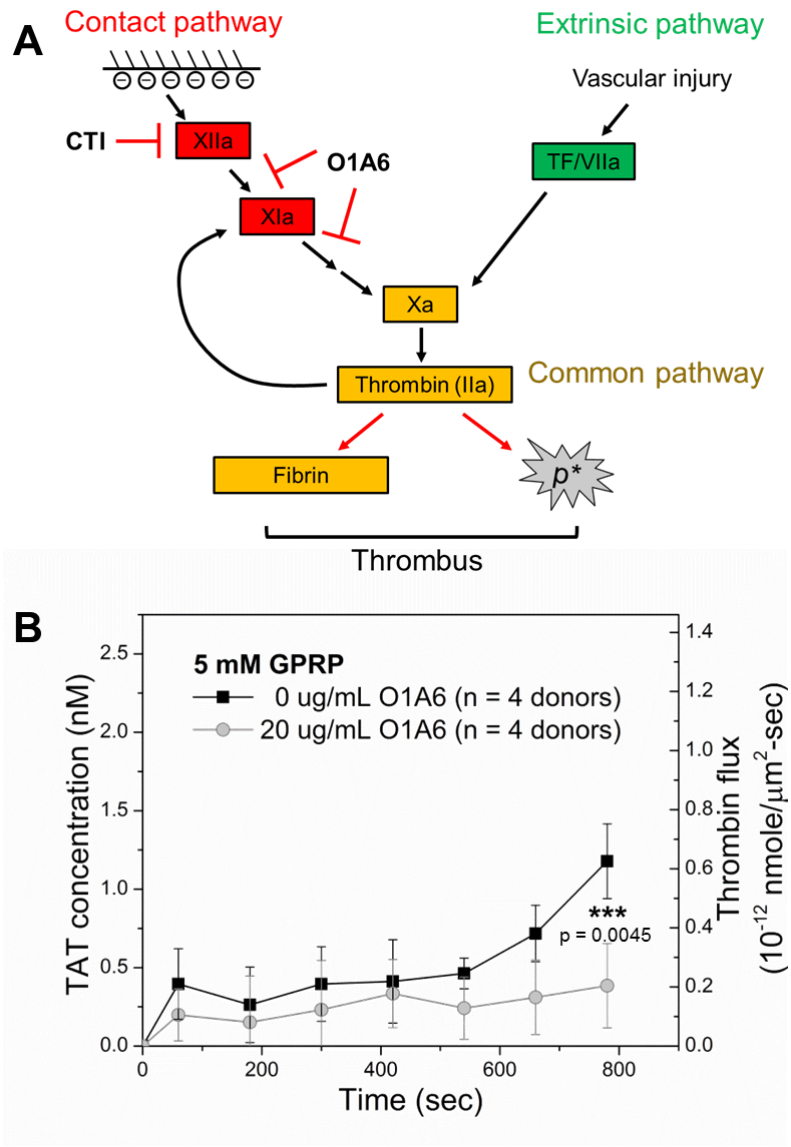

Figure 6-4 Thrombin flux is amplified after 500 sec of clotting via thrombin feedback generation of FXIa.

A, FXI antibody O1A6 disrupts thrombin feedback amplification loop by inhibiting FXIIa activation of FXI and blocking thrombin feedback activation of FXI. **B,** O1A6 (20 μg/mL, ○) abolished late stage increase in thrombin flux from growing thrombi during blood perfusion (40 μg/mL CTI, 5 mM GPRP) over collagen/high TF and caused significant reduction in final thrombin flux when compared to clotting without O1A6 (■) . *** $p < 0.005$.

6.3.5 The first layer of collagen-activated platelets generates the majority of thrombin

We tested the thrombin generating capacity of a monolayer of collagen-adherent platelets to that of a thick and dense platelet deposit. As previously observed [145], the glycoprotein IIb/IIIa ($\alpha_{IIb}\beta_3$) antagonist, GR144053 (500 nM), abolished secondary platelet deposition on collagen/high TF surface. For the first 500 sec of blood perfusion, the thrombin production was essentially the same for a platelet monolayer and a thick platelet deposit, indicating that the thick platelet mass was not diminishing thrombin production by limiting FX transport or by additional coverage/hindrance of surface TF. Interestingly, the accelerated increase of thrombin flux from 600 to 800 sec was largely prevented by GR144053 (**Figure 6-5A**), indicating a role for the thickened platelet deposit in thrombin-feedback activation of FXIa (**Figure 6-4B**) that was operative in this late-stage time regime (**Figure 6-5A**) and also consistent with platelet-dependent release of polyphosphate [199]. Additionally, in the absence of GPRP, a platelet monolayer was sufficient to support localized fibrin formation (**Figure 6-5B**).

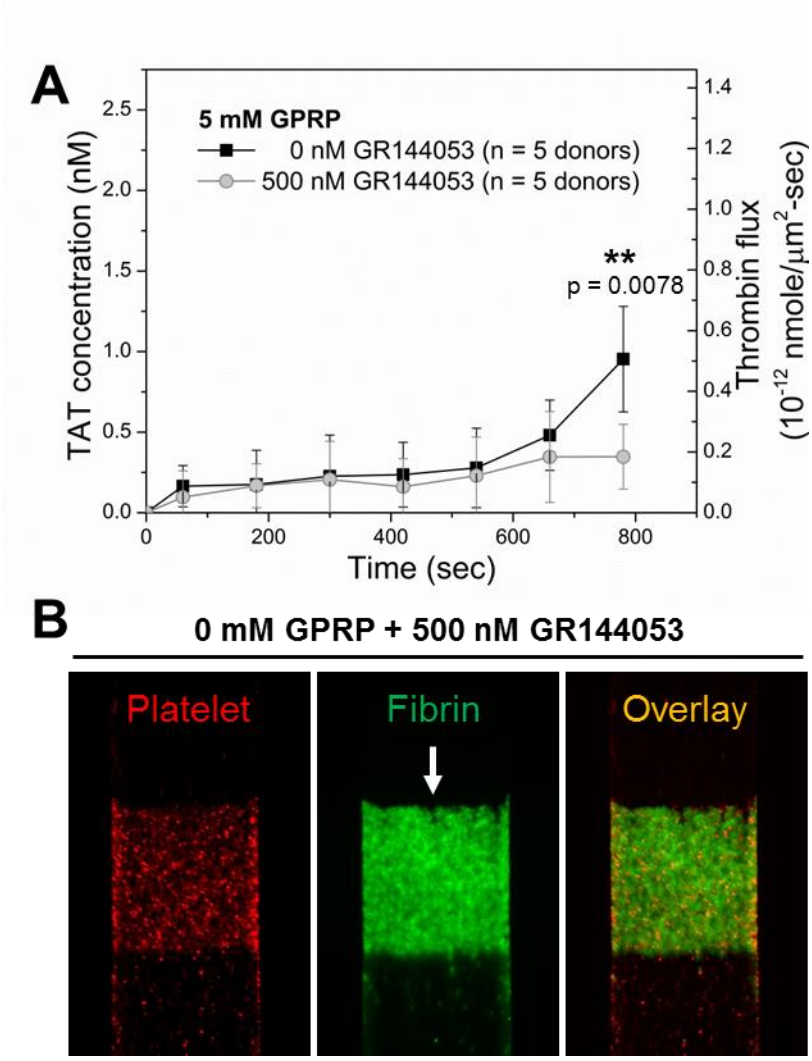

Figure 6-5 The first layer of collagen-activated platelets support initial thrombin production.

A, Dynamics of measured TAT concentration and thrombin flux from growing thrombi (■) or from the first layer of collagen-adherent platelets (○) during blood (40 μg/mL CTI, 5 mM GPRP) perfusion over collagen/high TF. The $\alpha_{IIb}\beta_3$ inhibitor, GR144053 (500 nM) was added to abolish platelet secondary aggregation and achieve a monolayer of platelet on collagen/high TF. Initial thrombin production during the first 500 sec of blood perfusion was intact whereas the final thrombin production on collagen/high TF was significantly reduced by GR144053. **B,** A platelet monolayer was sufficient to support localized fibrin formation when fibrin was allowed to polymerize in the absence of GPRP (B). ** $p < 0.01$.

6.3.6 Longer collagen/TF zones are less efficient in thrombin production

The TAT concentration in effluent collected downstream of 1000-μm long collagen/high TF was about 2x higher than the detected concentration in effluent from 250-μm long collagen/high TF (**Figure 6-6A**). However, the 1000-μm zone was less efficient in supporting overall thrombin generation on a per unit area basis. The overall thrombin flux from the entire 1000 μm-long zone of collagen/high TF was only half of the overall flux from the 250 μm-long zone of collagen/high TF (**Figure 6-6B**). On a 1000-μm zone, most of the platelet accumulation was observed on the first 250 μm, with significantly less platelet deposition between 250 and 1000 microns (**Figure 6-6C, D**). This is consistent with boundary layer depletion of depositing platelets in the red blood cell (RBC)-free layer of plasma nearest the collagen coating. Roughly half of detected thrombin flux from the 1000-μm collagen/high TF zone originated from the first 250 μm subregion of the 1000 μm long zone, assuming the first 250 μm had the exact efficiency in supporting thrombin generation as for the 250-μm long zone (**Figure 6-6E, F**).

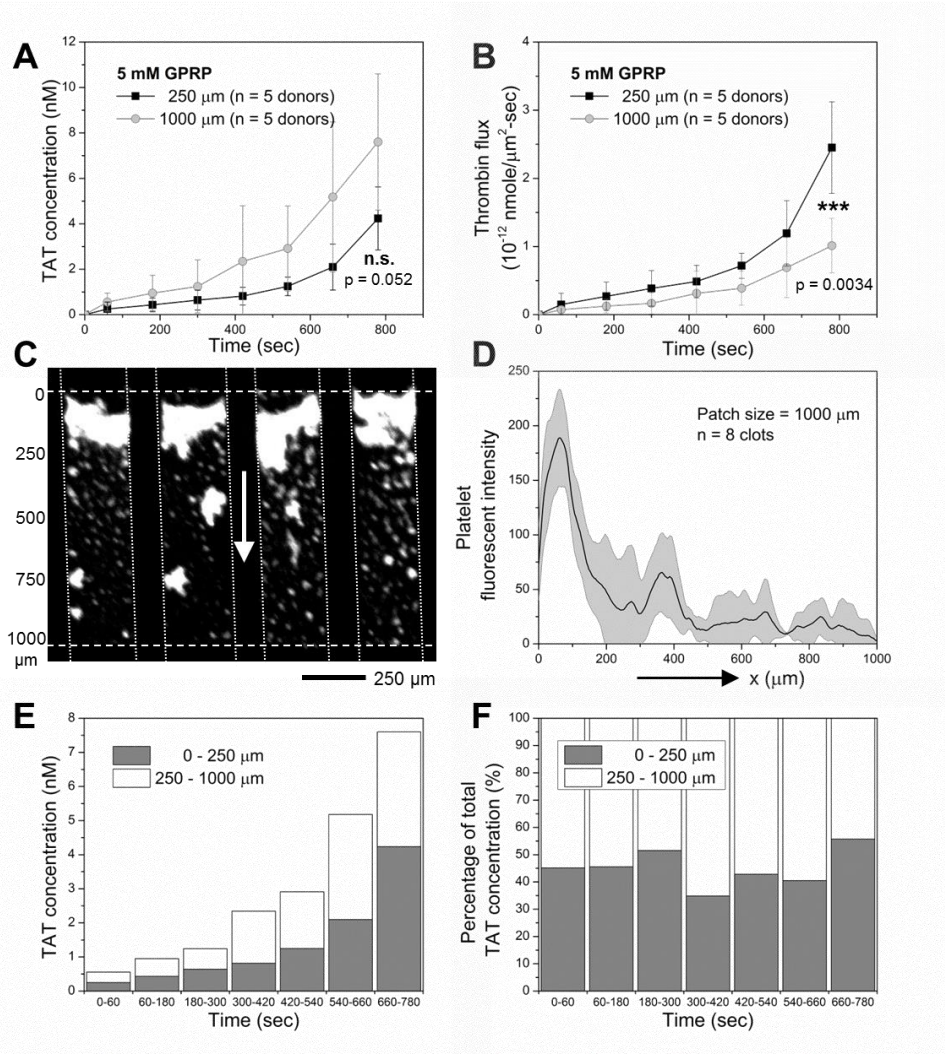

Figure 6-6 Longer collagen/TF zones were less efficient in thrombin production.

A, B, Measured TAT concentration and thrombin flux from blood perfusion (40 μg/mL CTI, 5 mM GPRP) over 250-μm long or 1000-μm long collagen/high TF (~1 molec/μm^2). Longer 1000-μm zones supported more thrombin production but less thrombin flux on a per unit area basis. **C, D,** Platelet accumulation was observed over the first 250 μm on 1000 μm collagen/high TF with far fewer platelets between 250 μm and 1000 μm along the flow direction. **E, F,** About half of the generated thrombin originated from the first 250 μm of the 1000-μm zone (E, F). ***, $p < 0.005$.

6.4 Discussion and Conclusions

In this study, ELISA allowed direct measurement of TAT in plasma isolated from whole blood samples collected from the outlet of a microfluidic thrombosis assay. Numerical simulation demonstrated the delay in thrombin detection in this setup was small (~10 sec) compared to the time interval (120 sec) between sample collections. Thus, TAT measurements can be directly converted to thrombin fluxes within each time interval. Previous theoretical and experimental studies suggested alterations in shear rates and surface TF affect coagulation reaction dynamics and cause substantial changes in thrombin flux [191, 192].

The microfluidic experiments were operated at a constant flow rate mode resulting in an initial wall shear rate of 200 s^{-1}. The thrombin flux released from growing thrombi on collagen/high TF (~ 1 molec/μm^2) increased over time and reached a level of ~10^{-12} nmole/μm^2-min by 800 sec at the end of the experiment. This final thrombin flux falls within the suggested range from previous computational models for similar shear conditions [191-193]. In our flow system, fibrin localized >85% of thrombin within the thrombus and traveled downstream, indicating that free thrombin lasted less than a second or two before its capture by fibrin. The TAT ELISA based measurement might underestimate the actual thrombin flux due to the following factors: (i) other protease inhibitors such as α_2-macroglobulin, even though far less effective than AT, also complex thrombin [194], (ii) thrombin bound to the clot by fibrin-independent mechanisms would not be detected in the plasma TAT-ELISA assay, and (iii) robust thrombin generation at

later time points boosted fibrin polymerization, which was not fully quenched by 5 mM GPRP (**Figure 6-7**).

A thrombin generation curve from 13 individual measurements provides the average dynamic change of thrombin flux from growing thrombi on 250 μm long collagen/high TF. We calculate that each TF molecule supported generation of ~92000 thrombin molecule via the extrinsic pathway during the first 500-sec time period. This curve displayed an accelerated increase in thrombin flux starting at about 500 sec. This accelerated increase was prevented by FXI antibody O1A6. Our previous work indicated that participation of the TF-triggered extrinsic pathway was required to generate enough thrombin to initiate the FXIa-dependent thrombin amplification mechanism, which can be interrupted by O1A6 [13]. This FXI function-blocking antibody also reduced platelet aggregation downstream of thrombi formed on collagen/TF suggesting a role of the FXI-thrombin axis in distal thrombi formation [200]. Therefore, thrombin flux after 500 sec is most likely augmented by the FXIa-dependent thrombin amplification loop. FXI inhibition did not significantly interfere with thrombin flux within the first 500 second indicating the extrinsic pathway is the major contributor of initial thrombin generation in CTI-inhibited whole blood clotting By 500 sec, ~70 % of collagen/TF had been covered with accumulated platelets (**Figure 6-3**), potentially reducing the access to surface immobilized TF and enhancing platelet-dependent pathways (such as polyphosphate pathways).

It is known that platelets provide lipid surface for prothrombinase assembly and therefore are essential for promoting coagulation [201, 202]. Interestingly, a monolayer of platelets provided enough lipid surfaces for robust thrombin generation in the initial

phase. The prevention of amplified thrombin generation during later times suggests the importance of aggregated platelets in aiding the FXI dependent thrombin feedback loop. It is possible that platelet aggregates promote thrombin generation by limiting flow dilution and active transport of activated coagulation factors. Additionally, the accumulated platelets release polyphosphate to act as a cofactor and promote thrombin activation of FXI [13, 82, 98] at later times.

We found increased collagen/TF patch length reduced the overall efficiency of thrombin generation on a per unit area basis, most likely owing to the decay in platelet deposition along the flow direction on 1000-μm long collagen/high TF patch. Furthermore, we have shown in our previous study that a single collagen/TF fiber (patch length < 1 μm) prompts a clotting response of multiple layers of platelet deposition and thrombin generation at a venous shear condition [203]. We suspect that the total thrombin generation might be greater on larger thrombotic patches, but thrombin generation on a per unit area basis decays once the patch size gets too large, which is probably due to boundary layer platelet depletion of the near-wall platelet layer and consequently reduced platelet deposition in downstream regions of larger patches.

In summary, we made direct measurements of TAT complex concentration in effluent from microfluidic thrombosis assay. We estimated thrombin flux from growing thrombi on collagen/TF surface can reach up to 10^{-12} nmole/μm^2-sec at a venous shear condition. Our results suggest polymerized fibrin fibers consume most of the free thrombin and likely serve as a mechanism of localizing clotting response near the injury site and potentially promoting a hierarchical structure of self-limiting clots. Furthermore,

aggregated platelets were found to play pivotal roles in amplifying thrombin generation via the FXI dependent feedback loop.

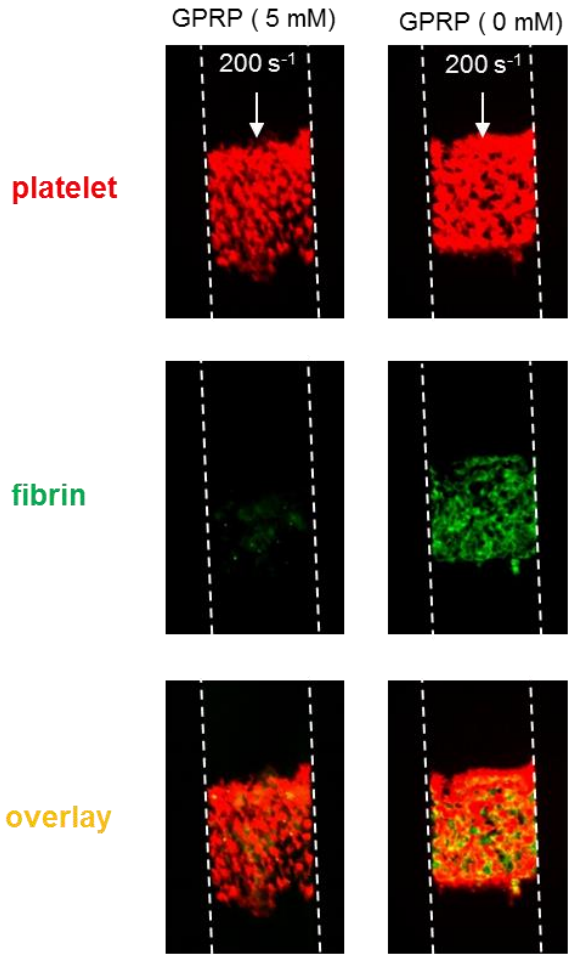

Figure 6-7 Substantial inhibition of fibrin polymerization by GPRP under flow.

GPRP (5 mM) blocked most, but not all, fibrin polymerization during blood perfusion (40 μg/mL CTI) over collagen/TF (1 molec/μm^2) at an initial wall shear rate of 200 s^{-1}. Fluorescent images were taken at the end of experiments (t = 800 sec). Flow direction: top to bottom. Dashed lines outline flow channels.

Chapter 7 : Future Work

7.1 Effect of flow pulsatility on thrombus growth

Due to small length scales within microfluidic devices, *in microfluidico* hemodynamic flows are generally at low Reynolds numbers (Re). In fact, rather extreme geometries are required to create boundary layer separation/impinging flow reattachment [160] in an effort to mimic laminar recirculation zones distal of a coronary stenosis (often described imprecisely as *"disturbed flow*" and incorrectly as turbulent). True fluid mechanical turbulence can be generated in blood in rare circumstances of arteriovenous fistulas, extreme stenosis, or mechanical heart valves. However, turbulence is extremely difficult to create using microfluidic devices due to the micron length scales that keep Re < 10-100. Additionally, most of the laboratory microfluidic systems operate at steady flow condition without incorporating the cyclic nature of blood flow and the complex wall shear stress profiles and transport conditions caused by flow pulsatility [52].

In Chapter 2 and Chapter 3, we developed microfluidic thrombosis assays showing that arterial thrombosis may be druggable by contact pathway inhibition when its triggered by low $[TF]_{wall.}$ However, arterial thrombosis occurs under pulsatile flow conditions due to the cardiac cycle and the flow complexity may affect dynamics of thrombus growth. Thus, performing microfluidic thrombosis assays under pulsatile flow condition may provide more accurate predictions on the inhibitory effect of contact pathway targeting drugs on arterial thrombosis.

In order to recreate pulsatile flow in the microfluidic system, we developed a LabVIEW protocol to control a programmable syringe pump [204]. Using this pumping

protocol, we were able to achieve pulsatile and reversing flows in the microfluidic system. Desired waveforms can be created in the LabVIEW user interface by manipulating three parameters: amplitude, offset (defines the direction) and frequency (**Figure 7-1**). The waveforms were then converted to a DC voltage signal which was then converted to analog and digital signals on a data acquisition card. The programmable syringe pump can read the signal and administer blood flow into microfluidic device. Pulsatile flow profiles can be validated by measuring the instantaneous displacements of small latex particles (2.45 μm diameter) in microfluidic channel (**Figure 7-2**).

We investigated the effect of pulsatile flow on platelet deposition dynamics in the absence of thrombin signaling pathway. Whole blood was treated with PPACK (100 μM) and apixaban (1 μM) before blood perfusion to achieve a complete knockout thrombin generation during experiment. In preliminary tests, we perfused whole blood over small collagen patches (250 μm × 20 μm, a typical patch size used in Chapter 5) in two separate 8-channel devices. One of the devices operated under constant Q mode (shear rate = 200 s^{-1} or 600 s^{-1}) while another device operated under pulsatile flow condition (average shear rate = 325 s^{-1}, amplitude = 375 s^{-1}, 1 Hz). The hypothesis was that platelet deposition on smaller collagen patches would be favored under pulsatile flow condition due to the increased instantaneous residence time of platelets at the injury site. However, in these experiments, platelet accumulation was not significantly affected by flow pulsatility or the slight flow reversal (**Figure 7-3**).

It has been known that vWF only plays significant role in facilitating platelet adhesion at elevated shear rates and is only essential for stable thrombus formation under high shear conditions [144, 205]. The contribution of vWF may be negligible in this

preliminary investigation since operating at a low average wall shear rate range. In order to investigate the effect of pulsatility on arterial thrombus growth and shear-dependent vWF function, future experiments have to be conducted at higher shear rates, representative of values in human arteries. Additionally, the current experiment targeted thrombin-independent platelet deposition even though increased instantaneous residence time at adhesion sites (due to pulsatility and flow reversal) may affect local thrombin generation kinetics and thus affect thrombus growth via thrombin dependent platelet signaling pathways or via the coagulation pathways. Blood perfusions over collagen/TF surfaces without thrombin inhibition are then required to elucidate the effect of pulsatile flow on thrombin dependent mechanisms. Furthermore, the current experiment focuses on the effect of flow pulsatility on platelet deposition on small collagen patches although larger patches will support more stable and more consistent thrombus formation across individual flow channels, especially at elevated shear rates. Flow experiments on larger patches (i.e. 250 μm × 250 μm) are more appropriate for studying the effect of pulsatile flow on arterial thrombosis.

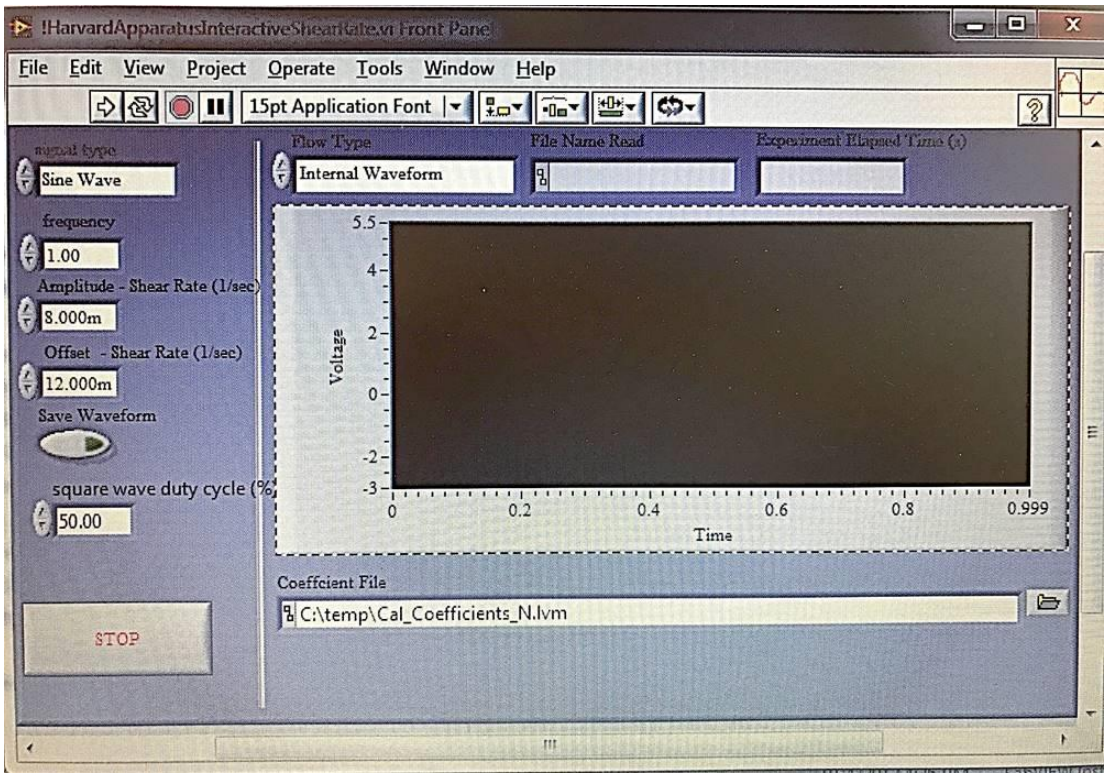

Figure 7-1 A LabVIEW program to control programmable syringe pump.

Screen shot of graphical user interface of the LabVIEW program used to control programmable syringe pump to generate pulsatile flow in microfluidic system.

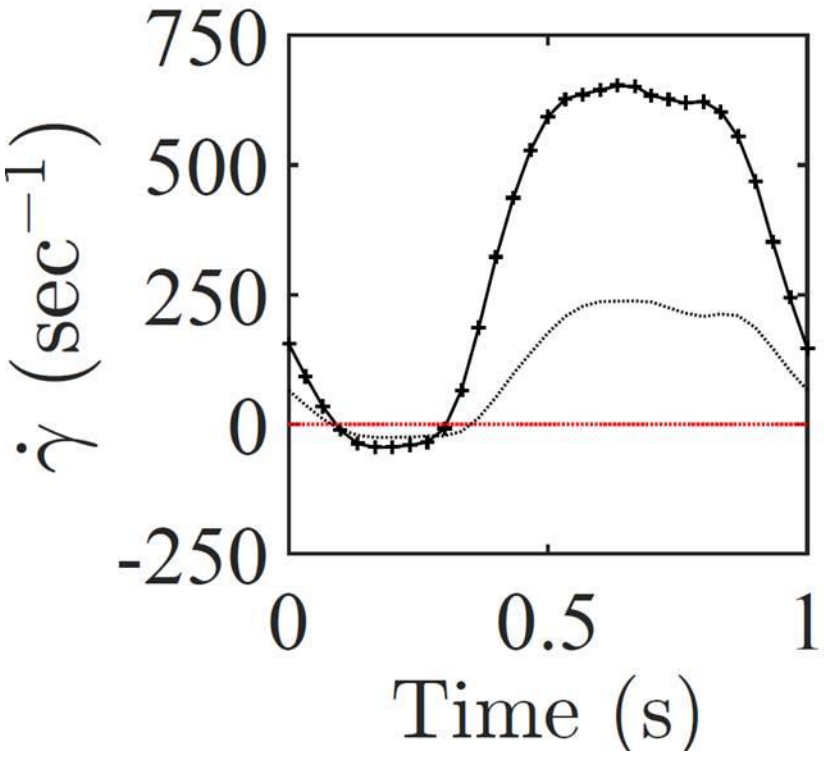

Figure 7-2 Representative shear rate profiles.

Two representative validated profiles of instantaneous shear rates within a single cycle calculated from displacements of latex tracer particles. Black line (with cross markers) shows a profile with an average shear rate of 325 s^{-1}. The amplitude is 375 s^{-1} (1 Hz). Black dashed line shows a profile with an average shear rate of 150 s^{-1} and the amplitude is 200 s^{-1} (1 Hz).

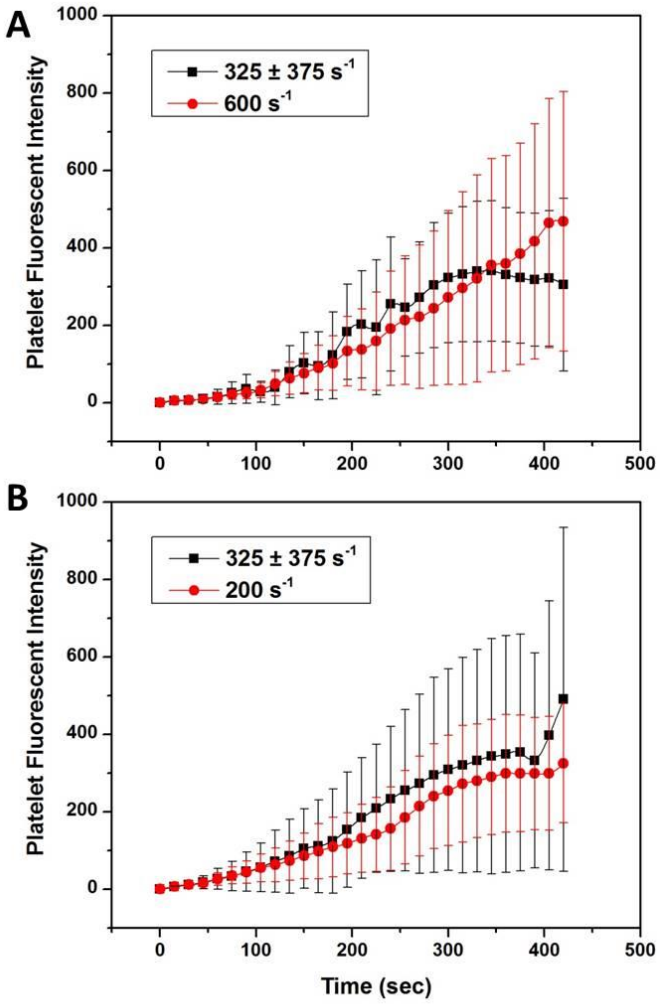

Figure 7-3 Dynamics of platelet adhesion and aggregation on small collagen patches.

A, Average kinetics of platelet accumulation measured by fluorescent intensity under pulsatile flow (black, 325 ± 375 s^{-1}, 1 Hz) and steady flow (red, initial wall shear rate = 600 s^{-1}) conditions (n = 6 clots). **B,** Average kinetics of platelet accumulation measured by fluorescent intensity under pulsatile flow (black, 325 ± 375 s^{-1}, 1 Hz) and steady flow (red, initial wall shear rate = 200 s^{-1}) conditions (n = 6 clots).

7.2 Microfluidic characterization of reaction dynamics of fibrin formation

In Chapter 5, we investigated the patch size threshold behavior of initiation of blood coagulation using the 8-channel microfluidic setup. In Chapter 6, we used the combination of the microfluidic thrombosis assay and TAT-ELISA assay to estimate the thrombin flux from clots growing on collagen/TF surface. The microfluidic system enables the study of coagulation dynamics under more physiological relevant conditions. However, there are limitations with using TAT complex measurement to estimate thrombin flux. We found most of the generated thrombin is localized by fibrin fibers and inhibition of fibrin polymerization was required to enable downstream thrombin detection (**Figure 7-4**). In some experiments, fibrin formation was observed at later times even in the presence of high level of GPRP. Additionally, there are more naturally occurring thrombin inhibitors other than antithrombin. Alternatively, conversion of prothrombin to thrombin releasing prothrombin fragment 1.2 (F1.2) and F1.2 can be used as an index of thrombin generation even in the presence of fibrin generation [206, 207]. Using the combination of the microfluidic thrombosis assay we developed in Chapter 6 and a F1.2-ELISA assay can achieve a more accurate estimation of thrombin flux.

In Chapter 6, we intentionally blocked fibrin polymerization in order to detect free thrombin. In reality, the presence of fibrin may affect clot structure and clot stability [4, 130]. Additionally, understanding the kinetics of fibrin generation within clots growing under flow condition may provide insights into the process of fibrinolysis, which is one of the important coagulation self-regulatory mechanisms. Thrombin cleaves fibrinopeptide A and B (FPA and FPB) and FPA is often used as an index of fibrin

generation [208]. We propose using the combination of the microfluidic thrombosis assay and a FPA-ELISA assay would provide a way of measuring fibrin generation kinetics in a growing clot under flow condition (**Figure 7-5**). Additionally, D-dimer (DD) is produced during fibrin degradation by plasmin and is often used as a marker of endogenous fibrinolysis in clinical models [209]. Tissue plasminogen activator (tPA) converts plasminogen to plasmin using fibrin as a substrate and plasmin can then initiate fibrinolysis [210]. In the microfluidic system, fibrinolysis is negligible due to the absence of endothelium, which is the major source of endogenous tPA [211, 212]. However, controlled fibrin degradation can be achieved by exogenously adding plasmin to initiate fibrinolysis. After microfluidic thrombosis assay, clots formed over collagen/TF surface need to be washed *in situ* with HBS buffer to remove blood cells and enzymes. All microfluidic channels should then be filled with plasmin containing buffer for at least 10 min for complete fibrin degradation in the clots. The fluids within microfluidic channels will be collected and subsequently be analyzed with ELISA assay to measure DD concentration. The cumulative amount of fibrin generated in the clots can then be calculated with endpoint DD measurement. In fact, measuring both total amount of fibrin generation with DD-ELISA assay and real-time fibrin formation with FPA-ELISA assay in the same experiment will offer a more accurate estimation of the real fibrin formation kinetics.

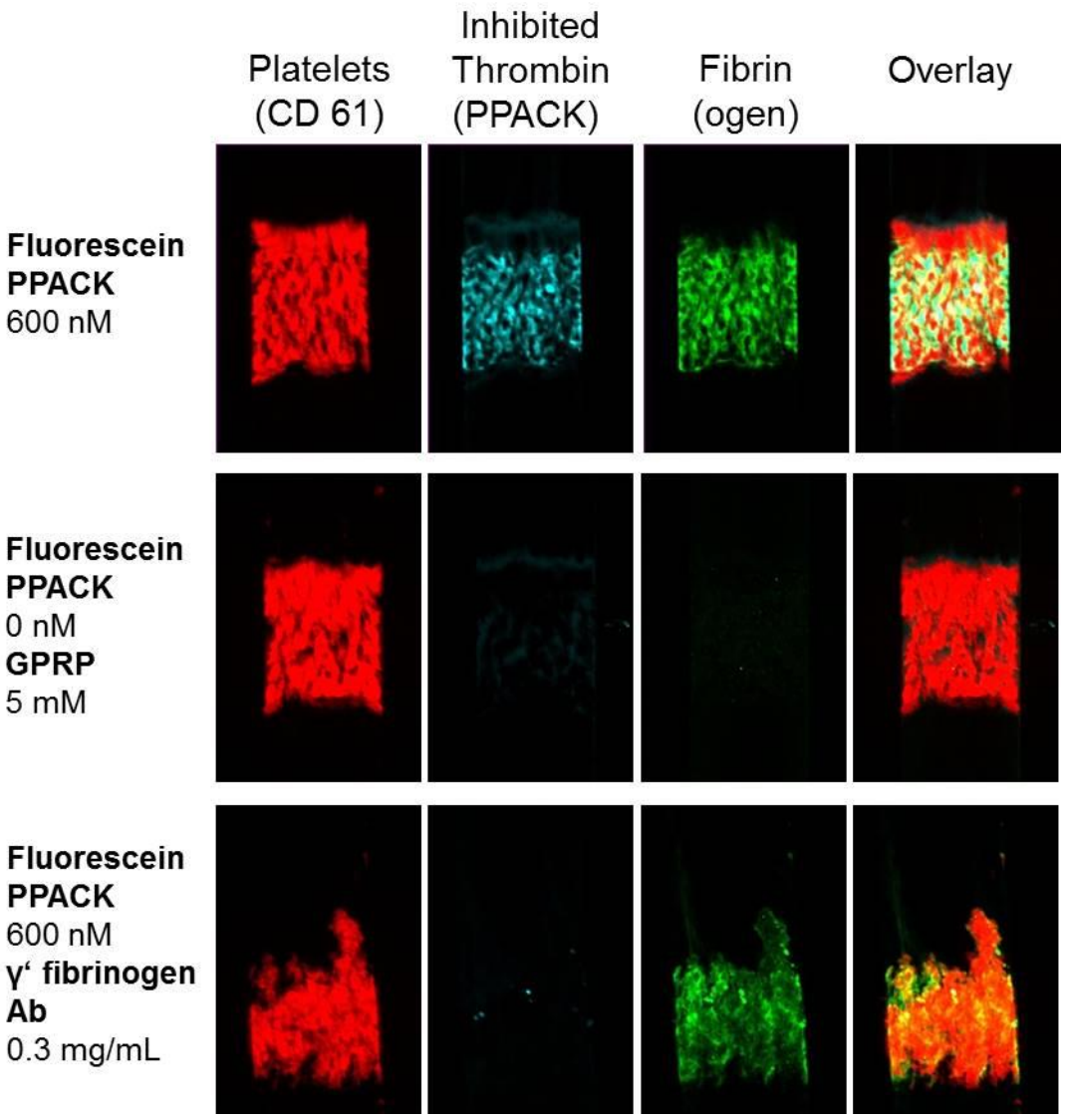

Figure 7-4 Fibrin localizes free thrombin via its antithrombin activity.

To confirm fibrin's antithrombin activity, extremely low concentration (600 nM) of fluorescein conjugated PPACk was used to label thrombin. This low level only labels localized thrombin without significantly affecting total thrombin generation. Labeled thrombin (cyan) co-localizes with fibrin (green). Once fibrin polymerization is inhibited with GPRP, there's very little thrombin signal suggestion fibrin localizes most of the formed thrombin. Antibody against fibrinogen γ' chain quenched fibrin-thrombin interaction. Images of individual clots formed on collagen/TF surfaces were taken at the end of the experiments (t =600 sec). Platelets are shown in red, fibrin fibers are shown in green and inhibited thrombin is in cyan.

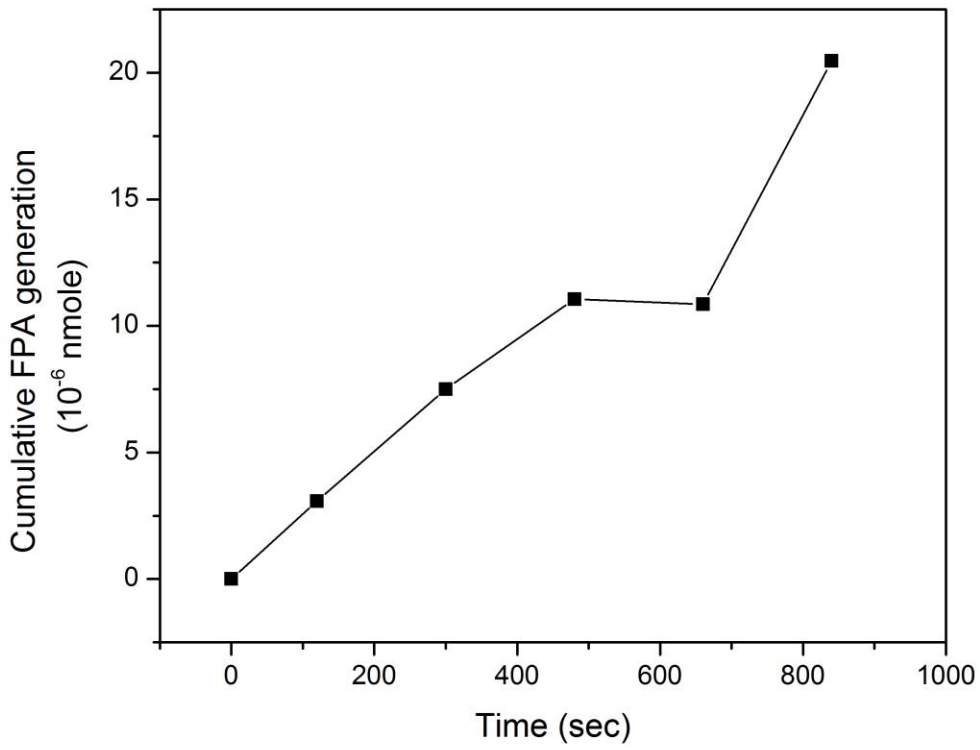

Figure 7-5 Cumulative FPA generation detected downstream of growing clots on collagen/TF surface from a single experiment.

Average cumulative FPA generation from 8 clots (1 donor) over 840 sec of blood perfusion (40 µg/mL) over collagen/TF surfaces.

BIBLIOGRAPHY

1. Colman RW. Are hemostasis and thrombosis two sides of the same coin? *J Exp Med*. 2006;203:493-5.
2. Jennings LK. Mechanisms of platelet activation: need for new strategies to protect against platelet-mediated atherothrombosis. *Thromb Haemost*. 2009;102:248-57.
3. Lundblad RL, Bradshaw RA, Gabriel D, Ortel TL, Lawson J, Mann KG. A review of the therapeutic uses of thrombin. *Thromb Haemost*. 2004;91:851-60.
4. Weisel JW. Structure of fibrin: impact on clot stability. *J Thromb Haemost*. 2007;5 Suppl 1:116-24.
5. Schmaier AH. The elusive physiologic role of Factor XII. *J Clin Invest*. 2008;118:3006-9.
6. Davie EW. A brief historical review of the waterfall/cascade of blood coagulation. *J Biol Chem*. 2003;278:50819-32.
7. Versteeg HH, Heemskerk JWM, Levi M, Reitsma PH. New Fundamentals in Hemostasis. *Physiol Rev*. 2013;93:327-58.
8. Freedman MD. Oral anticoagulants: pharmacodynamics, clinical indications and adverse effects. *Journal of clinical pharmacology*. 1992;32:196-209.
9. Adcock DM, Gosselin R. Direct Oral Anticoagulants (DOACs) in the Laboratory: 2015 Review. *Thromb Res*. 2015;136:7-12.
10. Sikka P, Bindra VK. Newer antithrombotic drugs. *Indian J Crit Care Med*. 2010;14:188-95.
11. Fitzmaurice DA, Blann AD, Lip GY. Bleeding risks of antithrombotic therapy. *BMJ*. 2002;325:828-31.
12. Zhu S, Diamond SL. Contact activation of blood coagulation on a defined kaolin/collagen surface in a microfluidic assay. *Thromb Res*. 2014;134:1335-43.
13. Zhu S, Travers RJ, Morrissey JH, Diamond SL. FXIa and platelet polyphosphate as therapeutic targets during human blood clotting on collagen/tissue factor surfaces under flow. *Blood*. 2015;126:1494-502.
14. Mann KG, Whelihan MF, Butenas S, Orfeo T. Citrate anticoagulation and the dynamics of thrombin generation. *J Thromb Haemost*. 2007;5:2055-61.
15. Hansson KM, Nielsen S, Elq M, Deinum J. The effect of corn trypsin inhibitor and inhibiting antibodies for FXIa and FXIIa on coagulation of plasma and whole blood. *J Thromb Haemost*. 2014;12:1678-86.
16. Butenas S, Mann KG. The effect of corn trypsin inhibitor and inhibiting antibodies for FXIa and FXIIa on coagulation of plasma and whole blood: comment. *J Thromb Haemost*. 2015;13:487-8.
17. Cheng Q, Tucker EI, Pine MS, Sisler I, Matafonov A, Sun M, et al. A role for factor XIIa-mediated factor XI acivation in thrombus formation in vivo. *Blood*. 2010;116:3981-9.
18. Kravtsov DV, Matafonov A, Tucker EI, Sun MF, Walsh PN, Gruber A, et al. Factor XI contributes to thrombin generation in the absence of factor XII. *Blood*. 2009;114:452-8.

19. Puy C, Tucker EI, Wong ZC, Gailani D, Smith SA, Choi SH, et al. Factor XII promotes blood coagulation independent of factor XI in the presence of long-chain polyphosphates. *J Thromb Haemost*. 2013;11:1341-52.
20. Maloney SF, Brass LF, Diamond SL. P2Y12 or P2Y1 inhibitors reduce platelet deposition in a microfluidic model of thrombosis while apyrase lacks efficacy under flow conditions. *Integr Biol*. 2009;2:183-92.
21. Colace T, Falls E, Zheng XL, Diamond SL. Analysis of morphology of platelet aggregates formed on collagen under laminar blood flow. *Ann Biomed Eng*. 2011;39:922-9.
22. Neeves KB, Maloney SF, Fong KP, Schmaier AA, Kahn ML, Brass LF, et al. Microfluidic focal thrombosis model for measuring murine platelet deposition and stability: PAR4 signaling enhances shear-resistance of platelet aggregates. *J Thromb Haemost*. 2008;6:2193-201.
23. Colace TV, Jobson J, Diamond SL. Relipidated tissue factor linked collagen surfaces potentiates platelet adhesion and fibrin formation in a microfluidic model of vessel injury. *Bioconjug Chem*. 2011;22:2104-9.
24. Colace TV, Muthard RW, Diamond SL. Thrombus growth and embolism on tissue factor-bearing collagen surfaces under flow: role of thrombin with and without fibrin. *Arterioscl Thromb Vasc Biol*. 2012;32:1466-76.
25. Okorie UM, Denney WS, Chatterjee MS, Neeves KB, Diamond SL. Determination of surface tissue factor thresholds that trigger coagulation at venous and arterial shear rates: amplification of 100 fM circulating tissue factor requires flow. *Blood*. 2008;111:3507-13.
26. Li R, Panckeri KA, Fogarty PF, Diamond SL. Recombinant factor VIIa enhances platelet deposition from flowing haemophilic blood but requires the contact pathway to promote fibrin deposition. *Haemophilia*. 2015;21:266-74.
27. Li R, Diamond SL. Detection of platelet sensitivity to inhibitors of COX-1, P2Y1, and P2Y12 using a whole blood microfluidic flow assay. *Thromb Res*. 2014;133:203-10.
28. Li R, Fries S, Li X, Grosser T, Diamond SL. Microfluidic assay of platelet deposition on collaen by perfusion of whole blood from healthy individuals taking aspirin. *Clin Chem*. 2013;68:610-8.
29. Li X, Fries S, Li R, Lawson JA, Propert KJ, Diamond SL, et al. Differential impairment of aspirin-dependent platelet cyclooxygenase acetylation by nonsteroidal antiinflammatory drugs. *Proc Natl Acad Sci U S A*. 2014;111:16830-5.
30. Kane RS, Takayama S, Ostuni E, Ingber DE, Whitesides GM. Patterning proteins and cells using soft lithography. *Biomaterials*. 1999;20:2363-76.
31. Colace TV, Fogarty PF, Panckeri KA, Li R, Diamond SL. Microfluidic assay of hemophilic blood clotting: distinct deficits in platelet and fibrin deposition at low factor levels. *J Thromb Haemost*. 2014;12:147-58.
32. Li R, Diamond SL. Detection of platelet sensitivity to inhibitors of COX-1, $P2Y_1$, and $P2Y_{12}$ using a whole blood microfluidic flow assay. *Thromb Res*. 2014;133:203-10.

33. Shankaran H, Alexandridis P, Neelamegham S. Aspects of hydrodynamic shear regulating shear-induced platelet activation and self-association of von Willebrand factor in suspension. *Blood*. 2003;101:2637-45.
34. Wolberg AS, Campbell RA. Thrombin generation, fibrin clot formation and hemostasis. *Transfus Apher Sci*. 2008;38:15-23.
35. Altman R, Hemker HC. Contact activation in the extrinsic blood blotting system. *Thromb Diath Haemorrh*. 1967;18:525-31.
36. Citarella F, Ravon DM, Pascucci B, Felici A, Fantoni A, Hack CE. Structure/function analysis of human factor XII using recombinant deletion mutants. Evidents for an additional region involved in the binding to negatively charged surfaces. *Eur J Biochem*. 1996;238:240-9.
37. Stavrou E, Schmaier AH. Factor XII: What does it contribute to our understanding of the physiology and pathology of hemostasis & thrombosis. *Thromb Res*. 2010;125:210-5.
38. Renne T, Pozgajova M, Gruner S, Schuh K, Pauer HU, Burfeind P, et al. Defective thrombus formation in mice lacking coagulation factor XII. *J Exp Med*. 2005;202:271-81.
39. Renne T, Nieswandt B, Gailani D. The intrinsic pathway of coagulation is essential for thrombus stability in mice. *Blood Cells Mol Dis*. 2006;36:148-51.
40. Pauer HU, Renne T, Hemmerlein B, Legler T, Frizlar S, Adham I, et al. Targeted deletion of murine coagulation factor XII gene-a model for contact phase activation *in vivo*. *Thromb Haemost*. 2004;92:503-8.
41. Smith JK. Facor XI deficiency and its management. *Haemophilia*. 1996;2:128-36.
42. Muller F, Gailani D, Renne T. Factor XI and XII as antithrombotic targets. *Curr Opin Hematol*. 2011;18:349-55.
43. Woodruff RS, Sullenger B, Becker RC. The many faces of the contact pathway and their role in thrombosis. *J Thromb Thrombolysis*. 2011;32:9-20.
44. Montfoort MLV, Meijers JCM. Anticoagulation beyond direct thrombin and factor Xa inhibitors: indications for targeting the intrinsic pathway? *Thromb Haemost*. 2013;110:223-32.
45. Zhuo R, Miller R, Bussard KM, Siedlecki CA, Vogler EA. Procoagulant stimulus pocessing by the intrinsic pathway of blood plasma coagulation. *Biomaterials*. 2005;26:2965-73.
46. Zhuo R, Siedlecki CA, Vogler EA. Competitive-protein adsorption in contac activation of blood factor XII. *Biomaterials*. 2007;28:4355-69.
47. Vogler EA, Siedlecki CA. Contact activation of blood-plasma coagulation. *Biomaterials*. 2009;30:1857-69.
48. Blezer R, George MW, Cahalan PT, Lindhout T. Initiation and propogation of blood coagulation at artificial surfaces studied in a capilary flow reactor. *Thromb Haemost*. 1998;79:296-301.
49. Johansson PI, Bochsen L, Andersen S, Viuff D. Investigation of the effect of kaolin and tissue factor-activated citrated whole blood, on clot forming variables, as evaluated by thromboelatography. *Transfusion*. 2008;48:2377-83.

50. Welsby IJ, Jiao K, Ortel TL, Brudney CS, Roche AM, Guerrero EB, et al. The kaolin-activation thrombelastograph predicts bleeding after cardiac surgery. *J Cardiothorac Vasc Anesth*. 2006;20:531-5.
51. Chatterjee MS, Denny WS, Jing H, Diamond SL. Systems Biology of Coagulation Initiation: Kinetics of Thrombin Generation in Resting and Activated Human Blood. *PLoS Comput Biol*. 2010;6:1-24.
52. Colace TV, Tormoen GW, McCarty OJ, Diamond SL. Microfluidics and coagulation biology. *Annu Rev Biomed Eng*. 2013;15:283-303.
53. Diaz CA, Xia Y, Rubino M, Auras R, Jayaraman K, Hotchkiss J. Fluorescent labeling and tracking of nanoclay. *Nanoscale*. 2013;5:164-8.
54. Smith SA, Morrissey JH. Rapid and efficient incorporation of tissue factor into liposomes. *J Thromb Haemost*. 2004;2:1155-62.
55. Welsh JD, Colace TV, Muthard RW, Stalker TJ, Brass LF, Diamond SL. Platelet-targeting sensor reveals thrombin gradients within blood clots forming in microfluidic assays and in mouse. *J Thromb Haemost*. 2012;10:2344-53.
56. Kawabata SI, Miura T, Morita T, Kato H, Fujikawa K, Iwanaga S, et al. Highly sensitive peptide-4-methylcoumaryl-7-amide substrates for blood clotting proteases and trypsin. *Eur J Biochem*. 1988;172:17-25.
57. Franco F, Perez-Maqueda LA, Perez-Rodriguez JL. The effect of ultrasound on the particle size and structural disorder of a well-ordered kaolinite. *J Colloid Interface Sci*. 2004;274:107-17.
58. Schroth BK, Sposito G. Surface charge properties of kaolinite. *Clays Clay Miner*. 1997;45:85-91.
59. Gachet C. The platelet P2 receptors as molecular targets for old and new antiplatelet drugs. *Pharmacol Ther*. 2005;108:180-2.
60. Hechler B, Cattaneo M, Gachet C. The P2 receptors in platelet function. *Semin Thromb Hemost*. 2005;31:150-61.
61. Radomski MW, Rees DD, Dutra A, Moncada S. S-nitroso-glutathione inhibits platelet acivation in vitro and in vivo. *Br J Pharmacol*. 1992;107:745-9.
62. Flamm MH, Colace TV, Chatterjee MS, Jing H, Zhou S, Jaeger D, et al. Multiscale prediction of patient-specific platelet function under flow. *Blood* 2012;120:190-8.
63. Tremoli E, Maderna P, Mannucci L, Colli S, Paoletti R. In vitro effects of iloprost on platelet aggregation in normal and hypercholesterolemia subjects. In: Gryglewski RJ SG, ed. *Prostacyclin and Its Stable Analogue Iloprost*. Berlin Heidelberg: Srpinger-Verlag; 1987:47-51.
64. Van der Mijden PEJ, Munnix ICA, Auger JMG-R, J.W.P., Cosemans JMEM, Kuijpers MJE, Spronk HM, et al. Dual role of collagen in factor XII-dependent thrombus formation. *Blood*. 2009;114:881-90.
65. Walsh PN, Griffin JH. Contributions of human platatelets to the proteolytic activation of blood coagulation factors XII and XI. *Blood*. 1981;57:106-18.
66. Matafonov A, Leung PY, Gailani AE, Grach SL, Puy C, Cheng Q, et al. Factor XII inhibition reduces thrombus formation in a primate thrombosis model. *Blood*. 2014;123:1739-46.

67. Larsson M, Rayzman V, Nolte MW, Nickel KF, Bjorkqvist J, Jamsa A, et al. A factor XIIa inhibitory antibody provides thromboprotection in extracorporeal circulation without increasing bleeding risk. *Sci Transl Med*. 2014;6:1-13.
68. Meijers JC. No contact, no thrombosis? *Blood*. 2014;123:1929.
69. Kuijpers MJE, van der Meijden PEJ, Feijge MAH, Mattheij NJA, May F, Govers-Riemslag J, et al. Factor XII regulates the pathological process of thrombus formation on ruptured plaques. *Arterioscler Thromb Vac Biol*. 2014
70. Makrism M, Van Veen JJ, Tait CR, Mumford AD, Laffan M, Haematology BCfSi. Guideline on the management of bleeding in patients on antithrombotic agents. *Br J Haematol*. 2013;160:35-46.
71. McFadyen JD, Jackson SP. Differentiating haemostasis from thrombosis for therapeutic benefit. *Thromb Haemost*. 2013;110:859-67.
72. Tucker EI, Marzec UM, White TC, Hurst S, Rugonyi S, McCarty OJ, et al. Prevention of vascular graft occlusion and thrombus-associated thrombin generation by inhibition of factor XI. *Blood*. 2009;113:936-44.
73. Wang X, Smith PL, Hsu MY, Gailani D, Schumacher WA, Ogletree ML, et al. Effects of factor XI deficiency on ferric chloride-induced vena cava thrombosis in mice. *J Thromb Haemost*. 2006;4:1982-8.
74. Rosen ED, Gailani D, Castellino FJ. FXI is essential for thrombus formation following FeCl3-induced injury of the carotid artery in the mouse. *Thromb Haemost*. 2002;87:774-6.
75. Gruber A, Hanson SR. Factor XI-dependence of suface- and tissue factor-initiated thrombus propagation in primates. *Blood*. 2003;102:953-5.
76. Yau JW, Liao P, Fredenburgh JC, Stafford AR, Revenko AS, Monia BP, et al. Selecive depletion of factor XI or factor XII with anisense oligonucleotides attenuates catheter thrombosis in rabbits. *Blood*. 2014;123:2102-7.
77. Yamashita A, Nishihira K, Kitazawa T, Yoshihashi K, Soeda T, Esaki K, et al. Factor XI contributes to thrombus propagation on injured neointima of the rabbit iliac artery. *J Thromb Haemost*. 2006;4:1496-501.
78. Leung PY, Hurst S, Berny-Lang MA, Verbout NG, Gailani D, Tucker EI, et al. Inhibition of factor XII-mediated activation of factor XI provides protection against experimental acute ischemic stroke in mice. *Transl Stroke Res*. 2012;3:381-9.
79. Matafonov A, Leung PY, Gailani AE, Grach SL, Puy C, CHENG Q, et al. Factor XII inhibition reduces thrombus formation in a primate thrombosis model. *Blood*. 2014;123:1739-46.
80. van Montfoort ML, Kuijpers MJE, Knaup VL, Bhanot S, Monia BP, Roelofs JJ, et al. Factor XI regulates pathological thrombus formation on acutely ruptured atherosclerotic plaques. *Arterioscl Thromb Vasc Biol*. 2014;34:1668-73.
81. Muller F, Mutch NJ, Schenk WA, Smith SA, Esterl L, Spronk HM, et al. Platelet polyphosphate are proinflammatory and procoagulant mediators in vivo. *Cell*. 2009;139:1143-56.
82. Choi SH, Smith SA, Morrissey JH. Polyphosphate is a cofactor for the activation of factor XI by thrombin. *Blood*. 2011;118:6963-70.

83. Smith SA, Mutch NJ, Baskar D, Rohloff P, Docampo R, Morrissey JH. Polyphosphate modulates blood coagulation and fibrinolysis. *Proc Natl Acad Sci*. 2006;103:903-8.
84. Choi SH, Smith SA, Morrissey JH. Polyphosphate accelerates factor V activation by factor XIa. *Thromb Haemost*. 2015;133:599-604.
85. Smith SA, Morrissey JH. Polyphosphate enhances fibrin clot structure. *Blood*. 2008;112:2810-6.
86. Mutch NJ, Engel R, Uitte de Willige S, Philippou H, Ariens RA. Polyphosphate modifies the fibrin network and down-regulates fibinolysis by atenuating binding of tPA and plasminogen to fibrin. *Blood*. 2010;2010:3980-8.
87. Smith SA, Choi SH, Collins JNR, Travers RJ, Cooley BC, Morrissey JH. Inhibition of polyphosphate as a novel strategy for preventing thrombosis and inflamation *Blood*. 2012;120:5103-10.
88. Gailani D. Future propects for contact factors as therapeutic targets. *Hematology Am Soc Hematol Educ Program*. 2014;2014:52-9.
89. Fogelson AL, Hussain YH, Leiderman K. Blood clot formation under flow: the importance of factor XI depends strongly on platelet count. *Biophys J*. 2012;102:10-8.
90. Buller HR, Bethune C, Bhanot S, Gailani D, Monia BP, Raskob GE, et al. Factor XI antisense oligonucleotide for prevention of venous thrombosis. *N Engl J Med*. 2015;372:232-40.
91. Flaumenhaft R. Making (anti)sense of factor XI in thrombosis. *N Engl J Med*. 2015;372:277-8.
92. Duarte JH. Anticoagulation therapy: Reducing factor XI with antisense oligonucleotides superior to endoxaparin for postoperative venous thromboembolism. *Nat Rev Cardiol*. 2015;23:66.
93. Puy C, Tucker EI, Matafonov A, Cheng Q, Zientek KD, Gailani D, et al. Activated factor XI increases the procoagulant activiaty of the extrinsic pathway by inactivating tissue factor pathway inhibitor. *Blood*. 2015
94. Oliver JA, Monroe DM, Roberts HR, Hoffman M. Thrombin activates factor XI on activated platelets in the absence of factor XII. *Arterioscl Thromb Vasc Biol*. 1999;19:170-7.
95. Bjorkqvist J, Nickel KF, Stavrou E, Renne T. In vivo activation and functions of the protease factor XII. *Thromb Haemost*. 2014;112:868-75.
96. Duckers C, Simioni P, Spiezia L, Radu C, Dabrilli P, Gavasso S, et al. Residual platelet factor V ensures thrombin generation in patients with severe congenital factor V deficiency and mild bleeding symptoms. *Blood*. 2010;115:879-86.
97. Werner TP, Amerhein N, Freimoser FM. Specific localization of inorganic polyphosphate (polyP) in fungal cell walls by selective extraction and immunohistochemistry. *Fungal Genet Biol*. 2007;44:845-52.
98. Smith SA, Choi SH, Davis-Harrison R, Huyck J, Boettcher J, Reinstra CM, et al. Polyphosphate exerts differential effects on blood clotting, depending on polymer size. *Blood*. 2010;2010:4353-9.

99. Nickel KF, Spronk HM, Mutch NJ, Renne T. Time-dependent degradation and tissue factor addition mask the ability of platelet polyphoaphates in activating FXII-mediated coagulation. *Blood*. 2013;122:3847-9.
100. Faxalv L, Boknas N, Strom JO, Tengvall P, Theodorsson E, Ramstrom S, et al. Putting polyphosphates to the test: evidence against platelet-induced activation of factor XII. *Blood*. 2013;122:3818-24.
101. Boknas N, Faxalv L, Strom KO, Tengvall P, Theodorsson E, Ramstrom S, et al. Response: Platelets do not generate activated FXII-how inappropriate experimental models have led to misleading conclusions. *Blood*. 2014;124:1692-4.
102. Lam WA, Chaudhuri O, Crow A, Webster KD, Li TD, Kita A, et al. Mechanics and contraction dynamics of single platelets and implications for clot stiffening. *Nat Mater*. 2011;10:61-6.
103. Thon JN, Peters CG, Machlus KR, Aslam R, Rowley J, Macleod H, et al. T granules in human platelets function in TLR9 organization and signaling. *J Cell Biol*. 2012;198:561-74.
104. Chen K, Detwiler TC, Essex DW. Characterization of protein disulphide isomerase released from activated platelets. *Br J Haematol*. 1995;90:425-31.
105. Essex DW, Chen K, Swiatkowska M. Localization of protein disulfide isomerase to the external surface of the platelet plasma membrane. *Blood*. 1995;86:2168-73.
106. Holbrook LM, Watkins NA, Simmonds AD, Jones CI, Ouwehand WH, Gibbins JM. Platelet release novel thiol isomerase enzymes which are recruited to the cell surface following activation. *Br J Haematol*. 2010;148:627-37.
107. Cho J, Furie BC, Coughlin SR, Furie B. A critical role for extracellular protein disulfide isomerase during thrombus formation in mice. *J Clin Invest*. 2008;118:1123-31.
108. Sharda A, Kim SH, Jasuja R, Gopal S, Flaumenhaft R, Furie BC, et al. Defective PDI release from platelets and endothelial cells impairs thrombus formation in Hermansky-Pudlak syndrome. *Blood*. 2015;125:1633-42.
109. Wu Y, Ahmad SS, Zhou J, Wang L, Cully MP, Essex DW. The disulfide isomerase ERp57 mediates platelet aggregation, hemostasis, and thrombosis. *Blood*. 2012;119:1737-46.
110. Zhou J, Wu Y, Wang L, Rauova L, Hayes VM, Poncz M, et al. The disulfide isomerase ERp57 is required for fibrin deposition in vivo. *J Thromb Haemost*. 2014;12:1890-7.
111. Wang L, Wu Y, Zhou J, Ahmad SS, Mutus B, Garbi N, et al. Platelet-derived ERp57 mediates platelet incorporation into a growing thrombus by regulating of the αIIbβ3 integrin. *Blood*. 2013;122:3642-50.
112. Passam FH, Lin L, Gopal S, Stopa JD, Bellido-Martin L, Huang M, et al. Both platelet- and endothelial cell-derived ERp5 supports thrombus formation in a laser-induced mouse model of thrombosis. *Blood*. 2015;125:2276-85.
113. Jordan PA, Stevens JM, Hubbard GP, Barrett NE, Sage T, Authi KS, et al. A role for the thiol isomerase protein ERp5 in platelet function. *Blood*. 2005;105:1500-7.
114. Burgess JK, Hotchkiss KA, Suter C, Dudman NPB, Szollosi J, Chesterman CN, et al. Physical proximity and functional association of glycoprotein 1bα and protein-

disulfide isomerase on the platelet plasma membrane. *J Biol Chem*. 2000;275:9758-66.
115. Manickam N, Sun X, Li M, Gazitt Y, Essex DW. Protein disulphide isomerase in platelet function. *Br J Haematol*. 2008;140:2168-73.
116. Cho J, Kennedy DR, Lin L, Huang M, Merrill-Skoloff G, Furies BC, et al. Protein disulfide isomerase capture during thrombus formation in vivo depends on the presence of β3 integrins. *Blood*. 2012;120:647-55.
117. Lahav J, Jurk K, Hess O, Barnes MJ, Farndale RW, Luboshitz J, et al. Sustained integrin ligation involves extracellular free sulfhydryls and enzymatically catalyzed disulfide exchange. *Blood*. 2002;100:2472-8.
118. Essex DW, Li M, Miller A, Feinman RD. Protein Disulfide Isomerase and Sulfhydryl-Dependent Pathways in Platelet Activation. *Biochemistry*. 2001;40:6070-5.
119. Lahav J, Wijnen EM, Hess O, Hamaia SW, Griffiths D, Makris M, et al. Enzymatically catalyzed disulfide exchange is required for platelet adhesion to collagen via integrin alpha2beta1. *Blood*. 2003;102:2085-92.
120. Khodier C, VerPlank L, Nag PP, Pu J, Wurst J, Pilyugina T, et al. Identification of ML359 as a Small Molecule Inhibitor of Protein Disulfide Isomerase. *Probe Reports from the NIH Molecular Libraries Program*. Bethesda MD; 2010.
121. Jasuja R, Passam FH, Kennedy DR, Kim SH, van Hessem L, Lin L, et al. Protein disulfide isomerase inhibitors constitute a new class of antithrombotic agents. *J Clin Invest*. 2012;122:2104-13.
122. Flaumenhaft R, Furie B, Zwicker JI. Therapeutic Implications of Protein Disulfide Isomerase Inhibition in Thrombotic Disease. *Arterioscler Thromb Vasc Biol*. 2015;35:16-23.
123. Chen VM, Ahamed J, Versteeq HH, Berndt MC, Ruf W, Hoqq PJ. Evidence for activation of tissue factor by an allosteric disulfide bond. *Biochemistry*. 2006;45:12020-8.
124. Ahamed J, Versteeq HH, Kerver M, Chen VM, Mueller BM, Hoqq PJ, et al. Disulfide isomerization switches tissue factor from coagulation to cell signaling. *Proc Natl Acad Sci*. 2006;103:13932-7.
125. Jasuja R, Furie B, Furie BC. Endothelium-derived but not platelet-derived protein disulfide isomerase is required for thrombus formation in vivo. *Blood*. 2010;116:4665-74.
126. Kim K, Hahm E, Li J, Holbrook LM, Sasikumar P, Stanley RG, et al. Platelet protein disulfide isomerase is required for thrombus formation but not for hemostasis in mice. *Blood*. 2013;122:1052-61.
127. Xu S, Sankar S, Neamati N. Protein disulfide isomerase: a promising target for cancer therapy. *Drug Discov Today*. 2014;19:222-40.
128. Reinhardt C, von Bruhl ML, Manukyan D, Grahl L, Lorenz L, Altmann B, et al. Protein disulfide isomerase acts as an injury response signal that enhances fibrin generation via tissue factor activation. *J Clin Invest*. 2008;118:1110-22.
129. Crimmins DL. Analysis of disulfide-linked homo- and hetero-peptide dimers with a strong cation-exchange sulfoethyl aspartamide column. *Pept Res*. 1989;2:395-401.

130. Welsh JD, Stalker TJ, Voronov R, Muthard RW, Tomaiuolo M, Diamond SL, et al. A system approach to hemostasis: 1. The interdependence of thrombus architecture and agonist movements in the gaps between platelets. *Blood*. 2014;124:1808-15.
131. Xu S, Butkevich AN, Yamada R, Zhou Y, Debnath B, Duncan R, et al. Discovery of an orally active small-molecule irreversible inhibitor of protein disulfide isomerase for ovarian cancer treatment. *Proc Natl Acad Sci*. 2012;109:16348-53.
132. Popescu NI, Lupu C, Lupu F. Extracellular protein disulfide isomerase regulates coagulation on endothelial cells through modulation of phosphatidylserine exposure. *Blood*. 2010;116:993-1001.
133. Stalker TJ, Traxler EA, Wu J, Wannemacher KM, Cermignano SL, Voronov R, et al. Hierarchical organization in the hemostatic response and its relationship to the platelet-signaling network. *Blood*. 2013;121:1875-85.
134. Michelet F, Guequen R, Leroy P, Wellman M, Nicolas A, Siest G. Blood and plasma glutathione measured in healthy subjects by HPLC: relation to sex, aging, biological variables, and life habits. *Clin Chem*. 1995;41:1509-17.
135. Furie B, Flaumenhaft R. Thiol isomerases in thrombus formation. *Circ Res*. 2014;114:1162-73.
136. Kastrup CJ, Runyon MK, Shen F, Ismaqilov RF. Modular chemical mechanism predicts spatiotemporal dynamics of initiation in the complex network of hemostasis. *Proc Natl Acad Sci U S A*. 2006;103:15747-52.
137. Kastrup CJ, Shen F, Runyon MK, Ismaqilov RF. Charaterization of the threshold response of initiation of blood clotting to stimulus patch size. *Biophys J*. 2007;93:2969-77.
138. Shen F, Kastrup CJ, Liu Y, Ismaqilov RF. Threshold response of initiation of blood coagulation by tissue factor in patterned microfluidic capillaries is controlled by shear rate. *Arterioscl Thromb Vasc Biol*. 2008;28:2035-41.
139. Bonderman D, Teml A, Jakowitsch J, Adlbrecht C, Gyongyosi M, Sperker W, et al. Coronary no-reflow is caused by shedding of active tissue factor from dissected atherosclerotic plaque. *Blood*. 2002;99:2794-800.
140. Walski M, Chlopicki S, Celary-Walska R, Frontczak-Baniewicz M. Ultrastructural alterations of endothelium covering advanced atherosclerotic plaque in human carotid artery visualised by scanning electron microscope. *J Physiol Pharmacol*. 2002;53:713-23.
141. Wilcox JN, Smith KM, Schwartz SM, Gordon D. Localization of tissue factor in the normal vessel wall and in the atherosclerotic plaque. *Proc Natl Acad Sci U S A*. 1989;86:2839-43.
142. Doggett TA, Girdhar G, Lawshe A, Schmidtke DW, Laurenzi IJ, Diamond SL, et al. Selectin-like kinetics and biomechanics promote rapid platelet adhesion in flow: the GPIb(alpha)-vWF tether bond. *Biophys J*. 2002;83:194-205.
143. Mody NA, King MR. Platelet adhesive dynamics. Part I: characterization of platelet hydrodynamic collisions and wall effects. *Biophys J*. 2008;95:2539-55.
144. Ruggeri ZM. The role of von Willebrand factor in thrombus formation. *Thromb Res*. 2007;120 Suppl 1:S5-9.

145. Colace TV, Diamond SL. Direct observation of von Willebrand factor elongation and fiber formation on collagen during acute whole blood exposure to pathological flow. *Arterioscler Thromb Vasc Biol*. 2013;33:105-13.
146. Franchini M, Lippi G. Von Willebrand factor and thrombosis. *Ann Hematol*. 2006;85:415-23.
147. Stalker TJ, Welsh JD, Tomaiuolo M, Wu J, Colace TV, Diamond SL, et al. A systems approach to hemostasis: 3. Thrombus consolidation regulates intrathrombus solute transport and local thrombin activity. *Blood*. 2014;124:1821-31.
148. Muthard RW, Diamond SL. Side view thrombosis microfluidic device with controllable wall shear rate and transthrombus pressure gradient. *Lab Chip*. 2013;13:1883-91.
149. Muthard RW, Diamond SL. Blood clots are rapidly assembled hemodynamic sensors: flow arrest triggers intraluminal thrombus contraction. *Arterioscl Thromb Vasc Biol*. 2012;32:2938-45.
150. Leiderman K, Fogelson AL. The influence of hindered transport on the development of platelet thrombi under flow. *Bull Math Biol*. 2013;75:1255-83.
151. Leiderman K, Fogelson AL. Grow with the flow: a spatial-temporal model of platelet deposition and blood coagulation under flow. *Math Med Biol*. 2011;28:47-84.
152. Beltrami E, Jesty J. The role of membrane patch size and flow in regulating a proteolytic feedback threshold on a membrane: possible application in blood coagulation. *Math Biosci*. 2001;172:1-13.
153. Brass LF, Diamond SL. Transport physics and biorheology in the setting of haemostasis and thrombosis. *J Thromb Haemost*. 2016
154. Fogelson AL, Neeves KB. Fluid Mechanics of Blood Clot Formation. *Annu Rev Fluid Mech*. 2015;47:377-403.
155. Yeh C, Eckstein EC. Transient lateral transport of platelet-sized particles in flowing blood suspensions. *Biophys J*. 1994;66:1706-16.
156. Vahidkhah K, Diamond SL, Bagchi P. Platelet dynamics in three-dimensional simulation of whole blood. *Biophys J*. 2014;106:2529-40.
157. Mannucci PM. Treatment of von Willebrand's Disease. *N Engl J Med*. 2004;351:683-94.
158. Hechler B, Nonne C, Eckly A, Magnenat S, Rinckel JY, Denis CV, et al. Arterial thrombosis: relevance of a model with two levels of severity assessed by histologic, ultrastructural and functional characterization. *J Thromb Haemost*. 2010;8:173-84.
159. Herbig BA, Diamond SL. Pathological VWF fibers resist tPA and ADAMTS13 while promoting the contact pathway and shear-induced platelet activation. *J Thromb Haemost*. 2015;19:1699-708.
160. Nesbitt WS, Westein E, Tovar-Lopez FJ, Tolouei E, Mitchell A, Fu J, et al. A shear gradient-dependent platelet aggregation mechanism drives thrombus formation. *Nat Med*. 2009;15:665-73.
161. Ross R. The pathogenesis of atherosclerosis: a perspective for the 1990s. *Nature*. 1993;362:801-9.
162. Davies MJ. The composition of coronary-artery plaques. *N Engl J Med*. 1997;336:1312-4.

163. Coughlin SR. Thrombin signalling and protease-activated receptors. *Nature*. 2000;407:258-64.
164. Wolberg AS. Thrombin generation and fibrin clot structure. *Blood Rev*. 2007;21:131-42.
165. Hornyak TJ, Bishop PD, Shafer JA. Alpha-thrombin-catalyzed activation of human platelet factor XIII: relationship between proteolysis and factor XIIIa activity. *Biochemistry*. 1989;28:7326-32.
166. Schwartz ML, Pizzo SV, Hill RL, McKee PA. Human Factor XIII from plasma and platelets. Molecular weights, subunit structures, proteolytic activation, and cross-linking of fibrinogen and fibrin. *J Biol Chem*. 1973;248:1395-407.
167. Krishnaswamy S, Church WR, Nesheim ME, Mann KG. Activation of human prothrombin by human prothrombinase. Influence of factor Va on the reaction mechanism. *J Biol Chem*. 1987;262:3291-9.
168. Krishnaswamy S, Jones KC, Mann KG. Prothrombinase complex assembly. Kinetic mechanism of enzyme assembly on phospholipid vesicles. *J Biol Chem*. 1988;263:3823-34.
169. Walker RK, Krishnaswamy S. The activation of prothrombin by the prothrombinase complex. The contribution of the substrate-membrane interaction to catalysis. *J Biol Chem*. 1994;269:27441-50.
170. Butenas S, Orfeo T, Gissel MT, Brummel KE, Mann KG. The significance of circulating factor IXa in blood. *J Biol Chem*. 2004;279:22875-82.
171. Brummel-Ziedins K, Vossen CY, Rosendaal FR, Umezaki K, Mann KG. The plasma hemostatic proteome: thrombin generation in healthy individuals. *J Thromb Haemost*. 2005;3:1472-81.
172. Brummel-Ziedins KE, Orfeo T, Gissel M, Mann KG, Rosendaal FR. Factor Xa generation by computational modeling: an additional discriminator to thrombin generation evaluation. *PloS one*. 2012;7:e29178.
173. Willems GM, Lindhout T, Hermens WT, Hemker HC. Simulation model for thrombin generation in plasma. *Haemostasis*. 1991;21:197-207.
174. Hockin MF, Jones KC, Everse SJ, Mann KG. A model for the stoichiometric regulation of blood coagulation. *J Biol Chem*. 2002;277:18322-33.
175. Nesheim ME, Tracy RP, Mann KG. "Clotspeed," a mathematical simulation of the functional properties of prothrombinase. *J Biol Chem*. 1984;259:1447-53.
176. Bungay SD, Gentry PA, Gentry RD. A mathematical model of lipid-mediated thrombin generation. *Math Med Biol*. 2003;20:105-29.
177. Sorensen EN, Burgreen GW, Wagner WR, Antaki JF. Computational simulation of platelet deposition and activation: I. Model development and properties. *Ann Biomed Eng*. 1999;27:436-48.
178. Sorensen EN, Burgreen GW, Wagner WR, Antaki JF. Computational simulation of platelet deposition and activation: II. Results for Poiseuille flow over collagen. *Ann Biomed Eng*. 1999;27:449-58.
179. Hoffman M, Monroe DM, 3rd. The action of high-dose factor VIIa (FVIIa) in a cell-based model of hemostasis. *Disease-a-month : DM*. 2003;49:14-21.

180. Zhu S, Welsh JD, Brass LF, Diamond SL. Platelet-targeting thiol reduction sensor detects thiol isomerase activity on activated platelets in mouse and human blood under flow. *J Thromb Haemost*. 2016;14:1070-81.
181. Voronov RS, Stalker TJ, Brass LF, Diamond SL. Simulation of intrathrombus fluid and solute transport using in vivo clot structures with single platelet resolution. *Ann Biomed Eng*. 2013;41:1297-307.
182. Kim OV, Xu Z, Rosen ED, Alber MS. Fibrin networks regulate protein transport during thrombus development. *PLoS Comput Biol*. 2013;9:e1003095.
183. Xu Z, Lioi J, Mu J, Kamocka MM, Liu X, Chen DZ, et al. A multiscale model of venous thrombus formation with surface-mediated control of blood coagulation cascade. *Biophys J*. 2010;98:1723-32.
184. Tomaiuolo M, Stalker TJ, Welsh JD, Diamond SL, Sinno T, Brass LF. A systems approach to hemostasis: 2. Computational analysis of molecular transport in the thrombus microenvironment. *Blood*. 2014;124:1816-23.
185. Meh DA, Siebenlist KR, Mosesson MW. Identification and characterization of the thrombin binding sites on fibrin. *J Biol Chem*. 1996;271:23121-5.
186. Lovely RS, Moaddel M, Farrell DH. Fibrinogen gamma' chain binds thrombin exosite II. *J Thromb Haemost*. 2003;1:124-31.
187. Fredenburgh JC, Stafford AR, Pospisil CH, Weitz JI. Modes and consequences of thrombin's interaction with fibrin. *Biophys Chem*. 2004;112:277-84.
188. Muthard RW, Welsh JD, Brass LF, Diamond SL. Fibrin, gamma'-fibrinogen, and transclot pressure gradient control hemostatic clot growth during human blood flow over a collagen/tissue factor wound. *Arterioscler Thromb Vasc Biol*. 2015;35:645-54.
189. Yeh CH, Fredenburgh JC, Weitz JI. Oral direct factor Xa inhibitors. *Circ Res*. 2012;111:1069-78.
190. Hemker HC, Giesen P, AlDieri R, Regnault V, de Smed E, Wagenvoord R, et al. The calibrated automated thrombogram (CAT): a universal routine test for hyper- and hypocoagulability. *Pathophysiol Haemost Thromb*. 2002;32:249-53.
191. Folie BJ, McIntire LV. Mathematical analysis of mural thrombogenesis. Concentration profiles of platelet-activating agents and effects of viscous shear flow. *Biophys J*. 1989;56:1121-41.
192. Kuharsky AL, Fogelson AL. Surface-mediated control of blood coagulation: the role of binding site densities and platelet deposition. *Biophys J*. 2001;80:1050-74.
193. Neeves KB, Illing DA, Diamond SL. Thrombin flux and wall shear rate regulate fibrin fiber deposition state during polymerization under flow. *Biophys J*. 2010;98:1344-52.
194. Downing MR, Bloom JW, Mann KG. Comparison of the inhibition of thrombin by three plasma protease inhibitors. *Biochemistry*. 1978;17:2649-53.
195. Ruhl H, Muller J, Harbrecht U, Fimmers R, Oldenburg J, Mayer G, et al. Thrombin inhibition profiles in healthy individuals and thrombophilic patients. *Thromb Haemost*. 2012;107:848-53.
196. Chandler WL, Velan T. Estimating the rate of thrombin and fibrin generation in vivo during cardiopulmonary bypass. *Blood*. 2003;101:4355-62.

197. Rivard GE, Brummel-Ziedins KE, Mann KG, Fan L, Hofer A, Cohen E. Evaluation of the profile of thrombin generation during the process of whole blood clotting as assessed by thrombelastography. *J Thromb Haemost*. 2005;3:2039-43.
198. Bird RB, Stewart WE, Lightfoot EN. *Transport Phenomena (2nd Edition)*. New York, NY: John Wiley & Sons, Inc.; 2006.
199. Ruiz FA, Lea CR, Oldfield E, Docampo R. Human platelet dense granules contain polyphosphate and are similar to acidocalcisomes of bacteria and unicellular eukaryotes. *J Biol Chem*. 2004;279:44250-7.
200. Zilberman-Rudenko J, Itakura A, Wiesenekker CP, Vetter R, Maas C, Gailani D, et al. Coagulation Factor XI Promotes Distal Platelet Activation and Single Platelet Consumption in the Bloodstream Under Shear Flow. *Arterioscler Thromb Vasc Biol*. 2016;36:510-7.
201. Swords NA, Mann KG. The assembly of the prothrombinase complex on adherent platelets. *Arterioscler Thromb*. 1993;13:1602-12.
202. Tracy PB, Mann KG. Prothrombinase complex assembly on the platelet surface is mediated through the 74,000-dalton component of factor Va. *Proc Natl Acad Sci U S A*. 1983;80:2380-4.
203. Zhu S, Tomaiuolo M, Diamond SL. Minimum wound size for clotting: flowing blood coagulates on a single collagen fiber presenting tissue factor and von Willebrand factor. *Integr Biol (Camb)*. 2016
204. Jimenez JM, Prasad V, Yu MD, Kampmeyer CP, Kaakour AH, Wang PJ, et al. Macro- and microscale variables regulate stent haemodynamics, fibrin deposition and thrombomodulin expression. *J R Soc Interface*. 2014;11:20131079.
205. Reininger AJ, Heijnen HF, Schumann H, Specht HM, Schramm W, Ruggeri ZM. Mechanism of platelet adhesion to von Willebrand factor and microparticle formation under high shear stress. *Blood*. 2006;107:3537-45.
206. Krishnaswamy S. The Transition of Prothrombin to Thrombin. *J Thromb Haemost*. 2013;11:265-76.
207. Wood JP, Silveira JR, Maille NM, Haynes LM, Tracy PB. Prothrombin activation on the activated platelet surface optimizes expression of procoagulant activity. *Blood*. 2011;117:1710-8.
208. Nossel HL, Yudelman I, Canfield RE, Butler VP, Jr., Spanondis K, Wilner GD, et al. Measurement of fibrinopeptide A in human blood. *J Clin Invest*. 1974;54:43-53.
209. Wells PS, Anderson DR, Rodger M, Forgie M, Kearon C, Dreyer J, et al. Evaluation of D-Dimer in the Diagnosis of Suspected Deep-Vein Thrombosis. *N Engl J Med*. 2003;349:1227-35.
210. Hoylaerts M, Rijken DC, Lijnen HR, Collen D. Kinetics of the activation of plasminogen by human tissue plasminogen activator. Role of fibrin. *J Biol Chem*. 1982;257:2912-9.
211. Huber D, Cramer EM, Kaufmann JE, Meda P, Masse JM, Kruithof EK, et al. Tissue-type plasminogen activator (t-PA) is stored in Weibel-Palade bodies in human endothelial cells both in vitro and in vivo. *Blood*. 2002;99:3637-45.
212. Levin EG, Santell L, Osborn KG. The expression of endothelial tissue plasminogen activator in vivo: a function defined by vessel size and anatomic location. *Journal of cell science*. 1997;110 (Pt 2):139-48.